SOLID STATE NMR STRUCTURAL EVALUATION OF THE SAF-P1/P2A CO-ASSEMBLING PEPTIDE NANOFIBER SYSTEM

A Thesis
Presented to
The Academic Faculty

By

Evan K. Roberts

In Partial Fulfillment
Of the Requirements for the Degree
Master of Science in the
School of Chemical & Biomolecular Engineering

Georgia Institute of Technology

August 2017

SOLID STATE NMR STRUCTURAL EVALUATION OF THE SAF-P1/P2A CO-ASSEMBLING PEPTIDE NANOFIBER SYSTEM

Approved By:

Dr. Anant K. Paravastu, Advisor
School of Chemical & Biomolecular Engineering
Georgia Institute of Technology

Dr. Martha A. Grover
School of Chemical & Biomolecular Engineering
Georgia Institute of Technology

Dr. Julie A. Champion
School of Chemical & Biomolecular Engineering
Georgia Institute of Technology

Date Approved: January 3rd, 2017

Satisfaction of one’s curiosity is one of the greatest sources of happiness in life.

— Linus Pauling

I would like to dedicate this work to:

My mother, Patricia Kellett, for never giving up on me and teaching me to never give up.

My advisor, Anant Paravastu, for believing in me, even in times when I did not.

The Georgia Tech ChBE community as a whole, whose overwhelming support has fostered my personal growth in a way that moves me beyond words.

Acknowledgements

Anant Paravastu for being the best research advisor, role model, and friend that I could have asked for.

Martha Grover for facilitating a TA role that made me realize my passion for educating others.

Julie Champion for agreeing to serve on my committee, and for motivating me to set a date for my defense while it was still feasible to do so with my chosen committee members.

Sarah R. Leonard, whose previous work in our lab inspired my research on SAF-p1/p2a, for supporting my efforts and making herself available to answer my questions.

Maxwell Zimmerman, formerly of the Paravastu lab, for writing the code for molecular modeling of co-assembling systems that was invaluable to the molecular modeling of SAF-p1/p2a.

The Georgia Tech Startup Fund and the National Science Foundation for funding my research.

Emory University and the staff of the Robert P. Apkarian Integrated Microscopy Core for allowing me to use their transmission electron microscope.

Yuan Gao for his patience and diligence in showing me how to perform the solid state NMR experiments that made this work possible.

Chris Elliot and particularly Cameron Black for their hard work in developing a 3D molecular model for the SAF-p1/p2a heterodimer and nanofiber.

Zachary Gunnz for his assistance in searching the literature, and for drafting the design for a benchtop sample preparation chamber that will make my future work on SAF-p1/p2a less stressful.

Yeongseon Jang of the Champion lab for kindly providing a staining agent (PTA) used in my electron microscopy experiments.

Rebecca Han for taking an interest in my work and helping me proofread this thesis.

TABLE OF CONTENTS

LIST OF TABLES

LIST OF FIGURES

NOMENCLATURE

Characterization/preparation methods and materials

TEM: Transmission Electron Microscopy

UA: Uranyl Acetate

PTA: Phosphotungstenic Acid

Lyophilized: Freeze-dried under vacuum

ESI+MS : Electrospray (+) Ionization-assisted Mass Spectrometry

HPLC: High Pressure Liquid Chromotography

MOPS: 3-(N-morpholino)-propanesulfonic acid

Fmoc: 9-Fluorenylmethyloxycarbonyl, used as a protecting group for the N-terminus during SPS of peptides and individual amino acids

Fmoc-protected: Describes individual amino acids or synthetic peptides that include an Fmoc protecting group bonded to the amine nitrogen or N-terminus, respectively

NMR Nomenclature

NMR: Nuclear Magnetic Resonance spectroscopy

Solid State NMR: NMR of solid samples

Labels: Magnetically-susceptible isotopes (*e.g.* ^{13}C) deliberately incorporated into a specific site of an amino acid and/or peptide for solid state NMR analysis

Uniformly ^{13}C-^{15}N labeled: All carbon and nitrogen atoms are magnetically susceptible

Selectively ^{nn}X-labeled: Some, but not all, atoms of element X in the amino acid are magnetically susceptible

Sensitivity: Limit of detection for a particular nucleus by NMR

Resolution: Describes broadness/sharpness of NMR spectral signals; may alternatively be used to describe the level of detail (*e.g.* molecular level, atomic-lenghth scale) accessible by a characterization method.

S/N: Signal-to-Noise Ratio

ν_L: Larmour frequency (in Hz or MHz)

γ_n : Gyromagnetic Ratio (in MHz/T or rad/T*s)

FID: Free-Induction Decay; generated by excitation of magnetically-susceptible nuclei in a static magnetic field

NMR Observable: The NMR peak resulting from a Fourier Transform of the FID

Minor Structure: In structurally heterogeneous peptide samples, any distinct structural population that is not the majority population

Minor Signal: An NMR observable corresponding to a nucleus that is part of a minor structure population in a structurally heterogeneous sample

CS: Chemical Shift (in ppm)

Δ**CS:** Secondary Chemical Shift (in ppm)

Upfield shift: A decrease in chemical shift for a given nucleus

Downfield shift: An increase in chemical shift for a given nucleus

RF pulse: Radiofrequency pulse, used to excite magnetically-susceptible nuclei in NMR

Probe: The electronic components of a spectrometer including multiple channels for each nucleus of interest, the amplifier, receiver, and coil that delivers pulses to the sample and transmits the FID following pulse excitation of nuclei

E-free probe: A probe specially designed to handle higher decoupling pulse powers and minimize heating of the sample from RF pulses

On-resonance: The condition of having the probe tuned to the resonant frequency of the nuclei of interest for the spectrometer magnetic field

Dual-resonance HX probe: Two-channel probe in which one channel is fixed for proton detection while the other channel may be set to detect a nucleus of the user's choice

Triple-resonance HCN probe: E-free probe with three channels fixed to detect ^{1}H, ^{13}C, and ^{15}N

MAS: Magic Angle Spinning; high-speed sample rotation at 54.7° relative to the z-axis

Rotor: A zirconia sample chamber of small diameter (*e.g.* 3.2 mm) that withstand the forces experienced under high-speed MAS conditions

Pulse Sequence: The order and cylindrical θ coordinate of each RF pulse in sequence for a specific experiment

$\boldsymbol{B_0}$: Static magnetic field in the *z*-direction; intrinsic to the spectrometer itself (in Teslas)

$\boldsymbol{B_1}$: Applied magnetic field in transverse magnetization plane resulting from delivery of an RF pulse through the coil within the probe about the sample (in Teslas)

CP: Cross-polarization

CPMAS: Cross-Polarization Magic Angle Spinning

Diagonal peak: Peaks corresponding to 1D NMR spectral signatures in 2D spectra; the diagonal divides 2D spectra into symmetric halves

Crosspeak: Peaks resulting from correlations of nuclear spins in close proximity to one another; ideally, only two nuclei participate in any one crosspeak

Through-bond transfer: Magnetization transfer between covalently bonded nuclei, or between nuclei in the same amino acid

Through-space transfer/contact: Magnetization transfer between nuclei that do not share covalent bonds or bonding partners, but are in close proximity within ~6 Å

fpRFDR: finite pulse Radiofrequency-Driven Recoupling

DARR: Dipolar-Assisted Rotational Resonance

τ_m: mixing time parameter for DARR experiments

Short-mixing DARR: DARR experiment with $\tau_m = 50$ ms

Long-mixing DARR: DARR experiment with $\tau_m = 500$ ms

REDOR: Rotational Echo Double Resonance – ^{13}C-^{15}N distance measurement

fsREDOR: frequency-selective REDOR

PITHIRDS-CT: not an acronym; ^{13}C-^{13}C distance measurement

Designer Peptide Nomenclature

***De novo*:** A novel peptide or peptide system developed using rational design principles

SAF (nonspecific): Stands for "Self-Assembling Fiber" despite all variants of SAF being co-assembling binary peptide systems

hSAF (nonspecific): Denotes a hydrogel-like variant of the SAF family of designer peptides

Assembly: The insoluble macromolecular structure formed by spontaneous aggregation and ordering of peptides, or the action thereof

Self-Assembly: Assembly of one peptide with other peptides of identical sequence

Co-assembly: Assembly of one peptide with one or more peptides of distinct sequence(s)

$\mathbf{t}_{\text{assembly}}$: Time elapsed after mixing peptides together to start an assembly

Secondary Structure: Repeated 3D conformation adopted by a peptide or assembly

Striations: Axial stripe-like patterns of regular periodicity that are visible in TEM micrographs of highly-ordered nanofibers

Residue: Defined here as the sidechain of an amino acid

Intraresidue contact: NMR crosspeaks between nuclei in the same amino acid

Interresidue contact: NMR crosspeaks between nuclei in different amino acids

Homodimer: Dimer formed by two identical peptides

Heterodimer: Dimer formed by two different peptides

Blunt-ended dimer: Peptide dimer that interfaces over the entire sequence

Sticky-ended dimer: Peptide dimer that interfaces over only part of the sequence, leaving one end of each peptide sequence in solution

Oligomer: A group of peptide monomers, dimers or n-mers that have associated into a larger aggregate

Protofibril: A longitudinal assembly of assembling peptides that can associate with other protofibrils to form a fibril

Supramolecular Structure: The macromolecule of uniform secondary structure formed by a peptide assembly

Polymorphism: Structural heterogeneity in a peptide sample resulting from secondary structural dynamics, rather than errors in sample preparation

Molecular Switch: An assembling peptide system that can convert from one supramolecular structure to another in response to a stimulus

C_α: The alpha carbon of an amino acid

C_β: The beta carbon of an amino acid

C_γ: The gamma carbon of an amino acid

C_δ: The delta carbon of an amino acid

C_ε: The epsilon carbon of an amino acid

SUMMARY

This work presents a structural investigation of two variants of SAF (Self-Assembling Fiber) binary peptides designed by Prof. Derek N. Woolfson and coworkers. SAF refers to pairs of complementary peptides that assemble into coiled coils upon mixing, which then associate with one another to form fibers. Design features hypothesized to drive co-assembly were evaluated by solid-state nuclear magnetic resonance (NMR) spectroscopy.

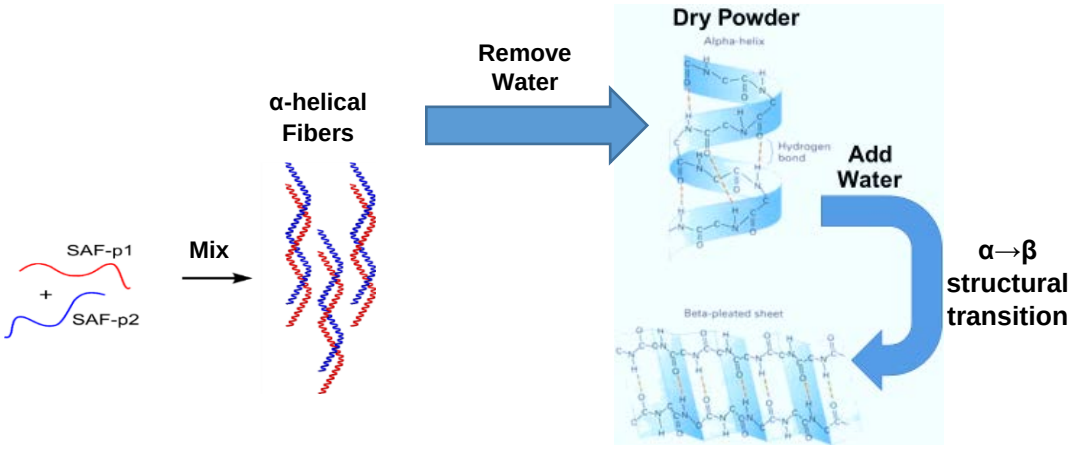

SAF peptides assemble into fibers when mixed and change structure upon rehydration.

Our results indicate that the SAF assembly mechanism proposed by Woolfson is partially correct. However, it was also discovered that the α-helical structure formed by the initial co-assembly can undergo conversion to a β-sheet structure, and that this conversion is triggered by rehydration of the dried α-helical nanofibers. To our knowledge, this is the first α-β structural transition ever observed in response to physiologically benign stimuli in a co-assembling *de novo* binary peptide system.

CHAPTER 1: INTRODUCTION

1.1 Co-assembling Designer Peptide Systems and Molecular Switches

The primary objective of this work is to evaluate the rational design of α-helical supramolecular structures formed by designer peptides, particularly in relation to *de novo* binary peptide systems that form nanofibers. The structures formed by such peptides are known as coiled-coils. The coiled-coil is a common and well-studied motif in nature as it relates to protein folding and nucleic acids (*1-6*). In fact, this foundation of study in naturally-occurring coiled-coils was the basis for developing the first design rules for α-helical designer peptides (*7*). In the context of rationally designed peptide systems, a coiled-coil refers to the twisting macromolecular structure formed when individual peptide subunits first orient parallel to their long axes, and then twist in the manner described by Pauling (*8*) as they associate longitudinally with other dimeric subunits. Since the inception of the field, a great many self-assembling coiled-coil designer peptides have been developed (*2, 3, 9-17*), but this work will cover coiled-coils formed by two complementary peptide sequences upon mixing—a phenomenon known as co-assembly.

An additional discussion is necessitated by my results which concerns the phenomenon of molecular switching. A "molecular switch" in this context is an assembling peptide system that is capable of transitioning between two types of secondary structure in response to a stimulus or set of stimuli (*18-20*). In particular, the conversion of dry α-helical coiled-coils to β-sheets in response to rehydration and mild heating will be examined in the context of

SAF. The potential implications of this discovery will be discussed as they relate to the design and fabrication of "smart" (*i.e.* stimulus-responsive) biomaterials for medical devices, regenerative medicine, and drug delivery applications.

1.1.1 Rational Design of Coiled-coil Peptide Assemblies

The primary structures of the coiled-coil are characteristic of an amino acid heptad-repeat (HPPHPPP, where H represents a hydrophobic residue and P represents a hydrophilic or polar residue). This approach to designing self-assembling peptide nanofibers will be described subsequently with the coiled-coil structures termed SAF. The positions *abcdefg* in the context of this work correspond to the heptad positions HPPHPPP. A schematic of the heptad helical wheel marked with the *abcdefg* positions is shown in Figure 1.

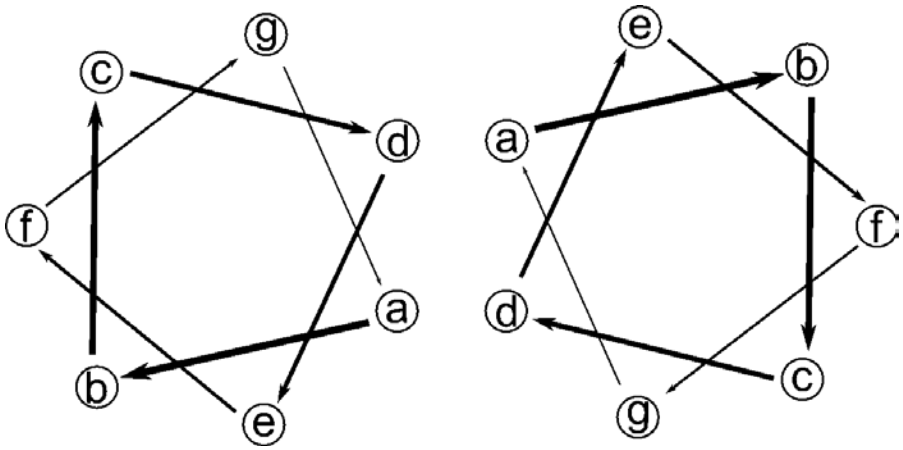

Figure 1: Helical wheel depiction of coiled-coil heptad marked with positions *abcdefg*.

This seven residue repeat of hydrophobic and polar residues served as the foundation for the design of the SAF co-assembling peptide family. Within the coiled-coil heptad,

[*abcdefg*]$_n$ positions *a*, *d*, *e*, and *g* are responsible for directing the dimer interface, and positions *b*, *c*, and *f* mediate lateral interactions between dimers (*21*).

For the designer peptides in this work, the *a* and *d* "core" positions signify hydrophobic residues that form the coiled-coil interface. The *e* and *g* "overhang" positions are occupied by charged residues which are intended to stabilize the coiled-coil and facilitate longitudinal co-assembly by pairing as *e*-to-*g* salt bridges between complementary peptides across the coiled-coil interface. The "surface" positions *b, c*, and *f* are mostly occupied by weakly hydrophobic (*i.e.* alanine) or polar hydrogen-bonding residues (*i.e.* glutamine).

1.1.2 The SAF Family of α-helical Co-assembling Peptides

The seminal work of Prof. Derek Woolfson and coworkers in developing the original "Self-Assembling Fiber" peptides, dubbed SAF-p1 and SAF-p2 (*22*), marked a milestone in rational peptide design. The conception of SAF-p1/p2 marked the first multicomponent *de novo* peptide system capable of spontaneously forming a coiled-coil nanostructure upon mixing. Specifically, the individually water-soluble peptide components were designed to undergo a molecular folding event when mixed to form sticky-ended heterodimers, which in turn assemble longitudinally into coiled-coil fibers, as depicted in Figure 2.

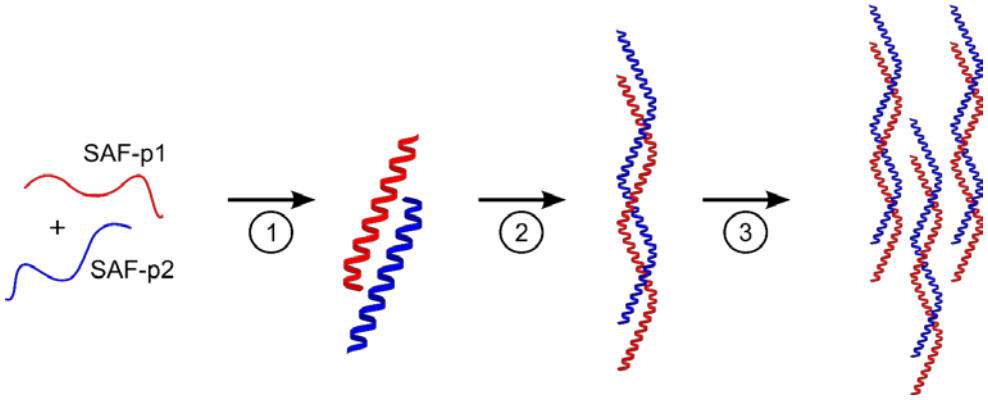

Figure 2: Schematic of the co-assembly pathway for SAF peptides as reported by Bromley *et al.(23)*. Upon mixing, the two component peptides associate to form heterodimers **(1)** which then associate longitudinally to form protofibrils **(2)** which continue to grow in length while associating laterally to form bundled fibrils **(3)**.

The conception of the SAF system was motivated by a desire to test *de novo* design principles derived from coiled-coils in nature (*22*), but the success of the first generation of SAF compelled further efforts to refine the system towards applications in tissue engineering as a biocompatible scaffold material for collagen-like cell cultures (*24-26*). Subsequent design iterations by the Woolfson lab would engender a whole family of SAF co-assembling binary peptide systems. A brief review is given here of their development towards the study of SAF-p1/p2a and hSAF$_{AAQ}$-p1/p2.

The Woolfson lab's novel approach to triggered co-assembly originates in bioinformatics—that is, the SAF peptide sequences were devised to form a specific supramolecular structure based on sequence-structure relationships found in nature. Woolfson applied several common structural features of heptad-based coiled coils in nature towards his design of the 28-residue peptides SAF-p1 and SAF-p2. First, the majority of

hydrophobic core positions *a* and *d* (Figure 3) were occupied by leucine (Leu, L) and isoleucine (Ile, I) at complementary positions to energetically favor the formation of leucine "zippers" along the plane of co-assembly when aqueous solutions of the peptides were mixed together. Secondly, to encourage the sticky-ended (as opposed to blunt-ended) formation of heterodimers, all *e* and *g* "overhang" positions were occupied by either lysine (Lys, K) and glutamate (Glu, E) such that the first two heptads of each peptide sequence carried only positive charges and the last two heptads carried negative charges. Finally, a single *a* position of each 28-residue peptide hosted an asparagine (Asn, N) residue instead of Leu or Ile, because Asn residues are known to pair with each other in coiled-coil interfaces through hydrogen bonding and encourage parallel alignment of the N-C termini (*9, 27, 28*). These three sequence-to-structure design features of the first-generation design of SAF were conserved amongst all subsequent generations of SAF; within the scope of this study, a structural evaluation of the leucine zipper and charged overhang pairings will be presented.

Table 1: SAF-p1/p2 and SAF-p2a amino acid sequences. Alterations to the SAF-p2 sequence in SAF-p2a are highlighted in yellow.

Peptide Name	Sequence				
Heptad repeat	*g*	*a b c d e f g*	*a b c d e f g*	*a b c d e f g*	*a b c d e f*
SAF-p1	K	IAALKQK	IASLKQE	IDALEYE	NDALEQ
SAF-p2	K	IAALKQK	NAALKQE	IAALEQE	IAALEQ
SAF-p2a	K	IRRLKQK	NARLKQE	IAALEYE	IAALEQ

The second generation of SAF includes the primary subject of study in this work, SAF-p1/p2a. As implied by the name, only the second component sequence was altered from the original design of SAF-p1/p2. Table 1 shows the sequences of the first and second generation SAF peptide sequences for comparison. The alterations leading to the SAF-p2a sequence were meant to enhance the observed propensity of SAF fibers to assemble laterally into thick (~50 nm) fibril-like structures by adding several positively-charged arginine (Arg, R) residues to the hydrophilic surface positions of the first two heptads (*24*). A tyrosine (Tyr, Y) residue was also incorporated at position 21 in SAF-p2a, although the reasoning for this design choice was not provided by the authors. The result of this redesign was the SAF-p1/p2a system, which produced the thickest and straightest fibers of any SAF variant to date.

Many more design iterations beyond the scope of this work were published after the second generation of SAF, including variants with increased surface charge (*29*), sequences extended by one heptad (*30, 31*), functional reactive group "caps" on the N- or C- termini (*32*), chromophore "tag" moieties (*33*), and a selection of variants called hSAF, which are capable of forming hydrogels (*25, 26*). An important unanswered question left over from these studies is why the SAF coiled-coil protofibrils laterally associate at all; most SAF variants form mature fibers that are more than an order of magnitude thicker than the fiber width of ~2 nm predicted by Woolfson's design (*22, 24, 27-33*).

The hydrogel-forming variants of SAF warrant some preliminary discussion for the purposes of this thesis. The importance of the Woolfson group's development of the hSAF

variants, from a design perspective, lies in their testing of substituent effects on the outer surface of the coiled-coil assembly, namely at the *f* position of the helical-wheel heptad model. The original hSAF literature (*25*) investigated the response to thermal stress by hydrogels rich in hydrogen-bonding surface residues (Gln in $hSAF_{QQQ}$) compared to hydrogels rich in hydrophobic surface residues (Ala in $hSAF_{AAA}$ and Ala/Trp in $hSAF_{AAA-W}$). My predecessor studied a hydrogel-like SAF variant called $hSAF_{AAQ}$, which was designed as a control against hydrogel formation in the original study (*25*), but was reported to form very thin (~2 nm thick) nanofibers. The complementary sequences for this variant are listed below in Table 2.

Table 2: $hSAF_{AAQ}$-p1/p2 amino acid sequences

Peptide Name	Sequence				
Heptad repeat	*g*	*a b c d e f g*	*a b c d e f g*	*a b c d e f g*	*a b c d e f*
$hSAF_{AAQ}$-p1	K	IAALKQK	IAALKQE	IAALEQE	NAALEQ
$hSAF_{AAQ}$-p2	K	IAALKQK	NAALKQE	IAALEQE	IAALEQ

1.1.3 Questions Raised by Previous Work on $hSAF_{AAQ}$-p1/p2

The investigation of $hSAF_{AAQ}$-p1/p2 shared similar objectives with my study of SAF-p1/p2a. The co-assembling coiled coils of the SAF family were the first of their kind, but until our lab's work with $hSAF_{AAQ}$-p1/p2, there had never been a high-resolution metric applied towards evaluating their design efficacy. Solid state NMR was used to probe the

design features of the coiled-coil interface, with the intention of subsequently moving forward to investigate the mechanism responsible for lateral assembly of SAF protofibrils into thick nanofibers.

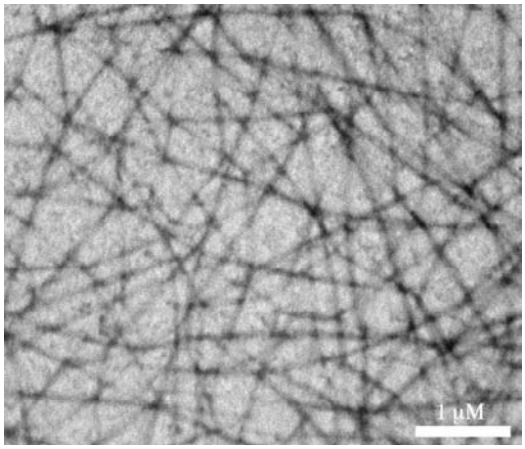

Figure 3: TEM of 200 µM $hSAF_{AAQ}$-p1/p2 nanofibers (scale bar: 1 µm) published by Banwell, Woolfson *et al.* (*25*)

My predecessor was interested in $hSAF_{AAQ}$ because it is the only SAF variant noted in the literature (*25*) as having fiber widths (~2 nm, Figure 3) matching the coiled-coil thickness predicted by Woolfson's design. This length scale allows straightforward interpretation of the paired interactions of core (*a* and *d* position) and overhang (*e* and *g* position) residues, which might be otherwise complicated by surface residue interactions between protofibrils. Similarly to my research on SAF-p1/p2a, the $hSAF_{AAQ}$-p1/p2 peptides were labeled to detect the Leu-Ile hydrophobic interaction and the Lys-Glu salt bridge at the overhang positions. However, the results of our structural evaluation of $hSAF_{AAQ}$-p1/p2 by solid state NMR were inconclusive. In fact, our study of $hSAF_{AAQ}$ had raised new questions.

Interpretation of the hSAF$_{AAQ}$-p1/p2 data was complicated by polymorphism (structural heterogeneity) in the sample; a more detailed discussion follows in Chapter 3. Preliminary analysis of the 2D NMR spectra for hSAF$_{AAQ}$-p1/p2 indicated that the Leu-Ile hydrophobic core interaction formed as hypothesized by Woolfson, while the presence of the hypothesized Lys-Glu salt bridge was rendered inconclusive due to spectral overlap. However, closer investigation of the hSAF$_{AAQ}$–p1/p2 data indicated that at least one minor structural population was present in the sample. Without knowing the nature of this minor structure, we could not conclusively determine if there was spatial proximity between the labeled Ile-Leu pair in the coiled-coil nanofiber. The reason for this is that the spectral signals suggesting a positive result for spatial proximity could instead be ordinary ^{13}C signals from a minor structure with a markedly different 3D conformation than the coiled-coil. Deconvolution of these two possibilities was impossible for this case, as we had no reference for how this unknown minor structure would appear in a 2D NMR spectra. Hence, we chose to study another variant of SAF for comparison.

1.1.4 SAF-p1/p2a Nanofibers: Testing the Design Hypothesis

I chose to study SAF-p1/p2a variant for three reasons. First, it was convenient to select a well-characterized variant from the literature that conserved both the sequence length of 28 and residues at the core (*a*, *d*) and overhang (*e*, *g*) heptad positions for better comparison with the hSAF$_{AAQ}$-p1/p2 structure. Second, SAF-p1/p2a appeared to be the most stable against forming kinetically-trapped minor structures, which may have complicated Dr. Leonard's study of hSAF$_{AAQ}$. According to the original literature for the hSAF series of peptides (*25*), the hSAF$_{AAQ}$ variant was developed as a negative control against hydrogel

formation, rather than as a rationally-designed peptide assembly in its own right. Homodimer formation by $hSAF_{AAQ}$-p1 and/or $hSAF_{AAQ}$-p2 was considered to be the most likely source of structural heterogeneity in our samples due to TEM evidence of self-assembly (Chapter 3). While many SAF variants could be considered stable against homodimer formation, the highly ordered structure of SAF-p1/p2a and its reported cooperative unfolding mechanism under thermal stress (*30*) made it a particularly attractive candidate for preparing structurally-uniform samples. The third and final reason I chose SAF-p1/p2a has to do with the regularly-spaced axial striations uniquely observed in transmission electron microscopy (TEM) images of SAF-p1/p2a nanofibers (*23, 30, 31*). Examples of these striations in my samples and those from literature (*30*) are shown in Figure 4. These striations repeat every ~4.2 nm in the literature (*23, 31*), which corresponds to the length of a 28-residue α-helix within a coiled-coil (*34*). These striations imply a remarkable level of structural regularity that is rarely attained by rational design.

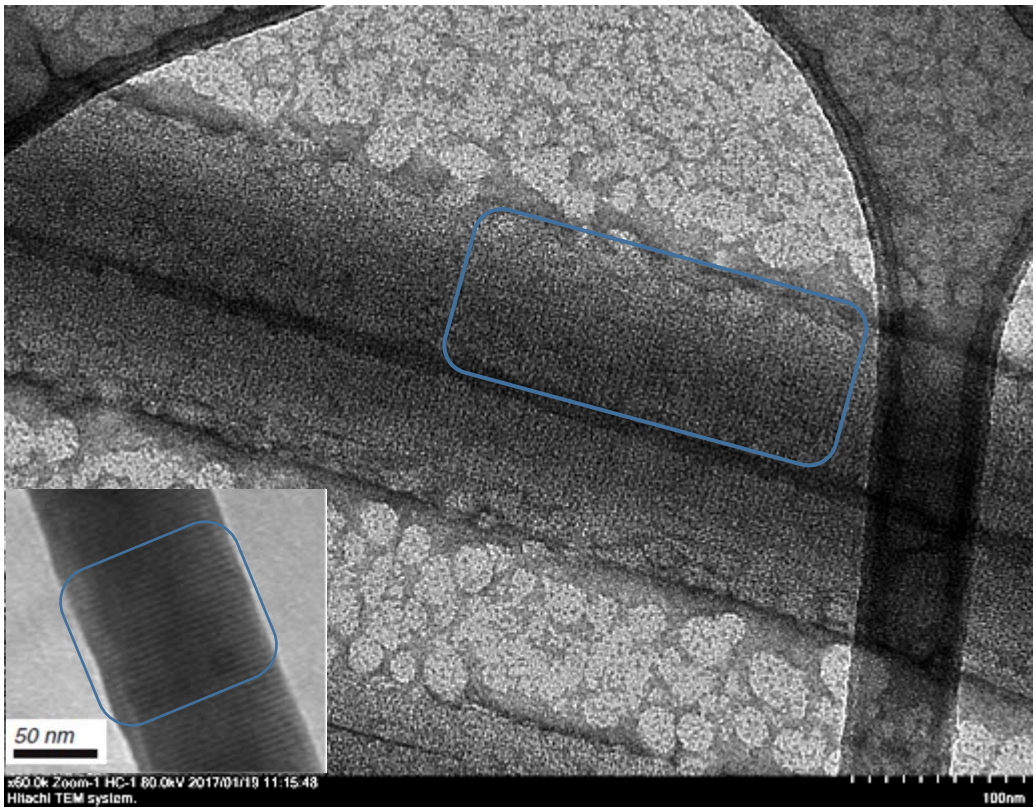

Figure 4: TEM of mature SAF-p1/p2a fibers stained with UA and imaged at 60k magnification; scale bar is 100 nm. Inset image from Smith, Woolfson *et al.* (*30*) shown for comparison. For each image, a group of striations is boxed in blue.

1.2 Molecular Switches and Their Applications

The supramolecular assembly of designer peptide systems can be broadly categorized in terms of secondary structure by one of two motifs: α-helix or β-sheet. These two conformations differ considerably in terms of 3-dimensional geometry and energetic favorability, such that a peptide system that assembles according to one of these structural topographies typically cannot form the other. However, a number of notable exceptions to this generality have been observed in assembling peptide systems, which are called molecular switches when a structural conversion is triggered by a change in conditions. Triggering conditions for conversion between structural motifs are diverse even for these exceptional cases, with conformational shifts in molecular switch assemblies of a single peptide sequence variously observed in the literature to be a function of pH (*35-37*), temperature (*38-40*), solvent composition (*41, 42*), or humidity (*43, 44*). Molecular switching may also be triggered by exposure to light (*45*), metal cations (*46, 47*), or certain enzymes (*48*). For a dual-responsive system, two of these triggers (most commonly temperature and pH) are required to induce molecular switching, and as a result the structural transition can be controlled with greater precision (*20*). However, The task of rationally designing a molecular-switching peptide system becomes more complicated as the number of peptide sequences increases and the triggering conditions become more specific (*18, 20, 49, 50*). As such, the vast majority of molecular switch systems include only one *de novo* peptide sequence and a single environmental trigger (*20, 50, 51*).

The task of rationally engineering a multicomponent α-to-β molecular switch from distinct co-assembling peptide sequences is such that, to date, no successful attempts have been reported in literature (*20*, *50*).

Remarkably, my work uncovered evidence that Woolfson's group serendipitously achieved this feat with SAF-p1/p2a, but remained unaware of its molecular switching property. The importance of this discovery lies in its potential to provide a starting point for the rational design of smart biomaterials made from co-assembled peptides that can be triggered to undergo the α-to-β structural shift under benign physiological conditions. The following is a topical review of biomedical engineering applications that could advance through the implementation of co-assembled molecular switch biomaterials featuring similar structural dynamics to SAF-p1/p2a.

1.2.1 Drug Delivery

Arguably the most straightforward application for a smart α-to-β molecular switching biomaterial would be as a drug delivery vehicle. The simplest example for a system like SAF-p1/p2a would be extended-release delivery drugs (especially for localized delivery of poorly soluble drugs), wherein drug molecules are trapped between protofibrils during co-assembly of the coiled-coil nanofibers (*52*) such that they are gradually released *in vivo* as the structure unfolds and rearranges to form a β-sheet (*53*). A more complex drug-delivery platform could involve a triggered-release drug carrier that is hermetically sealed within an implant sporting a design feature to break the seal (*52*, *53*) in response to a stimulus (*e.g.* host-guest molecular recognition of a pathological biomarker), which would then allow

biological fluids to contact the peptide assembly and affect the structural transition to finally release the drug into the body. Accurate models of both time-dependent structural rearrangement and *in vivo* degradation of a candidate molecular switch would be necessary to evaluate its potential as a drug carrier.

In the context of my project, drug delivery applications are of particular interest because the surface morphology of both structural states in SAF-p1/p2a differs drastically from those of the liposomal and micellar peptide drug carriers that are well-studied as nanoscale drug delivery vehicles (*54-57*). Also, the peptide assembly itself is insoluble up to the point of *in vivo* biodegradation, so it could be advantageous for extended-release pharmaceutical therapies that are meant to be targeted to a single location within the body. As such, a drug delivery platform based on a molecular switch like SAF-p1/p2a could, in theory, be subcutaneously localized on a pathological surface that would otherwise be incompatible with nanospherical drug delivery vehicles, which would be expected to degrade more rapidly in the body (*58, 59*). Targeted gene and/or pharmaceutical therapies for bone disease, including osteoporosis (*59-61*) and bone cancers (*58*), could be made more effective through use of such a delivery platform.

1.2.2 Biosensors and Biochips

A co-assembling binary peptide system featuring the α-to-β molecular switch properties of SAF-p1/p2a could improve the *ex vivo* fabrication and *in vivo* deployment of biosensor devices and biochips (*19*). At present, there is high demand for transducers and tissue-to-sensor interface biomaterials for implanted medical devices that exhibit good

biocompatibility—that is, the materials used must not elicit an inflammatory immune response in the host (*62, 63*). Furthermore, biomimetic materials that are structurally reproducible and amenable to functionalization with covalently-attached biomolecule surface moieties are preferable for the safety and efficacy of interfacial molecular recognition functionality between a biosensor and host tissue (*62-65*). It is challenging to engineer biomaterials that can meet these criteria in a practical manner. However, there is a possibility that α-to-β molecular switch peptide biomaterials could overcome these challenges in certain cases.

The co-assembly of coiled-coil nanofibers at physiological pH is an environmentally-friendly procedure that is simple to control and yields a finely powdered product upon lyophilization. The α-helical nanofiber powder can fill voids down to the micron scale within the biosensor chassis. When humidity is introduced to the interior of the sensor and its temperature rises to that encountered *in vivo* (37 °C), the powder will gradually convert to a flexible and continuous β-sheet network with greater resistance to shear deformation than the coiled-coil architecture (*66*). The structural continuity of the β-sheet structure allows for optical and electrical functionality that would not be possible for an amorphous powder of discrete nanofibers (*67*). Additionally, a β-sheet network of small (<5000 Da) peptides such as those in the SAF family (~3100-3500 Da) carry a low risk of adverse immunogenicity following implantation (*62, 63*). Hence, the approach of manufacturing biosensors using a smart molecular switch similar to SAF-p1/p2a is advantageous by virtue of convenient, finely-controlled fabrication using the coiled-coil nanofibers to ultimately yield a functionalized and resilient β-sheet material.

Possible extensions of this application could involve the integration of photonic and optically-active dopants (e.g. Eu, Tb) with photosensitizers (e.g. salicylic acid; 1,10-phenanthroline) to impart photoluminescent functionality to biosensor components for diagnostic and ophthalmic implants (*67, 68*).

1.2.3 Fusion Peptide Architectures

Fusion peptides—designer peptides decorated with covalently-grafted biomolecules—add an additional dimension to the potential functionality of a molecular-switching peptide co-assembly. Folded proteins could be covalently attached onto one of the component peptides at a surface site (*i.e.* at a Cys-substituted *b*, *c*, or *f* heptad position) prior to co-assembly into coiled-coil nanofibers. The advantage of this approach lies in the improved capacity of co-assembly to precisely control formation of a structurally well-defined and reproducible supramolecular biomaterial with high bioactivity (*63, 65*). Ideally, a well-established protocol for grafting proteins to a smart biomaterial similar to SAF-p1/p2a could lead to advances in a diverse array of fields in biotechnology, from enzymatic biocatalysis in industry (*65, 69*) to molecular recognition-based diagnostics in medicine (*53, 70*). The approach of fusion peptide integration into α-to-β molecular switch biomaterials is notable in that it has the theoretical potential to improve almost any molecular switch developed for either of the two biomedical application categories discussed previously.

1.3 Structural Elucidation of Peptide Assemblies by Solid State NMR

1.3.1 Introduction to Solid State NMR

Solid state nuclear magnetic resonance (NMR) is a powerful technique for structural studies of peptide assembly. Chemically-distinct populations of nuclei with magnetic moments are identified by NMR signal frequency and intensity, and this data is overlaid in two dimensions to create a correlation map of magnetic interactions between these nuclei. The pattern of these correlations is unique for each structure, enabling structural evaluation at a resolution inaccessible to other experimental methods. My work focuses on interpretation of ^{13}C or ^{15}N NMR signals to extract structural information from isotopically-labeled peptide samples. The samples we study are produced by chemical synthesis (*71*) such that they are incorporated with uniformly or selectively labeled amino acids (Figure 5) at specific sequence positions of interest to overcome the limits of NMR signal sensitivity to nuclei with low natural abundances (1% for ^{13}C and 0.4% for ^{15}N).

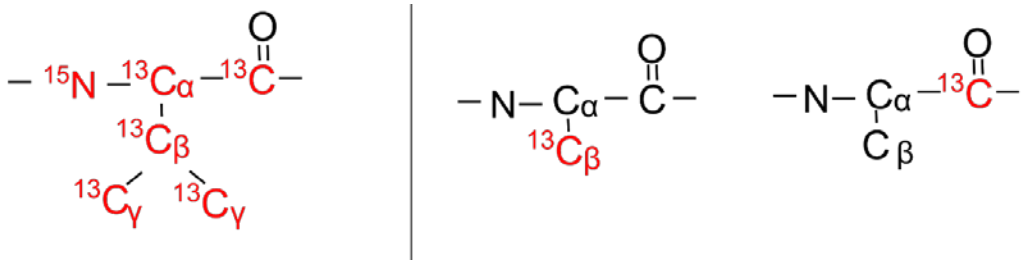

Figure 5: Schematic of **(A)** uniformly ^{13}C-^{15}N labeled valine. **(B)** Selectively ^{13}C labeled alanine, labeled at Cβ or CO

An in-depth treatment of the quantum phenomena and hardware that enable our experiments is beyond the scope of this thesis. However, at its most fundamental level, NMR spectroscopy can be considered a three-step technique: 1) placement of samples into large static magnetic fields (represented by vector $\mathbf{B_0}$ in this work); 2) excitation of nuclear spins (nuclei with magnetic moments) by resonant radio frequency magnetic fields delivered via induction by a coil around the sample; and 3) detection of current induced in the coil by time-dependent nuclear magnetization, which is known as the free induction decay (FID). A schematic of this experimental setup for solid state NMR is shown in Figure 6. The NMR peak (also called the "observable") results from a Fourier Transform of the FID generated from the precession of nuclear magnetization transverse to the plane of $\boldsymbol{B_0}$ following pulses of the applied magnetic field $\boldsymbol{B_1}$. Each nucleus that contributes to the FID has a corresponding peak in the NMR spectrum, which contains all peaks from a 1D NMR experiment. The peak position, known as the chemical shift (CS, units of ppm or Hz), is our primary quantity of interest.

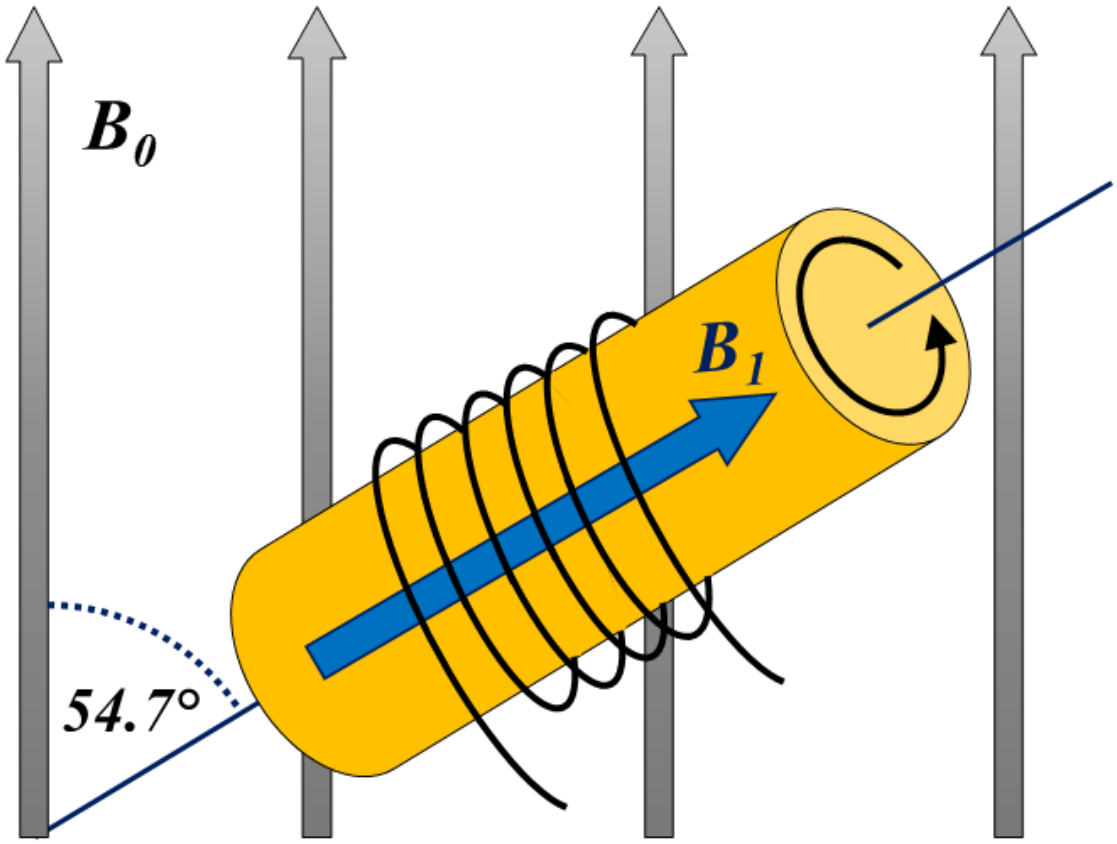

Figure 6: Depiction of sample rotation (colored cylinder) at the magic angle. $\mathbf{B_0}$ is the static magnetic field of the spectrometer, and $\mathbf{B_1}$ is the applied magnetic field generated by radiofrequency pulses delivered through the probe coil.

Some adjustments to the traditional (solution state) setup for NMR are necessary to effectively assess the local electronic environment and secondary structure at sites with magnetically susceptible nuclei in solids. One obstacle to obtaining useful data is the fact that molecular solids do not tumble in space on a sufficiently fast timescale to average out position-dependent inhomogeneities in the magnetic field experienced at each site. The cumulative effect of these local inhomogeneities is a broadening of peaks that results in poor resolution compared to the narrow linewidths obtained in solution state NMR. One technique of critical importance to solid state NMR signal resolution is magic angle

spinning, or MAS (*72*). MAS is the high-frequency (>10 kHz) spinning of the sample about the z-axis at the "magic" angle of 54.7° (Figure 6) to average away some of the peak-broadening inhomogeneities that negatively impact resolution. All NMR experiments reported in this work use MAS to improve resolution. A fundamental practice to improve solid state NMR strength is cross-polarization (CP), which transfers highly abundant ^{1}H magnetization to weakly abundant spins (^{13}C and ^{15}N) (*73, 74*). CP is used in conjunction with MAS to enhance weakly abundant spin signals at an acceptable level of resolution (*75*). To actually observe the FID for the weakly abundant spin nuclei, CP must be followed by a decoupling pulse sequence. Decoupling is the high-power radiofrequency excitation of ^{1}H to eliminate dipolar couplings to ^{13}C or ^{15}N that are not fully removed by MAS (*76, 77*), thereby improving resolution even further than with MAS alone. Decoupling parameters (*e.g.* power levels of ^{1}H excitation pulses) must be optimized for each sample. Pulse patterns and relevant parameters for CP and decoupling will be discussed further in the Methodology section.

1.3.2 Applications to Structural Study of Peptide Assemblies

Solid state NMR is the experimental method of choice for probing the structure of soft matter at an atomic-length scale resolution. Biological amyloid and designer peptide assemblies are insoluble, thus precluding analysis by solution state NMR, and typically do not possess sufficient long-range structural order for characterization by X-ray crystallography (*78*). Computational methods (*79-81*) are often very helpful in predicting peptide assembly structures, especially when used in conjunction with NMR-derived structural constraints (*82-86*), but solid state NMR remains the only experimental means

of testing these predictions at a sufficient level of detail to "close the design loop" for *de novo* systems.

1.3.3 The Problem of Polymorphism

The success of a solid state NMR structural investigation often requires that a sample have only one well-defined molecular structure. The presence of minor structures within a sample creates spectral crowding that complicates data interpretation, sometimes past the point of being able to extract conclusive results. As such, care must be taken to ensure structural homogeneity of the sample during preparation. Because peptide assembly is a complex phenomenon, it can be difficult to prepare a structurally-uniform sample when multiple energetically-favorable assembly pathways exist for a system. The formation of different supramolecular structures by assembly of the same peptide system is called polymorphism, because peptide assemblies with different molecular structures exhibit distinct morphologies (*e.g*. nanofiber width, protofilament core packing geometry) when observed using electron/atomic force microscopy or X-ray diffraction-based techniques. For example, the naturally-occurring amyloidogenic peptides central to the pathology of Alzheimer's disease are known to assemble along multiple energetically similar pathways to distinct amyloid fibril structures (*82, 87, 88*). Amyloidogenic peptides are known to also form non-fibrillar species of distinct secondary structure that have been described as oligomers and protofibrils (*84, 89-91*). There have been fewer studies of assembly pathways for designer peptides, but in the case of SAF-p1/p2a, there is at least one study that examines the oligomeric and protofibril states as they occur on the assembly pathway towards mature fibers (*23*). However, it is important to note that the "oligomeric" and

"protofibril" states of SAF-p1/p2a (and coiled-coils in general) have a common α-helical secondary structure, and are therefore not defined equivalently to those for pathological amyloids (*92*). The Nomenclature contains more general definitions that are applicable to SAF-p1/p2a. A molecular switch peptide system is engineered specifically to exhibit controlled (*i.e.* triggered) polymorphism. Molecular switches can be readily identified by solid state NMR, but the triggering conditions for structural transition must be controlled to maximize structural homogeneity during any single experiment if more detailed structural characterization by NMR is desired. The problem of polymorphism, as it relates to solid state NMR, is that variation of structure at the molecular length scale hinders interpretation of signals originating from the atomic length scale.

1.4 Purpose and Scope of Study

This work started out as an effort to settle conflicting interpretations of the puzzling data for $hSAF_{AAQ}$-p1/p2. Over time, it became clear that further study would be required to do this, and my focus turned then to SAF-p1/p2a. I was ultimately successful in settling the debate concerning $hSAF_{AAQ}$, but I must admit that I owe this success, at least in part, to a serendipitous discovery that none of us expected or imagined to be possible. The structural evaluation of SAF-p1/p2a detailed herein raised at least as many questions as it answered due to an observation of structural dynamics that is, to the best of our knowledge, a first in the scientific community for any binary peptide system of rational design under biologically-benign conditions. The following chapters will present a technical basis for the structural elucidation of the SAF-p1/p2a nanofiber assembly by solid state NMR, the experimental results of this investigation, interpretations thereof, and a discussion of how to proceed in answering the questions that remain.

CHAPTER 2: METHODOLOGY

2.1 Description of Solid State NMR Experiments

2.1.1 ^{1}H-^{13}C CPMAS

As previously discussed, cross-polarization (CP) is an essential experimental technique in solid-state NMR to obtain higher sensitivity for isotopically dilute nuclear spins (*i.e.* weakly abundant relative to ^{1}H), namely ^{13}C or ^{15}N for peptide studies. Figure 7 illustrates the pulse sequence for ^{1}H-^{13}C CP. CP may be used to generate a 1D NMR spectrum in what is called a CPMAS experiment (*75*). For the measurements on rehydrated SAF-p1/p2a, a 110 kHz pulse was initially applied to excite the protons and generate transverse magnetization before more complicated pulse. During the dry sample experiments, an E-free probe (one designed to reduce heating of the sample by radiofrequency pulses) had been installed on the spectrometer and 100 kHz decoupling power was used instead to the same effect. A 2 ms contact time was then applied to allow for polarization transfer from protons to nearby carbons via dipolar interactions. After the cross-polarization transfer, the protons are dipolar decoupled at 110 kHz (or 100 kHz for the E-free probe) while the carbon FID is observed. The CPMAS pulse sequence is used to obtain a 1D NMR spectrum, giving an indication of structural order and insight into secondary structure. This simple sequence was also used to optimize hydrogen and carbon pulse power levels for the 2D NMR ^{13}C-^{13}C experiments described subsequently.

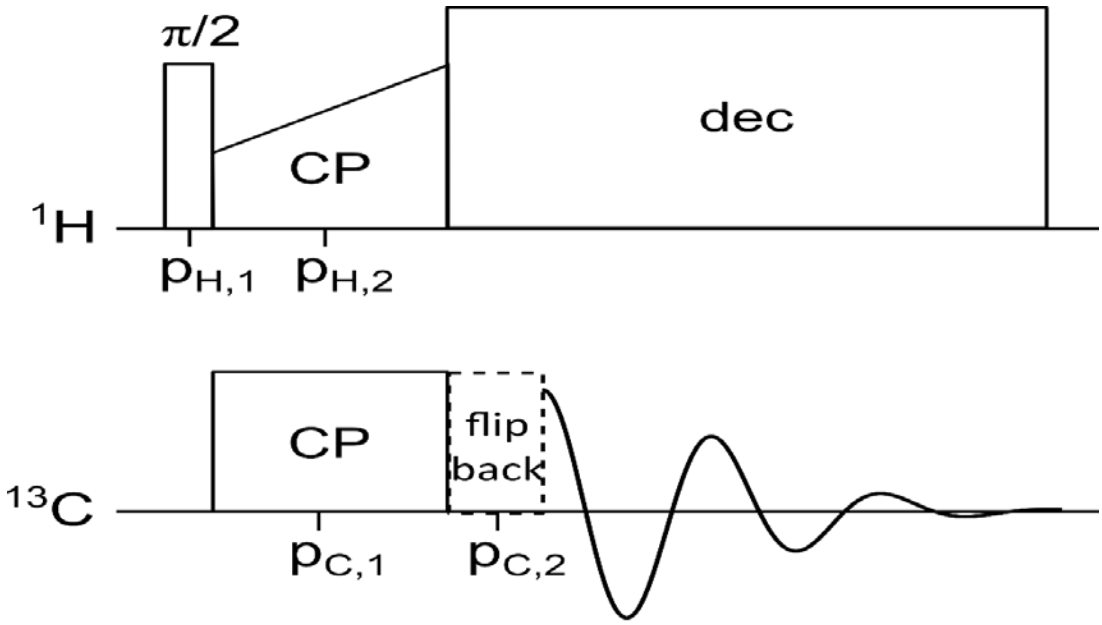

Figure 7: The ^{1}H-^{13}C CPMAS pulse sequence.

2.1.2 ^{13}C-^{13}C fpRFDR

The finite pulse radiofrequency-driven recoupling (fpRFDR) pulse sequence shown in Figure 8 was used to obtain 2D ^{13}C-^{13}C chemical shift correlation NMR data. This sequence was developed to consider the non-negligibility of the time elapsed over an applied pulse width at the timescale of sample rotation under fast MAS (*76, 93, 94*). To work around this complication, the fpRFDR sequence instead accounts for finite pulse lengths, hence its name. Similar to the CPMAS experiment, fpRFDR utilizes cross-polarization at the beginning of the sequence to prepare the ^{13}C transverse magnetization. Following the chemical shift evolution period t_1, the dipolar couplings are refocused in the transverse plane, and a rotor-synchronized π-pulse fusillade is used to restore ^{13}C-^{13}C dipolar couplings to enhance spin exchange during the rotational period (τ_r) of the sample at high-

speed MAS conditions. A final refocusing pulse is applied, and the carbon FID is observed during the acquisition period τ_2 (spin-spin relaxation time). The value of t_1 determines the coupled spin resonance frequencies that contribute to the FID observed during τ_2 for a single iteration of the pulse sequence (*i.e.* a single scan). Many scans (*e.g.* 64 scans) are performed per t_1 value to improve signal-to-noise for each 1D experiment included in the 2D data set. Varying t_1 will result in a different FID, effectively creating a new 1D experiment to contribute to the data set. By consecutively scanning at many values of t_1 (typically, 350 or more t_1 values), as many 1D spectra contribute to the data set, which ultimately takes the form of a ^{13}C-^{13}C 2D exchange spectrum. Using this 2D spectrum, precise peak assignments can be made using statistical correlations between ^{13}C isotropic chemical shift and molecular conformation. This is the preferred method of assigning ^{13}C chemical shifts in our lab due to its high resolution and low propensity for spectral overlap (*84, 95*), as fpRFDR typically only reports on single-bond transfer correlations (*e.g.*, between ^{13}C labeled C_α and C_β sites). These properties result from the high spinning speeds used (22 kHz for my study) and the very short mixing time for polarization transfer (τ_r = 1.28 ms for my study) (*93, 94*).

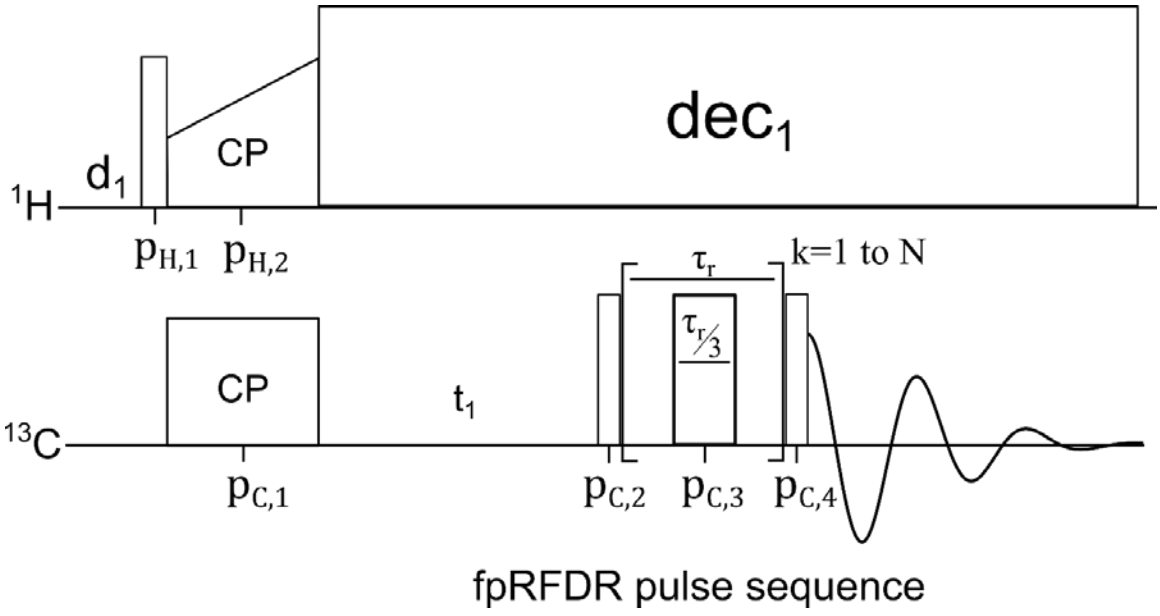

Figure 8: The finite pulse radio frequency driven recoupling (fpRFDR) pulse sequence.

Chemical shift assignments made by fpRFDR may be used to calculate secondary chemical shifts (Δ CS), which are reported as the difference in chemical shift values for a nucleus in the sample and the same nucleus on the same amino acid for the corresponding random coil peptide (*96, 97*). Analysis of Δ CS for ^{13}C atoms near the peptide backbone (carbonyl, C_α, C_β) has been used to assess secondary structure (*98, 99*). In addition, comparisons of crosspeak positions and line shapes have been used as a basis for evaluating structural variation between different samples (*100-102*). Simulated (generic) fpRFDR assignment pathways for the α-helical and β-sheet configurations of isoleucine are given in Figure 9 for comparison.

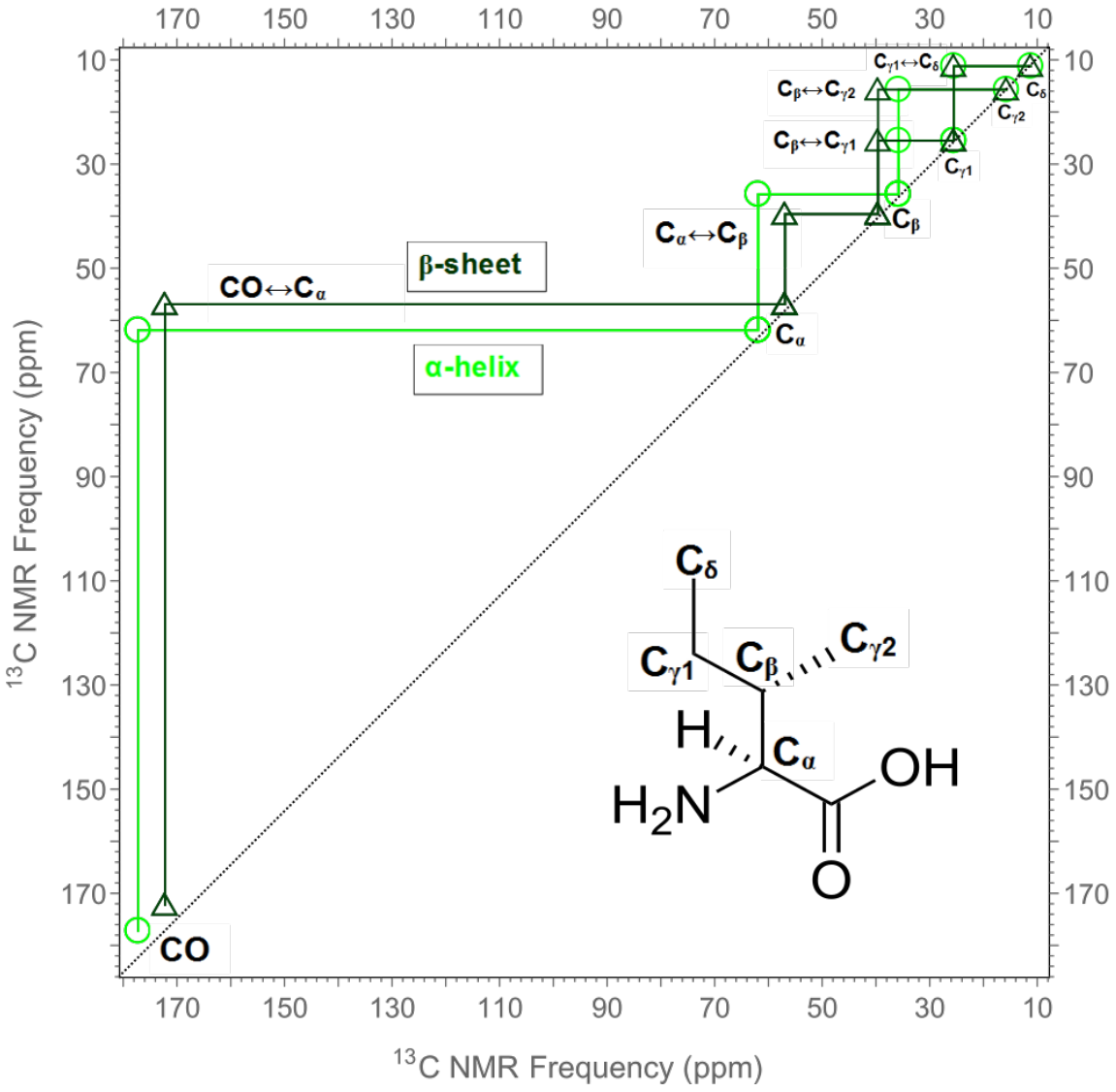

Figure 9: Simulated fpRFDR assignment pathways for a uniformly ^{13}C-labeled isoleucine residue incorporated within α-helix (light green) or β-sheet (dark green) secondary structure.

2.1.3 ^{13}C-^{13}C DARR

The dipolar-assisted rotational resonance (DARR) experiment (*103*) produces a ^{13}C-^{13}C 2D exchange spectrum similar to the 2D fpRFDR experiment, but without the need for high power ^{1}H decoupling during the mixing period. Consequently, the experiment can be performed with a wider range of possible mixing times. At mixing times of ~20 ms or less, 2D DARR spectra exhibit crosspeaks that correspond mostly to ^{13}C atoms within a single amino acid. As mixing times are increased to 50-100 ms, additional crosspeaks can be observed that correspond to amino acids that are adjacent in the primary structure. With mixing times at 500 ms or above, crosspeaks include those that report on amino acids that are brought together by the molecular fold within an effective range of about ~0.6 nm (*95*, *104*). The DARR pulse sequence is shown in Figure 10.

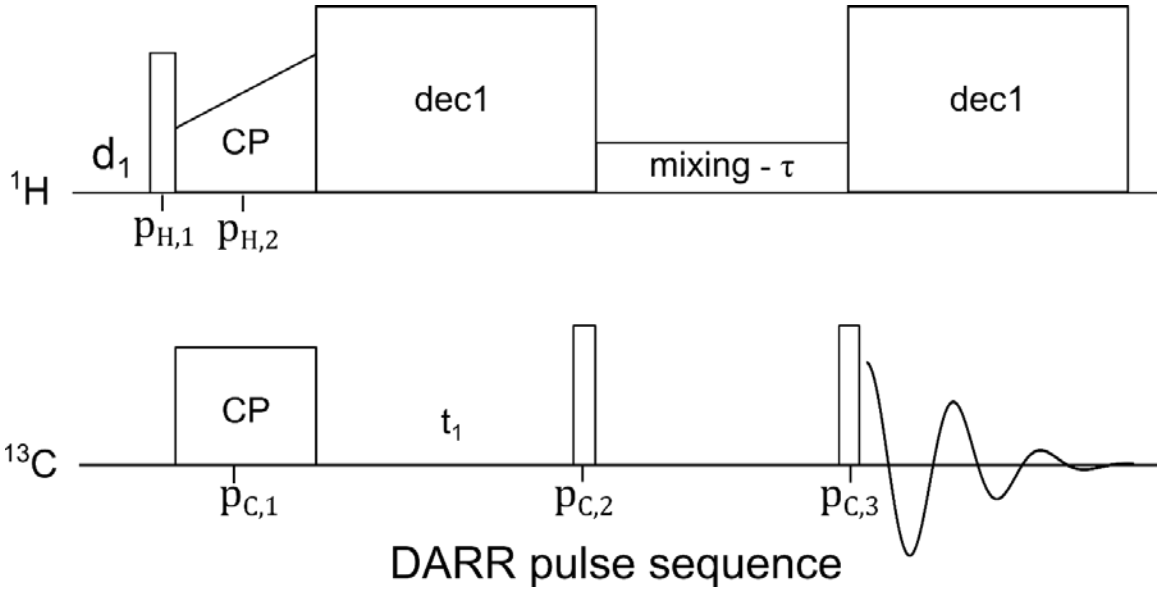

Figure 10: The Dipolar Assisted Rotational Resonance (DARR) pulse sequence.

At longer mixing times, crosspeak patterns in 2D DARR spectra can become crowded, as was the case for the SAF-p1/p2a DARR spectra. Concerns about spectral overlap with spinning sidebands are relevant to 2D DARR spectra, such that the MAS rate must be chosen to avoid interference of observable signals by spinning sidebands. Crosspeaks corresponding to longer distances (above ~0.5 nm) are also more difficult to detect when MAS speeds are too fast (above ~20 kHz; MAS rates of 10 kHz and 11 kHz were used for the DARR experiments reported here).

The DARR sequence shown in Figure 10 was used to observe long-range ^{13}C-^{13}C couplings in SAF-p1/p2a, specifically to probe through-space couplings in both the dry and rehydrated samples. For the rehydrated sample, DARR was applied at different mixing times to help distinguish between through-bond correlations in the spin system of each labeled residue (obtained through short-mixing DARR) and through-space couplings (obtained through long-mixing time DARR) in the overlaid spectra. Following the transfer of polarization from the excited protons to carbon, a period of t_1 passes for chemical shift evolution—as with fpRFDR, this t_1 value is varied between scanning sets to facilitate construction of a 2D NMR spectrum. Following t_1, magnetization is flipped about the transverse plane by a second pulse and undergoes spin exchange during the mixing time, τ_m. A final refocusing pulse is applied, and the carbon FID can be observed during τ_m (*103*). The ^1H radio frequency decoupling field amplitude is set equal to the spinning speed during both t_1 and τ_2.

2.2 Experimental Design

2.2.1 Choice of Isotopic Labeling Scheme

SAF-p1 K6L12 and SAF-p2a E15I23 were selected for isotopic enrichment to test Woolfson and coworkers' hypothesized alignment of heptad core positions *a* and *d* upon mixing, and also to test for the presence of the stabilizing electrostatic interaction between heptad overhang positions *e* and *g*. Specifically, my proposed labeling scheme was intended to allow the conclusive determination of the existence and local secondary structure of the SAF-p1 L12/SAF-p2a I23 hydrophobic core interaction and the SAF-p1 K6/SAF-p2a E15 salt bridge at its proximal overhang position. This particular labeling scheme also allows for a direct comparison to previous work on $hSAF_{AAQ}$-p1/p2, excepting the A4 residue in $hSAF_{AAQ}$-p2, which is not conserved in the SAF-p2a sequence. It is also worth noting that all four labeled residues are conserved in sequence amongst all sticky-ended heterodimer-forming variants of SAF, and are posited in the literature to interact as described previously (*22, 24-26, 29-32*). Chemical shift assignments reporting on local secondary structure at labeled residues of lyophilized and minimally rehydrated (1 μL/mg) SAF-p1/p2a nanofibers from ^{13}C-^{13}C fpRFDR experiments will enable sidechain co-proximity determination by DARR performed at short (50 ms) and long (500 ms) mixing times. SAF-p1/p2a nanofibers with this isotopic labeling scheme will display DARR off-diagonal crosspeaks between residues SAF-p1 K6 and SAF-p2 E15 and also between SAF-p1 L12 and SAF-p2 I23 if they co-assemble according to Woolfson's design hypothesis (*23, 31*).

2.2.2 Choice of Assembly Conditions and Staining for TEM

TEM images were collected of matured ($t_{assembly}$ = 24 hr) and propagating ($t_{assembly}$ < 24 hr) SAF-p1/p2a fibers from assemblies in 10 mM MOPS (3-*N*-morpholino-propanesulfonic acid), 200 mM MOPS, and ultra-pure water (UPW). Fibers were stained separately using 1% uranyl acetate (UA) and 1% phosphotungstenic acid (PTA) to identify stain-selective observability of topological features (*i.e.* striation patterns in the seminal literature for SAF-p1/p2a). During previous side-by-side assemblies using 10 mM MOPS and UPW, it was observed that the SAF/MOPS solution would always become turbid before the SAF/UPW solution by a margin of hours. The assembly media buffer concentration was varied for TEM to determine if the co-assembly of SAF-p1/p2a into its signature unbranched fiber morphology depended on the presence of MOPS, and if so, whether it was sensitive to the buffer concentration.

2.3 Procedures

2.3.1 Synthesis, Assembly, and Rehydration of SAF Nanofibers

Peptide Synthesis:

SAF-p1 and SAF-p2a were synthesized by CPC Scientific, Inc. (Sunnyvale, CA) using uniformly ^{13}C-^{15}N labeled amino acids from our inventory that were purchased from Cambridge Isotope Laboratories, Inc. Peptides were supplied at >90% purity as determined by reverse-phase high performance liquid chromatography (RP-HPLC). The molecular weights of SAF-p1 and SAF-p2a were measured to be 3188.6 g/mol and 3337.9 g/mol, respectively, by electrospray ionization-assisted mass spectrometry (ESI+). Documentation of chemical analysis was provided by CPC Scientific and can be found in Appendix A, Figure 25A-F.

$hSAF_{AAQ}$-p1 and $hSAF_{AAQ}$-p2 were synthesized in-house by Sarah Leonard at Florida State University. Peptides were synthesized following standard fluorenylmethylcarbonyl (Fmoc) synthesis procedures (*71*) using an Applied Biosystems Model 433A Peptide Synthesizer with HBTU/HoBt activation. Fmoc-protected amino acids were purchased from Anaspec. After recovering the product from the peptide synthesizer, Sarah purified her peptides using RP-HPLC and verified their molecular weights using matrix-assisted laser desorption ionization-time of flight mass spectrometry (MALDI-TOF).

For both SAF-p1/p2a and $hSAF_{AAQ}$-p1/p2, samples were stored with desiccant at -40 °C until ready for assembly.

Assembly of SAF-p1/p2a Nanofibers:

The method described by Bromley and Woolfson *et al. (23)* was followed for SAF-p1/p2a nanofiber assembly. Pre-made 0.2 M MOPS (Alfa Aesar) at pH 7.4 was diluted to 10 mM with pure water, and the labeled SAF-p1 (19.3 mg) and SAF-p2a (20.1 mg) were each made into 30 mL stocks of 200 µM each such that, when mixed together, they would form 60 mL of assembly media at a concentration of 100 µM in each peptide. The media volume was spread out between four 15 mL centrifuge tubes and for the first 5-10 min after mixing, the tubes were left on ice to prevent the seeding of any kinetically-trapped minor structures. The tubes were then taken off ice and allowed to sit for 24 hours at room temperature to allow the fibers to mature. After 24 hours, the tubes were centrifuged at 18,000 rpm for 15 minutes to spin down the SAF-p1/p2a nanofibers. The sample was then frozen in liquid nitrogen, lyophilized overnight, and stored at -40°C until being packed in a rotor for experimentation.

Although there was not a DI H_2O rinse step to remove residual MOPS prior to lyophilization, the supernatant was lyophilized to estimate an upper bound of 9.5 mg MOPS incorporated into the sample. The SAF-p1/p2a nanofibers were then recovered at a minimum 58.6% yield (23.1 mg SAF-p1/p2a).

Rehydration of the SAF-p1/p2a nanofibers was performed using 1 µL ultra-pure water (UPW) per mg material. An additional 10 µL UPW was added one week after initial

rehydration because ^{1}H spectra collected following the 50 ms and 500 ms DARR experiments exhibited drastically reduced water peaks (Appendix A.2, Figure 26).

Assembly of $hSAF_{AAQ}$-p1/p2 Nanofibers

Co-assembled $hSAF_{AAQ}$-p1/p2 samples (1649 μM in total peptide, 824 μM in each component) were produced using equal volumes of fresh $hSAF_{AAQ}$-p1 (5 mg/mL) and $hSAF_{AAQ}$-p2 (5 mg/mL) stock solutions prepared in DI H_2O. The choice of DI H_2O (rather than 10 mM MOPS) for the assembly media was deemed necessary to enable recovery of the sample after centrifugation. Samples were self-assembled for 24 hours, frozen in liquid nitrogen, and then lyophilized overnight. To study the individual components, $hSAF_{AAQ}$-p1 and $hSAF_{AAQ}$-p2 were freshly prepared at 5 mg/mL in DI H_2O. After 3 hours they were frozen in liquid nitrogen and lyophilized overnight.

2.3.2 TEM Sample Preparation and Image Processing

Transmission Electron Microscopy (TEM) imaging performed at the Robert P. Apkarian Integrated Microscopy Core at Emory University on a Hitachi HT-7700 electron microscope at an accelerating voltage of 80 keV. Unlabeled SAF-p1/p2a assemblies were performed at concentrations of 100 μM (in each peptide) in either UPW (VWR, Inc.) or low-endotoxin MOPS (supplied at pH 7.4 by Alfa Aesar) at buffer concentration of either 10 mM or 0.2 M (twenty-fold buffer excess). Duplicate 5 μL aliquots of assembly media were taken at approximately 3 h, 6 h, 18 h, and 24 h of elapsed assembly time; these were

placed on lacey carbon-coated 400-mesh copper specimen grids (Ted Pella, Inc.) and allowed to sit for two minutes before moisture was wicked away with filter paper and grids were rinsed with 5 µL of UPW for 1 minute and wicked again prior to staining. One of each duplicate aliquot was stained with 1 wt% UA from our inventory; the other was stained with 1 wt% PTA, kindly provided by Yeongseon Jang of the Champion lab. Both stains were allowed to sit for 1 min and then wicked dry before storing the grids.

Striation periodicity was calculated by averaging 15 measurements made on 3 high-magnification (120k) TEM images using contrast filtering and a pixel ruler referenced to the 100-nm scale bar in Inkscape v. 0.91 (Free Software Foundation, Inc.) .

2.3.3 Solid State NMR Experimental Timeline and Setup

All solid state NMR experiments were performed on a Bruker DRX 500 MHz narrow-bore spectrometer and processed using Bruker TopSpin 3.5 at the Georgia Institute of Technology NMR Center. Dry samples in a single-tipped zirconia rotor (Bruker) were pulsed using an E-free 3.2 mm HCN triple-resonance probe at spinning speeds of 22 kHz (fpRFDR), 10 kHz (DARR, lyophilized sample). The rehydrated sample was pulsed using a 3.2mm HX dual-resonance probe at spinning speeds of 22 kHZ (fpRFDR) or 11 kHz (DARR, rehydrated sample) on the same spectrometer. Processed data sets were analyzed using Wolfram Mathematica version 11.0 code developed in-house by Anant Paravastu and coworkers.

Choice of MAS speed was important for the 2D NMR experiments. Atomic sites with large anisotropies (orientation dependences) in chemical shift (large line widths without MAS) exhibit spinning sidebands under MAS. Spinning sidebands occur at frequencies of the primary NMR peak plus and minus the sample rotation rates, converted on the Hz-to-ppm scale. It was desirable to push spinning sidebands originating from the carbonyl region (170-185 ppm) to ~100 ppm, where the spinning sidebands could not interfere with any signals from labeled ^{13}C sites. In choosing a spinning speed, it was important to consider the fact that polarization transfer efficiencies for recoupling methods used during mixing periods are highly dependent on MAS speed for the 2D NMR experiments presented here. For the fpRFDR experiment, which has a very short (<2 ms) mixing period, it is optimal to acquire data at the highest spinning speed attainable that does not risk damage to the spectrometer (*94*). A MAS rate of 22 kHz was found to be optimal for fpRFDR. For DARR experiments, which have longer mixing periods (in my case, τ_m of 50 ms and 500 ms), polarization transfer is optimal at a low MAS rate that still returns an acceptable level of resolution (*103*). For the dry SAF-p1/p2a DARR at τ_m = 500 ms, a MAS rate of 10 kHz was used, but this setting yielded poor spectral resolution, so the MAS rate was increased to 11 kHz for DARR experiments with the rehydrated sample.

2.3.4 Molecular Modeling

Virtual Molecular Dynamics (VMD version 1.0.9) software (*105*) was used to render models for SAF-p1/p2a. Importing the two component peptides into one VMD file for

heterodimer modeling was done using in-house Mathematica code for heterodimer fibrillogenesis simulation developed by Maxwell Zimmerman and operated by Chris Elliott. Coordinate positioning and image rendering for the heterodimer and protofibril models of SAF-p1/p2a in VMD was done by Cameron Black. A Nanoscale Molecular Dynamics (NAMD) simulation (*79*) is currently in progress to optimize the 3D positioning of the SAF-p1/p2a components according to distance constraints derived from DARR results.

$hSAF_{AAQ}$-p1/p2 nanofibers were modeled by Maxwell Zimmerman using VMD and NAMD. For the NAMD simulation, the $hSAF_{AAQ}$-p1 and $hSAF_{AAQ}$-p2 components were loaded into the same simulation and solvated in a waterbox at 310 K as the initial condition. Energy minimization was performed for 10 ps simulation time; a total simulation time of 4 ns was used to position the molecules. The NAMD output was sent to VMD for final image rendering.

CHAPTER 3: RESULTS AND DISCUSSION

3.1 Transmission Electron Microscopy

TEM imaging confirmed successful reproduction of SAF-p1/p2a fibers, with striations clearly visible in assemblies from 10 mM MOPS and stained by 1% uranyl acetate (UA). These striations (Figure 11) are detectable at or below $t_{assembly}$= 18 hours, and match those published in the Woolfson lab literature for SAF-p1/p2a (*23, 30*).

TEM of SAF-p1/p2a assembled at 10 mM MOPS confirmed the successful reproduction of highly ordered, unbranched nanofibers, comprised of densely-packed protofibrils, featuring a smooth surface morphology and, for samples stained with uranyl acetate (UA), striation patterns matching those reported in literature for SAF-p1/p2a (*23, 30*).This light-to-dark striation pattern repeats ~2.5 times per 10 nm fiber length, consistent with two ~4.2 nm lengths of a 28-residue coiled-coil helix [*i.e.*, 28 * 0.148 nm = 4.144 nm, where 0.148 nm is the rise per residue in a coiled coil (*34*).

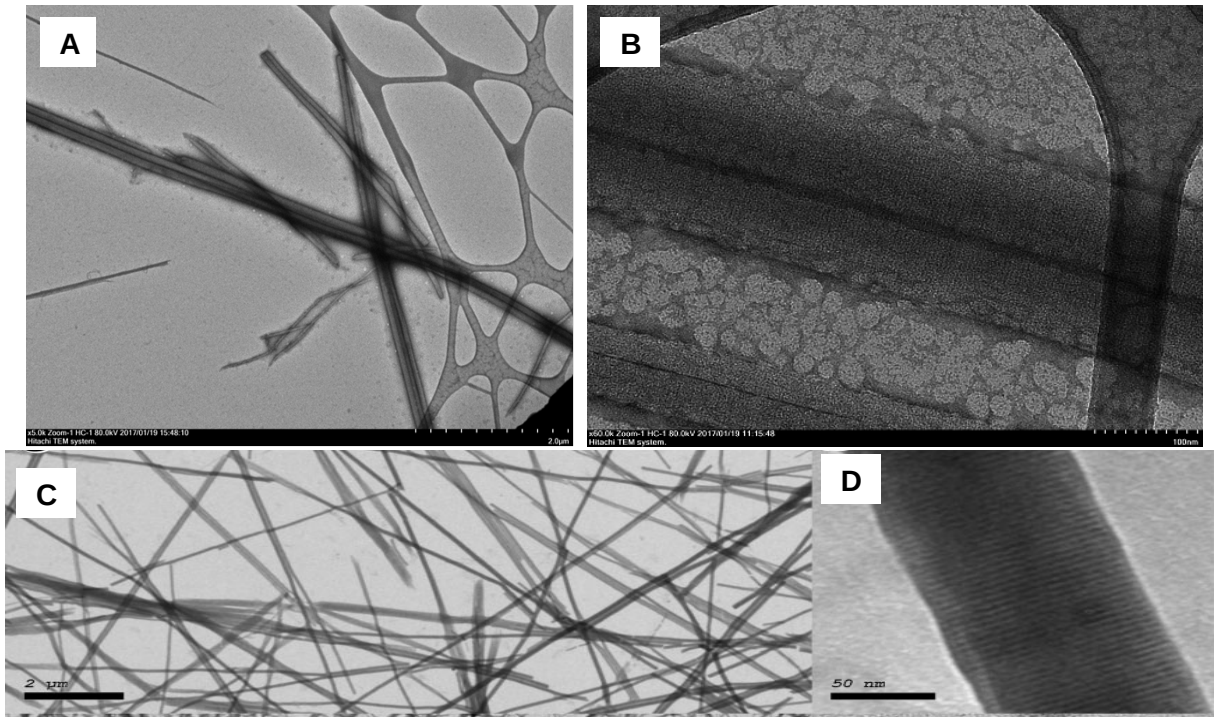

Figure 11: TEM of SAF-p1/p2a assembled for this study from 10 mM MOPS at magnification of **(A)** 5k, scale bar 2 µm, and **(B)** 60k, scale bar 100nm, with striations visible. Bottom row images are TEM of SAF-p1/p2a published by Smith, Woolfson *et. al.*, 2006 (*30*) scale bars are **(C)** 2 µm and **(D)** 50 nm, with striations visible.

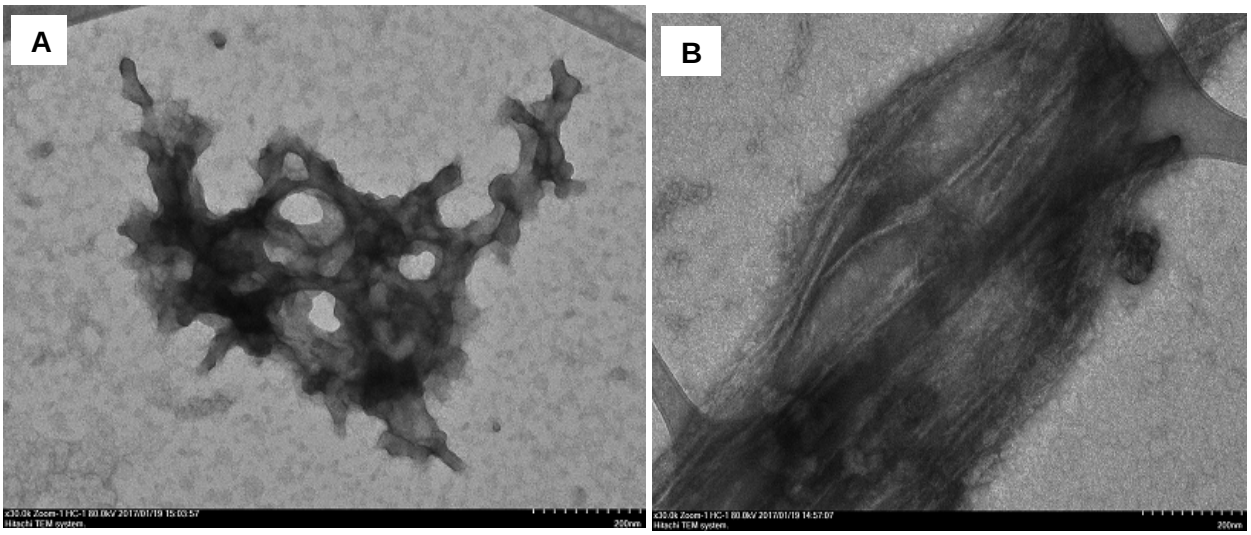

Figure 12: TEM of SAF-p1/p2a assembled from pure water and stained with PTA. **(A)** Mature SAF-p1/p2a conglomerate and **(B)** loose-bundled protofibril core. Both images are at 30k magnification; scale bars are 200 nm.

In contrast, TEM images of SAF-p1/p2a assemblies from ultrapure water (UPW) show conglomerations of highly-branched nanofibers with loose-packed protofibril cores and a lumpy surface morphology (Figure 12). Interestingly, a comparable degree of branching and lumpiness was observed in TEM images of SAF-p1/p2a assemblies from a twenty-fold excess (200 mM) of MOPS (Figure 13), although these images do not include any visible protofibrils that could allow for a qualitative-comparison of core packing densities. Of the three assembly conditions studied, only 10 mM MOPS (the buffer and concentration used in all of Woolfson's reports on SAF-p1/p2a) facilitated assembly of nanofibers capable of displaying striations, and these striations were only visible after staining with UA.

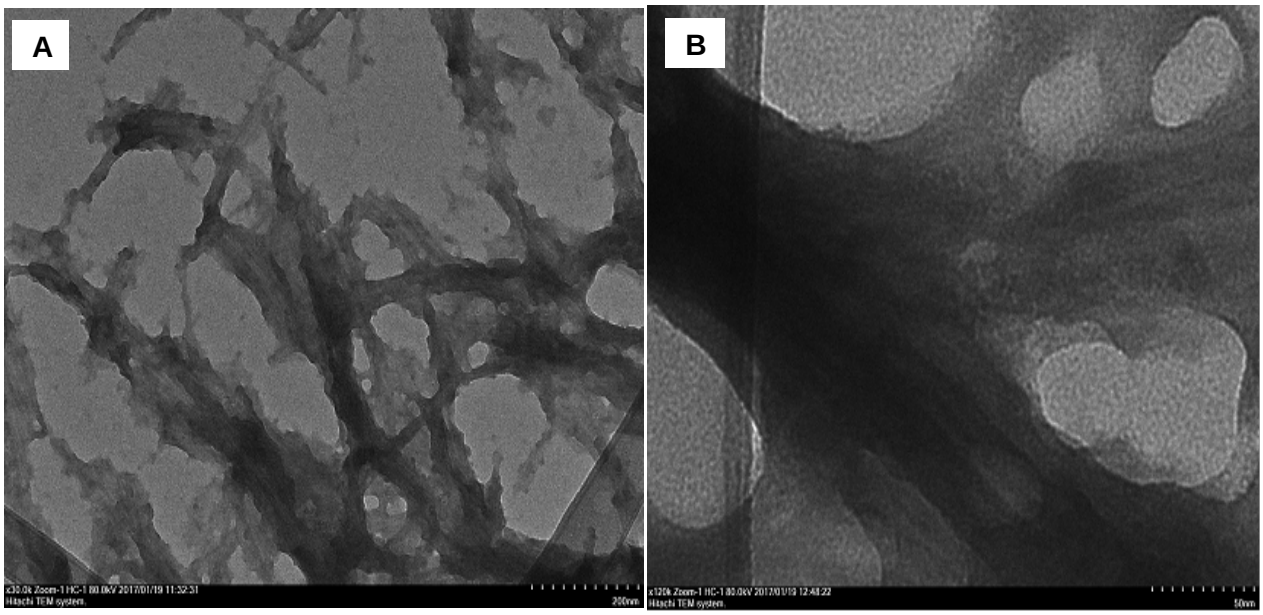

Figure 13: TEM of SAF-p1/p2a assembled from 200 mM MOPS and stained with UA. **(A)** Mature SAF-p1/p2a branched fibers, imaged at 30k magnification, 200 nm scale bar shown. **(B)** A branching fiber nexus, imaged at 120k magnification, 50 nm scale bar shown.

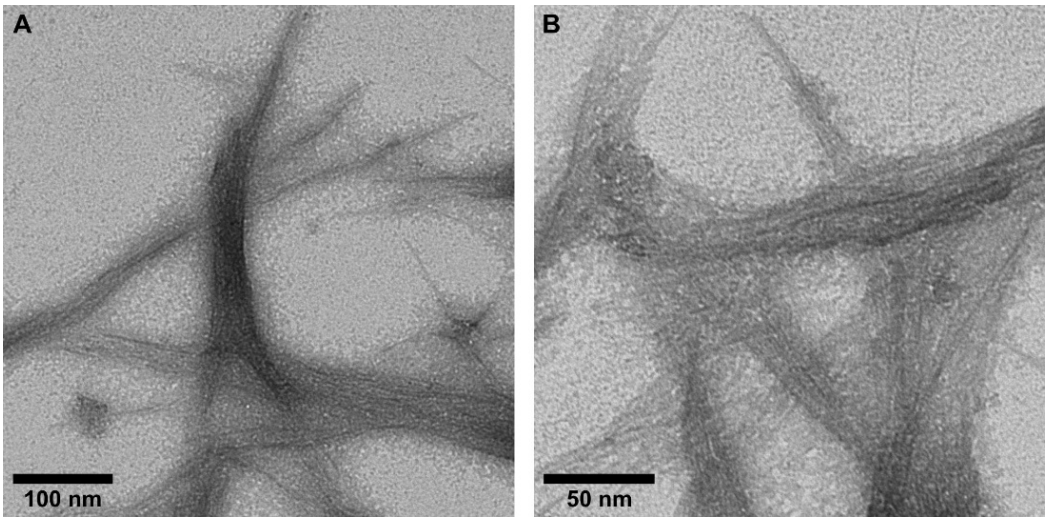

Figure 14: TEM images of **(A)** freshly prepared $hSAF_{AAQ}$-p1/p2 nanofibers deposited on the TEM grid immediately after mixing the individual components and **(B)** freshly prepared $hSAF_{AAQ}$-p1 deposited on the TEM grid immediately after solvating in H2O at 5 mg/mL. Imaged by Sarah R. Leonard, 2014.

TEM images of $hSAF_{AAQ}$-p1/p2 and self-assembled $hSAF_{AAQ}$-p1 (Figure 14) show significantly thicker nanofibers than the ~2 nm $hSAF_{AAQ}$-p1/p2 nanofibers (Figure 3) reported by Woolfson and coworkers (*25*). However, the protofibrils bundled within the fibers in Figure 14 appear to match the anticipated ~2 nm fiber width. A particularly interesting result is pictured in Figure 14B, which shows a cluster of fibers formed by self-assembly of $hSAF_{AAQ}$-p1. Unlike other variants of SAF, at least one component of the $hSAF_{AAQ}$ analogue is evidently capable of standalone self-assembly. This result gives credence to the hypothesized presence of at least one minor structure population in the $hSAF_{AAQ}$-p1/p2 sample used for solid state NMR structural analysis.

3.2 Solid State NMR Spectroscopy

3.2.1 ^{1}H-^{13}C CPMAS

A 1D CPMAS spectrum was acquired following lyophilization of the SAF-p1/p2a nanofibers. Additional CPMAS spectra were collected before and after each 2D NMR experiment, beginning 4 days after rehydration and ending 8 days after rehydration. The water content of the sample was monitored by collecting ^{1}H spectra before and after each experiment during this time; an additional aliquot of 1 mL water/mg sample was added after the water peak of the ^{1}H spectra fell to an unusually low intensity (Appendix A.2 Figure 26C). Figure 15 shows the ^{1}H-^{13}C CPMAS spectra for the dry sample, spectra collected ~4 days after initial hydration, and ~36 hours after the supplemental water was added (8 days after initial rehydration).

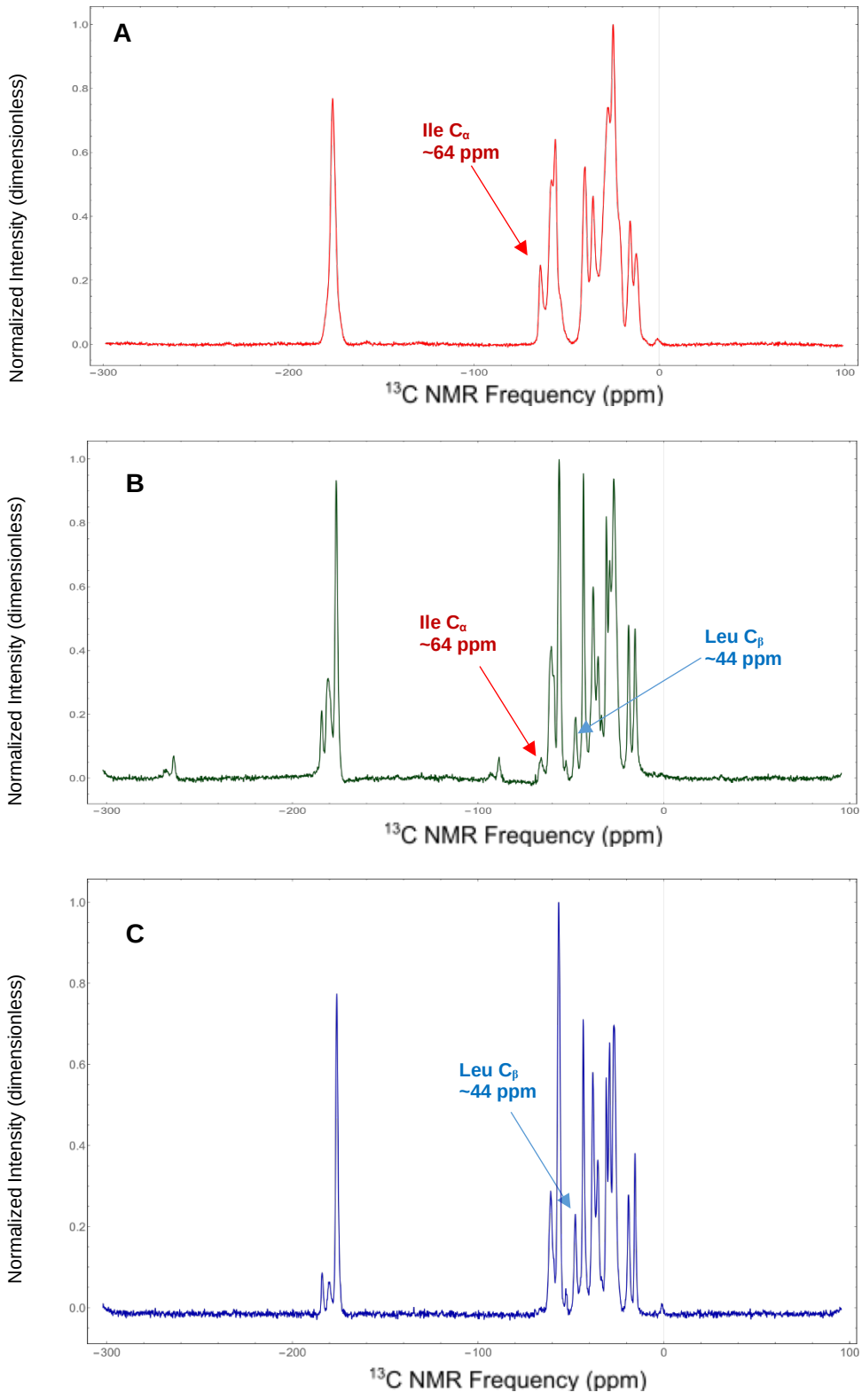

Figure 15: CPMAS Spectra of SAF-p1/p2a nanofibers **(A)** freshly lyophilized **(B)** 4 days after minimal rehydration and **(C)** 36 hours after supplementary rehydration (8 days after initial rehydration).

Inspection of the CPMAS spectra reveals evidence of a time-dependent structural transition. For typical solid peptide samples (*i.e.* those that do not undergo hydration-triggered structural conversions), peaks will sharpen following rehydration, but "new" peaks that appear are actually due to improved resolution afforded by the molecular motion of water in the sample. In other words, most peptide samples analyzed by this methodology only show signals that were already present (albeit weakly resolved) in the dry sample following rehydration. SAF-p1/p2a does not conform to this trend. Following rehydration of the lyophilized SAF-p1/p2a, characteristic α-helical chemical shift signals (*106*) of the labeled alpha carbons and backbone carbonyl carbons gradually disappear from the spectra altogether, shifting upfield (*i.e.* lower ppm value) to peak positions characteristic of a β-sheet secondary structure. An example highlighted to illustrate this phenomenon in the CPMAS spectra (Figure 15A-B) is the SAF-p2a I23 C_α signal, which migrates from ~64 ppm to 54.5 ppm over the course of 8 days following rehydration. In turn, peaks that were not present in the dry sample materialize in the region of characteristic β-sheet C_β chemical shifts following rehydration. The SAF-p1 L12 C_β peak is a clear example of this in Figure 15B-C, as it fills the gap in signal observed around ~44 ppm in the CPMAS spectrum of the dry sample.

3.2.2 ^{13}C-^{13}C fpRFDR

fpRFDR of Dry SAF-p1/p2a Nanofibers

For the dry sample, fpRFDR chemical shift assignments of the backbone and beta carbons (Figure 16) confirm that the assembled nanofibers are indeed α-helical. Large downfield (*i.e.* higher ppm value) Δ CS of all four alpha carbons, accompanied by smaller (but statistically significant) upfield Δ CS of their carbonyl and beta carbons, unambiguously identify the lyophilized SAF-p1/p2a nanofibers as helical in secondary structure (*98, 106*). This finding supports the realization of a coiled-coil assembly as intended by design.

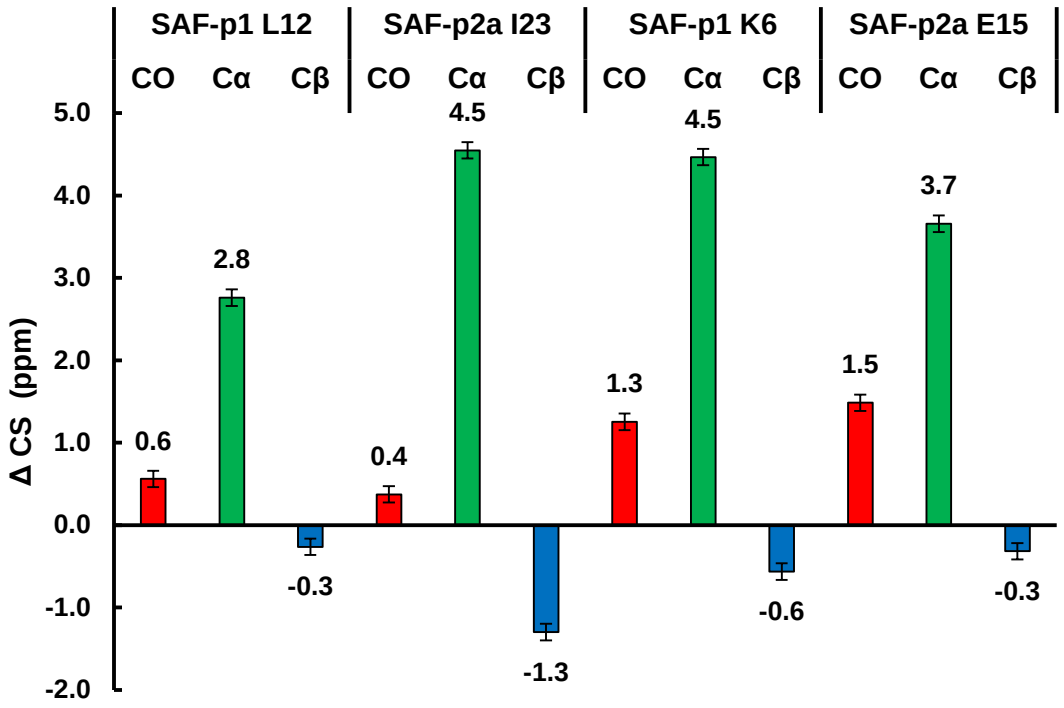

Figure 16: Secondary chemical shifts of labeled backbone CO (red), C_α (green), and C_β (blue) derived from fpRFDR of lyophilized SAF-p1/p2a nanofibers.

Sidechain carbon Δ CS from fpRFDR assignments (Figure 17) are not typically observed in peptide assemblies, because the sidechain atoms beyond C_β are not systematically compelled to experience a Δ CS by supramolecular secondary structure. However, the orientation of sidechain carbons are anisotropic in nature for solid samples (*98*), meaning that a given sidechain carbon is sensitive to local secondary structure about its sidechain. Hence, the significant Δ CS observed in SAF-p2a for the E15 and I23 sidechain carbons indicate that they are in an atypical local conformation relative to their random-coil structural state (*107*), although neither the specific nature of this conformational perturbation nor its relationship to the leucine zipper or salt bridge design motifs may be conclusively determined from Δ CS data alone. However, it is notable that the K6 C_ε does not show signs of shielding effects (upfield shift) from the increased electron density on the adjacent terminal amine that would be expected from a charge interaction with the E15 sidechain carboxyl group.

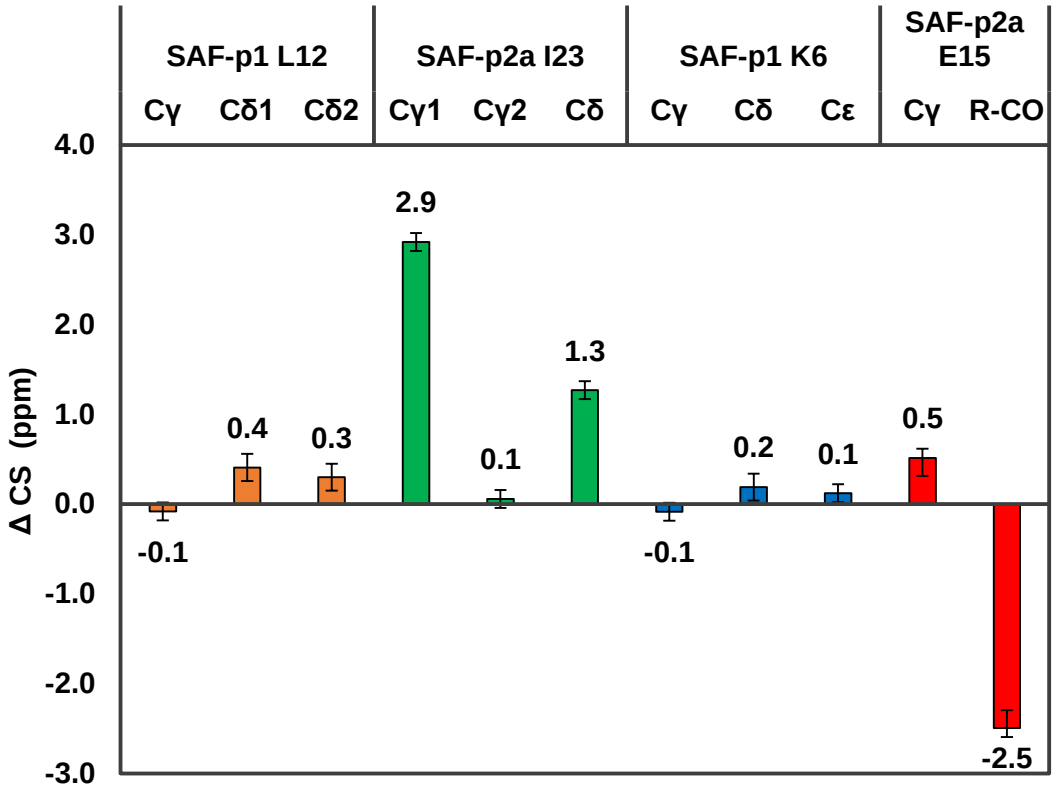

Figure 17: Secondary chemical shifts of labeled sidechain carbons assigned by fpRFDR of lyophilized SAF-p1/p2a nanofibers.

The fpRFDR spectrum of the dry sample suffers from poor resolution (Appendix B.1 Figure 27A), which complicates assignment of chemical shifts for crosspeaks near the diagonal, but this is not atypical for solid state NMR of lyophilized peptides. The α-helical structure population is large enough that the signal-averaged peak positions found by 2D Gaussian fitting can be considered accurate for the sample as a whole. However, the presence of minor structures in the dry sample cannot be ruled out entirely. In low-resolution spectra, minor signals can blend in with broad peaks from the major signals. Subsequent observation of the sample undergoing a structural conversion upon rehydration implies that the presence of an energetically-favored minor structure population is likely to exist in the dry sample.

fpRFDR of Rehydrated SAF-p1/p2a Nanofibers

The 2D fpRFDR spectrum of the minimally rehydrated sample (Appendix B.1 Figure 27B) shows the opposite trend in secondary structural population distribution from the dry sample. All labeled backbone and beta carbon Δ CS switch sign from their dry sample values (Figure 18), uniformly exhibiting the trend of strong upfield carbonyl carbon Δ CS, moderate upfield C_α Δ CS, and strong downfield C_β Δ CS characteristic of a β-sheet assembly (*98*).

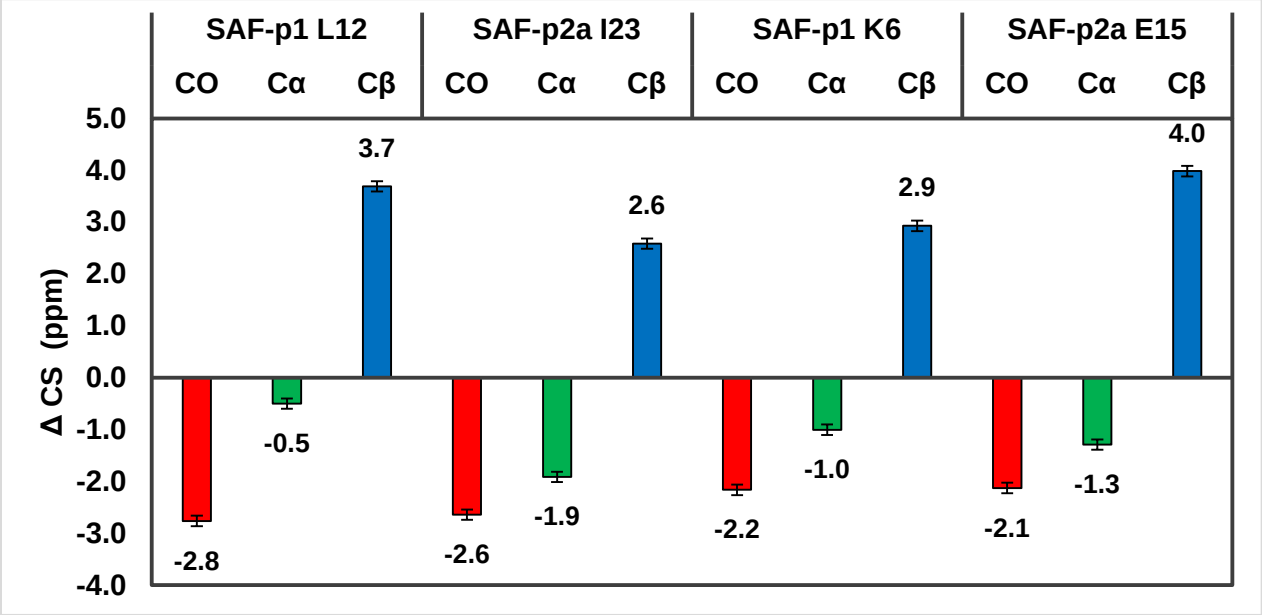

Figure 18: Secondary chemical shifts of labeled backbone CO (red), C_α (green), and C_β (blue) derived from fpRFDR of rehydrated SAF-p1/p2a.

Significant sidechain carbon Δ CS in the rehydrated sample (Figure 19) are more numerous, but on average less intense, than those observed in the dry sample. Again, this observation identifies perturbations in the local secondary structure of these sidechains,

but does not allow us to conclude anything specific about their nature. Absence of the upfield Δ CS that would be expected for a Lys C_ε engaged in a salt-bridge interaction is once again noted in the rehydrated sample.

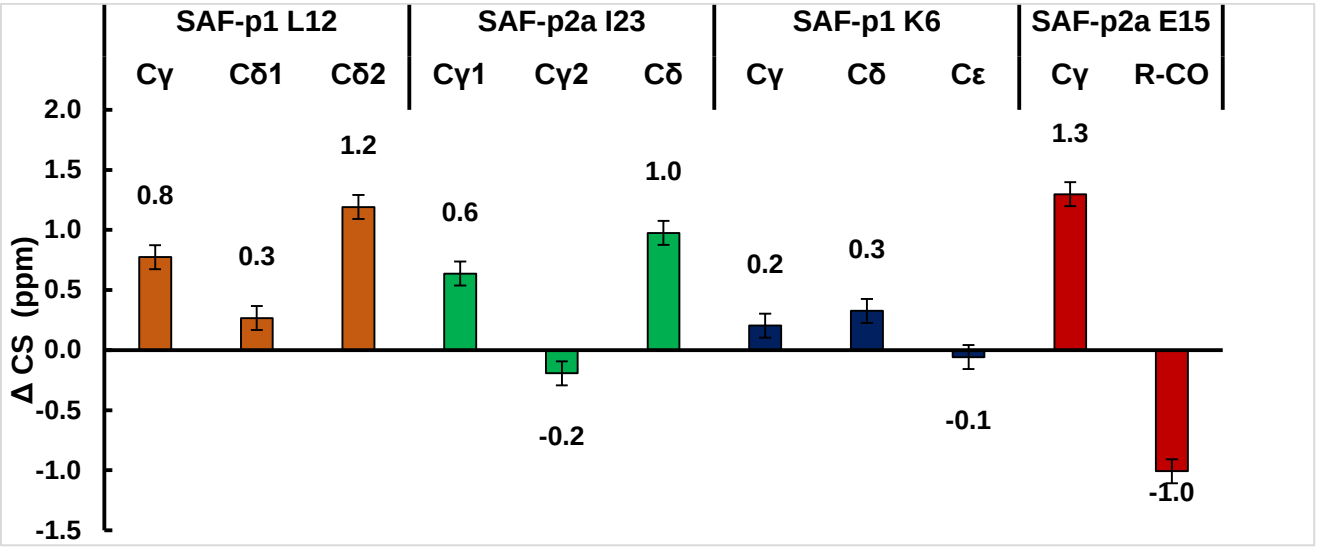

Figure 19: Secondary chemical shifts of labeled sidechain carbons assigned by fpRFDR of rehydrated SAF-p1/p2a.

Of the three 2D NMR experiments on the rehydrated sample, the fpRFDR spectrum has the least number of minor signals due to it being the last experiment performed, and then following a supplemental hydration aliquot (Appendix A.2, Table 4). Further discussion of minor structures for the rehydrated sample is offered subsequently, and in a more appropriate context, alongside the results of the DARR experiments.

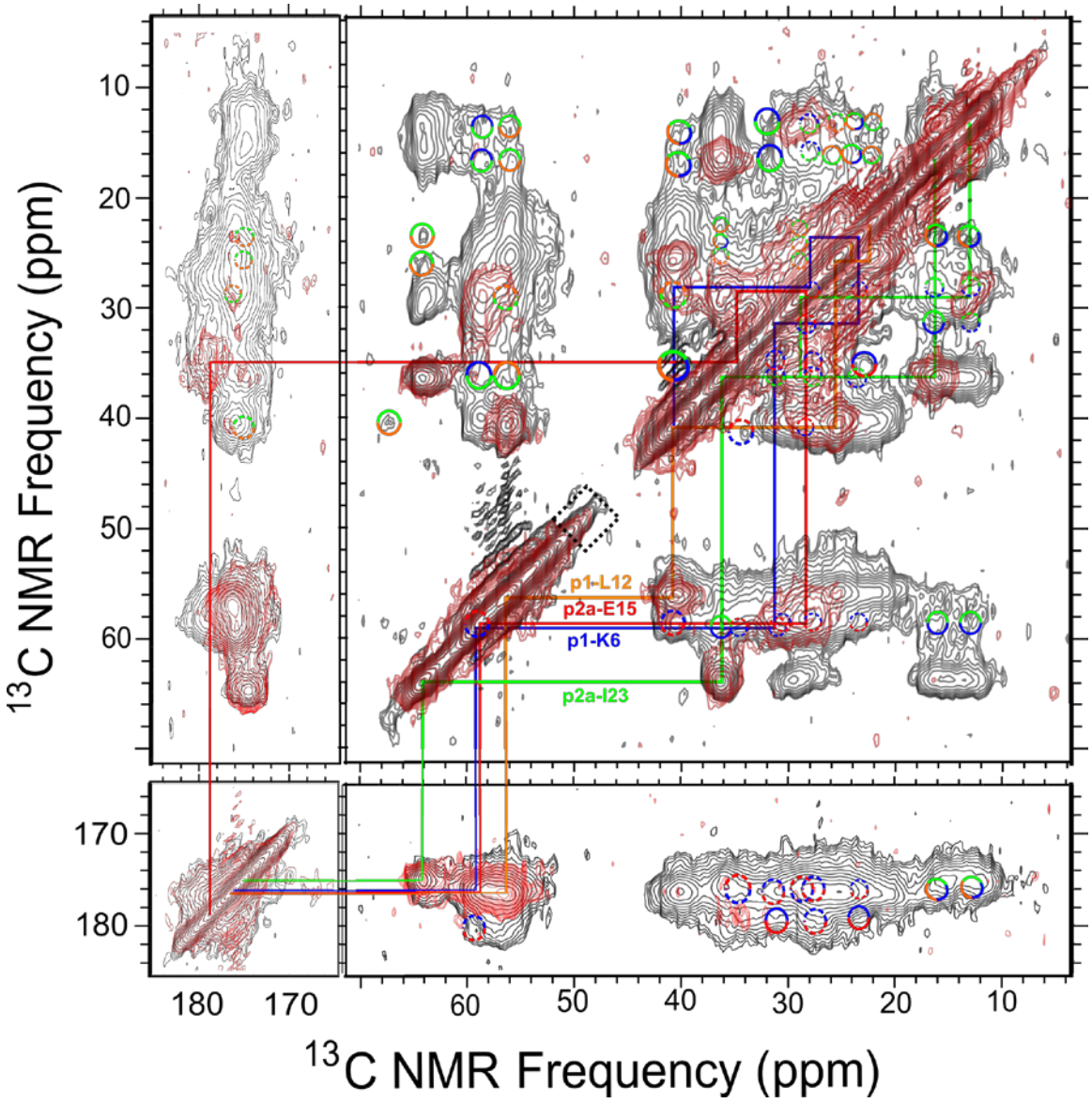

Figure 20: fpRFDR (red) and 500 ms DARR (black) spectral overlays for the lyophilized SAF-p1/p2a nanofibers. Bicolored circles mark interresidue DARR crosspeaks between ^{13}C sites, with the topmost color indicating the amino acid of the vertical coordinate; solid circles mark likely through-space contacts, dashed circles mark suspected through-space contacts susceptible to overlap by fpRFDR and/or 50 ms DARR spectra. Tricolored circles mark ambiguous through-space crosspeak assignments, with the topmost color indicating the unambiguously involved amino acid of the crosspeak pairing. The dashed diamond marks a suspected ^{13}C natural abundance signal from MOPS at 48.5 ppm (*108*).

3.2.3 ^{13}C-^{13}C DARR

DARR of Dry SAF-p1/p2a Nanofibers

A ^{13}C-^{13}C 2D DARR spectrum of lyophilized SAF-p1/p2a nanofibers was collected at a mixing time (τ_m) of 500 ms (Figure 20). This spectrum reveals through-space contacts between all labeled sidechain carbons of SAF-p1 L12 and SAF-p2a I23. While this result confirms that these two sidechains are co-proximal within the DARR detection limit of ~6 Å (*104*), the notable absence of a C_α- C_α contact implies that SAF-p1 L12 and SAF-p2a I23 are not close enough to each other to fully realize the model hypothesis put forth by Woolfson and coworkers (*30, 31*).

The DARR spectrum of the dry nanofibers also yielded some intriguing information concerning the SAF-p1 K6 and SAF-p2a E15 residues. Despite heavy spectral overlap, unambiguous through-space contacts are observed from the E15 sidechain carbonyl carbon to K6 C_β and C_γ, indicating co-proximity of these residues (Figure 20). However, there is also a conspicuous absence of a contact between K6 C_ε and the glutamate sidechain carbonyl carbon, which is arguably the most important through-space contact for determining the formation of a Lys-Glu salt bridge.

It is worth noting that, in our preparation of the SAF-p1/p2a nanofibers, we evacuate water from the sample by lyophilization, which in turn removes the driving force for spontaneous hydrophobic interactions. However, examples from literature (*109*) have demonstrated that lyophilization is an effective method of structural preservation of amphipathic α-helical

peptide assemblies, rather than a means of degradation. Our confidence in our results is strengthened by the fact that the lyophilized nanofibers experience no external forces that could be reasonably expected to drive dissociation of the hydrophobic core prior to experimentation.

DARR of Rehydrated SAF-p1/p2a Nanofibers

The majority of signals observed in the long-mixing (τ_m=500 ms) DARR spectrum are duplicates of those in the short-mixing (τ_m=50 ms) DARR spectrum of rehydrated SAF-p1/p2a (Figure 21). Long-mixing DARR reports on both through-bond and through-space ^{13}C-^{13}C contacts. That is, all intraresidue (through-bond) contacts within a given labeled residue are observed as crosspeaks on the same spectrum as interresidue (through-space) contacts between ^{13}C nuclei that are within ~6 Å of one another in the molecular fold (*104*). The short-mixing DARR experiment reports on all ^{13}C-^{13}C intraresidue contacts as well, but it is not sensitive to through-space contacts. Overlaying these two spectra allows one to accurately categorize each crosspeak. For rehydrated SAF-p1/p2a, considerable overlap of these spectra indicate that only one crosspeak from the long-mixing DARR experiment is a true through-space contact. ^{13}C-^{13}C fpRFDR assignment pathways superimposed upon the overlaid 50 ms/500 ms DARR spectra for the rehydrated β-motif structure (Figure 21) show that the lone through-space correlation signal resides at a point of overlap for all four labeled amino acid spin systems. Identifying the source of this signal is therefore impossible with the current choice of labels.

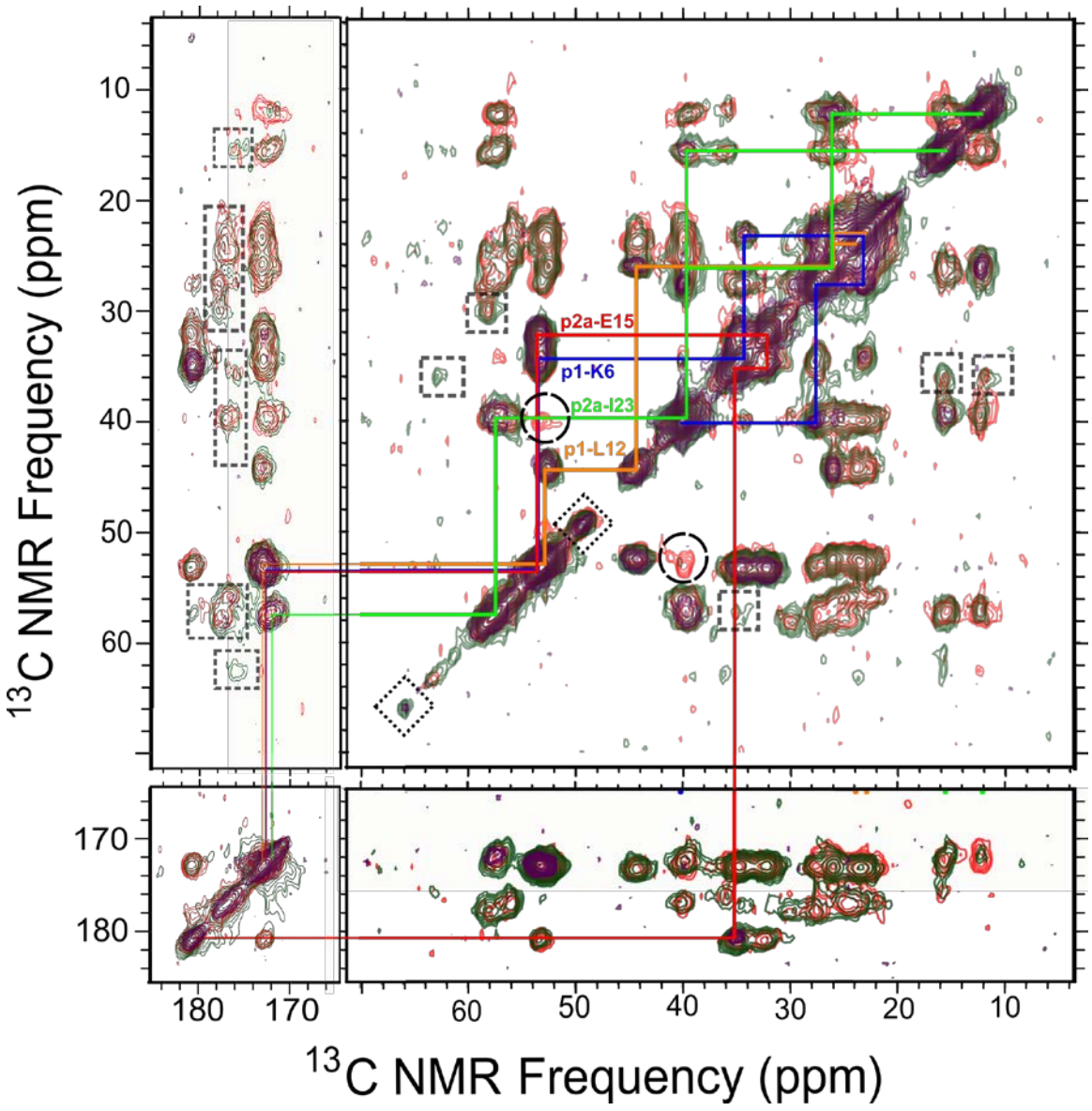

Figure 21: fpRFDR (purple), 50 ms DARR (dark green) and 500 ms DARR (red) spectral overlays for rehydrated SAF-p1/p2a β-sheet structure. Black circles mark the only certain through-space contact from the 500 ms DARR spectrum. Grey boxes highlight α-helical minor structure signals from the DARR experiments. Dashed black diamonds are MOPS carbon signals at 48.5 ppm and 65.1 ppm (*108*).

The α-helical minor structure population present in the rehydrated SAF-p1/p2a is indicated by relatively weak fpRFDR and DARR cross peaks matching the chemical shift assignments for the dry sample. The select minor signals that did not vanish into the noise are shown in Figure 21 and correspond to backbone and beta carbons, whose chemical shifts are sensitive to changes in secondary structure as illustrated in Figure 9. For spectra of the rehydrated sample, a decrease in both quantity and intensity of the minor signals was observed which can be correlated to the time elapsed since the initial rehydration of the sample (Appendix A.2, Table 4). This effect is particularly pronounced in the final experiment of this sequence (fpRFDR). Immediately following the 500 ms DARR experiment, a routinely collected ^{1}H spectrum showed a vanishing water peak (Appendix A.2, Figure 26C) which prompted delivery of an additional 10 μL UPW to the sample prior to the fpRFDR experiment. Only three unambiguously resolved minor signals from the helical structure are observed in the fpRFDR spectrum overlaid in Figure 21. Quantitative comparison of minor signal populations amongst the DARR and fpRFDR spectra strongly suggest that the α-to-β structural transition observed in rehydrated SAF-p1/p2a is time-dependent, with the extent of structural conversion correlated to the extent of rehydration.

3.3 Molecular Modeling of SAF-p1/p2a

Efforts are still ongoing to optimize our molecular models for SAF-p1/p2a heterodimers and nanofibers using NAMD (*79*). Figure 22 shows a manually-positioned model for each, based on a $C_\alpha - C_\alpha$ distance of ~6 Å between SAF-p1 L12 and SAF-p2a I23.

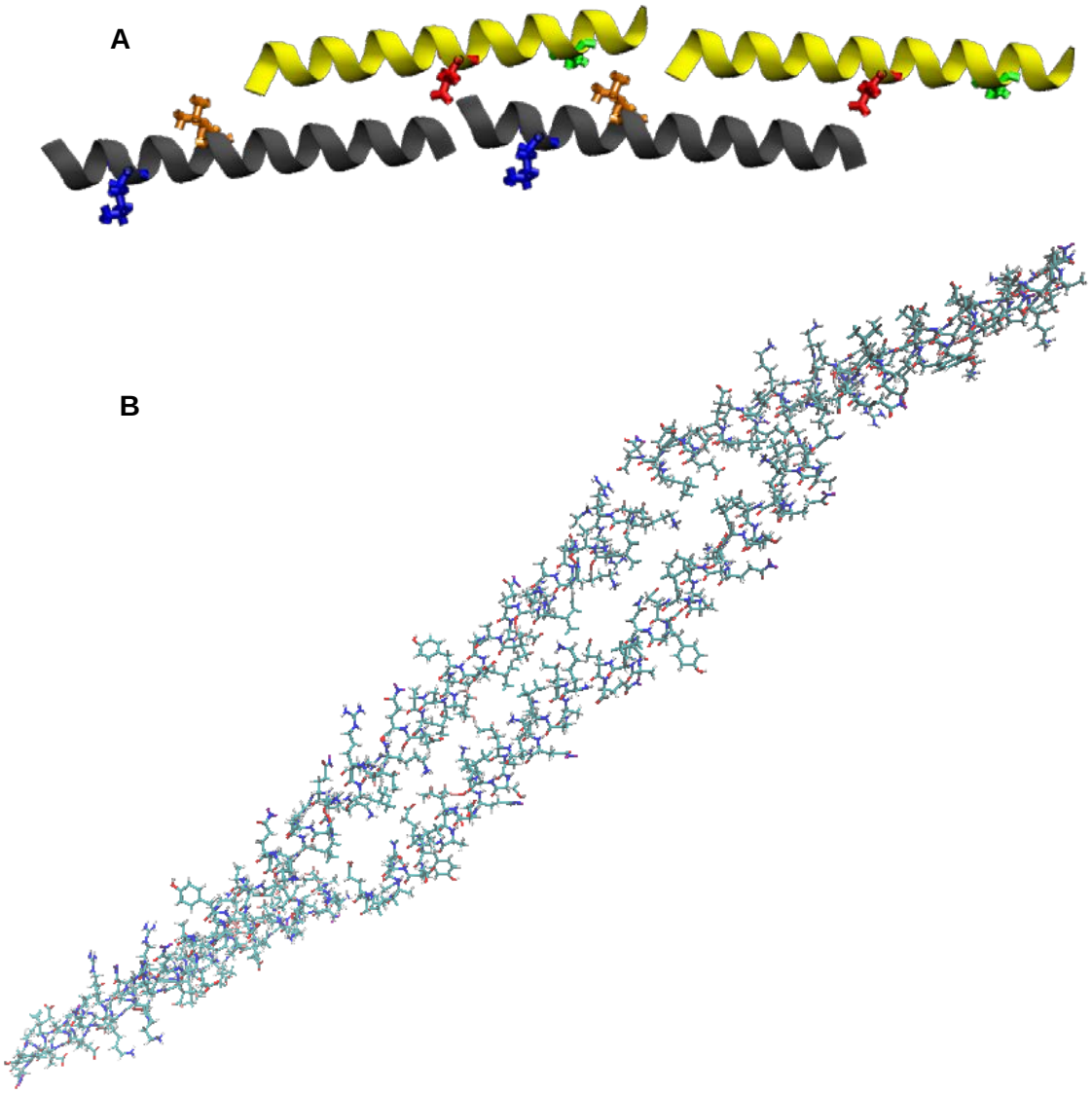

Figure 22: (A) sticky-ended heterodimer model for SAF-p1/p2a, **(B)** an all-atom molecular model representation of a SAF-p1/p2a coiled-coil protofibril positioned according to DARR data for the dried sample.

3.4 Comparison of hSAF$_{AAQ}$-p1/p2 and SAF-p1/p2a data

The α-helical minor structure signals in 2D NMR spectra of rehydrated SAF-p1/p2a are comparable in quantity and magnitude to those of the β-sheet minor structure in rehydrated hSAF$_{AAQ}$-p1/p2. An example of the β-sheet structural shift exhibited by a minor population of hSAF$_{AAQ}$ is highlighted on the overlaid dry/rehydrated fpRFDR spectra of polymorphic hSAF$_{AAQ}$ in Figure 23.

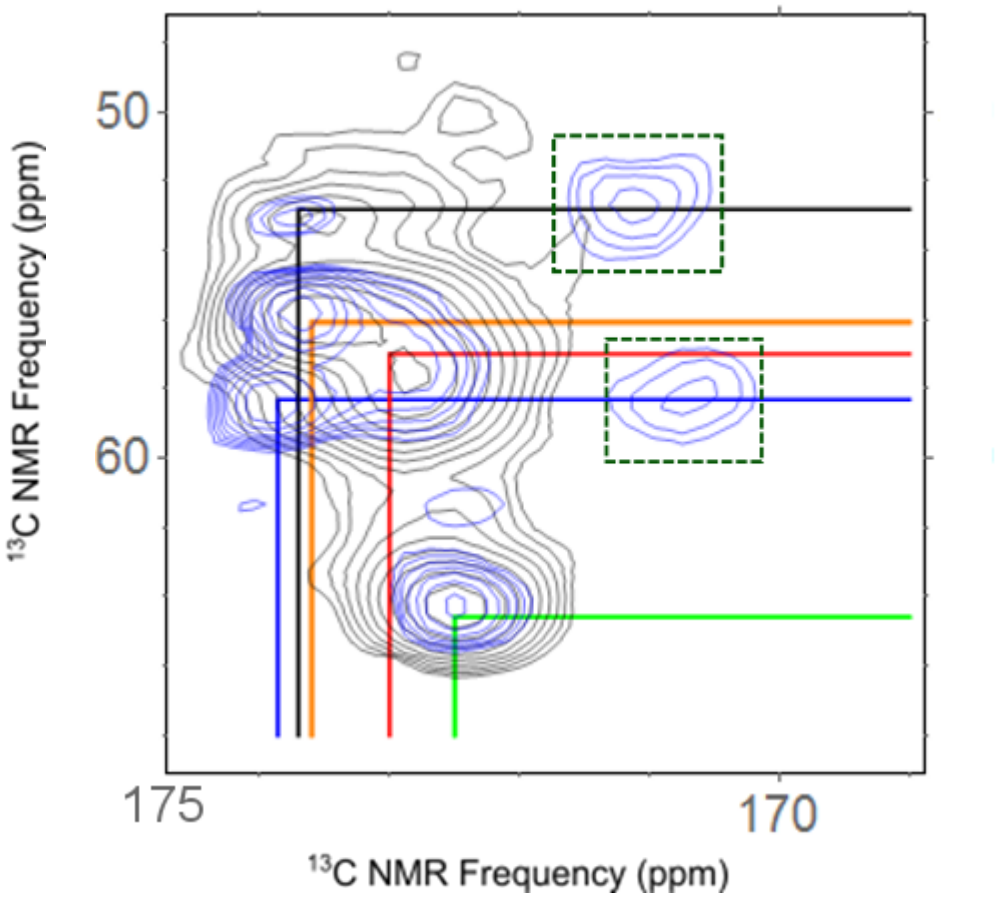

Figure 23: Overlaid ^{13}C-^{13}C fpRFDR spectra in the CO-C$_\alpha$ correlation region of dry (gray) and minimally rehydrated (blue) hSAF$_{AAQ}$-p1/p2. Green dashed boxes highlight minor signals indicating a shift to β-sheet secondary structure following rehydration.

However, unlike SAF-p1/p2a, the $hSAF_{AAQ}$-p1/p2 sample did not shift into a majority β-sheet structure following rehydration, which explains why this structural shift went unnoticed during the first study of $hSAF_{AAQ}$. According to chemical shift data obtained by fpRFDR analysis (Table 3), the majority of the $hSAF_{AAQ}$-p1/p2 sample retained α-helical secondary structure following rehydration.

Table 3: Chemical shift assignments for ^{13}C-^{15}N labeled sites within rehydrated $hSAF_{AAQ}$-p1/p2 nanofibers based on 2D fpRFDR NMR data. CO, C_α, and C_β secondary shifts are shown in parentheses.

Residue	CO	C_α	C_β	$C_{\gamma1}$	$C_{\gamma2}$	$C_{\delta1}$	$C_{\delta2}$	C_ϵ
A4	177.5 (1.4)	52.9 (2.1)	16.5 (-0.9)	-	-	-	-	-
K6	176.0 (1.1)	58.3 (3.8)	30.0 (-1.4)	23.0	-	27.6	-	40.3
L12	177.5 (1.6)	56.1 (2.7)	40.1 (-0.6)	25.0	-	21.5	21.3	-
E15	176.0 (1.1)	57.1 (2.2)	25.9 (-2.3)	30.6	-	175.4	-	-
I23	175.1 (0.4)	64.2 (4.7)	35.9 (-1.2)	15.1	29.1	12.4	-	-

This result contrasts with the near-totality of β-sheet structural conversion in rehydrated SAF-p1/p2a, and leads us to an interesting point of discussion. $hSAF_{AAQ}$-p1/p2 is more resistant to structural conversion, yet its coiled-coil nanofibers do not pack tightly and are less ordered than those formed by SAF-p1/p2a. Additionally, $hSAF_{AAQ}$-p1 has been shown to self-assemble (Figure 14), whereas neither SAF-p1 nor SAF-p2a are capable of individual assembly. The coiled-coil structures for both peptide systems are shown to be metastable by undergoing a time-dependent structural transition, but it appears that the

susceptibility of each system to doing so is correlated with the level of order realized in their α-helical supramolecular structures. Hence, the mechanism of this structural transition may be comparable to that for thermal denaturation of a peptide assembly (*30*), in the sense that highly-ordered assemblies tend to unfold cooperatively around a certain critical temperature, while less-ordered or polymorphic assemblies tend to unfold over a broad temperature range. If this comparison is accurate, then the more highly-ordered SAF-p1/p2a may cooperatively "unfold" in response to rehydration as if it were being denatured, but assumes a self-templating amyloidogenic structure (*110*) instead of a solubilized random-coil state.

In comparing the full set of NMR data for $hSAF_{AAQ}$-p1/p2 (Figure 24A) with the data for SAF-p1/p2a, some similar themes emerge. First, there is evidence of spatial proximity between $hSAF_{AAQ}$-p1 L12 and $hSAF_{AAQ}$-p2 I23. The replication of a positive result for sidechain proximity between these two hydrophobic core residues among two variants of SAF further supports Woolfson's design hypothesis. However, as noted for SAF-p1/p2a, spectral overlap again precludes any conclusive evaluation of the K6-to-E15 salt bridge for $hSAF_{AAQ}$-p1/p2.

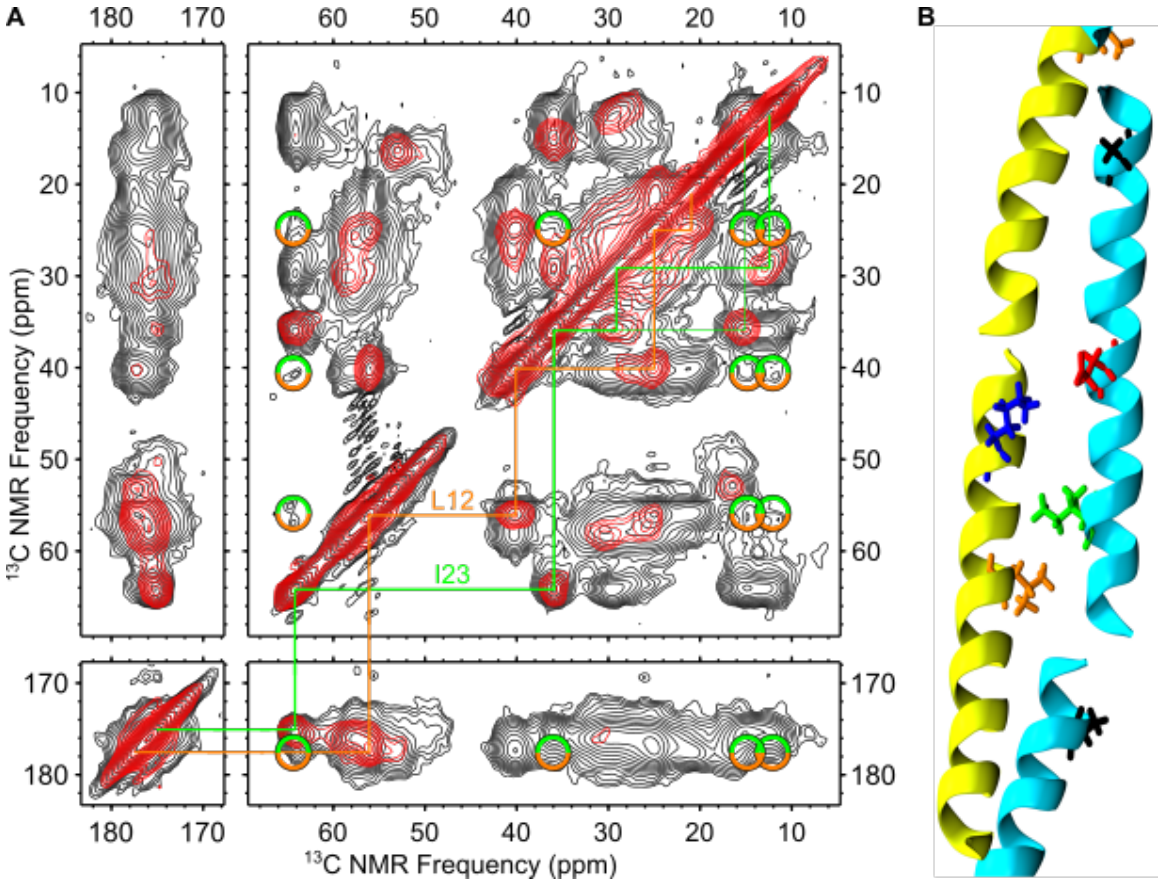

Figure 24: (A) fpRFDR/DARR spectral overlay showing positions of Leu-Ile DARR contacts in lyophilized hSAF$_{AAQ}$-p1/p2. Data collected by Sarah R. Leonard, 2014.

(B) Molecular model of hSAF$_{AAQ}$-p1/p2 sticky-ended heterodimer. Model developed by Maxwell Zimmerman, 2014.

CHAPTER 4: CONCLUSIONS

Chemical shift data derived from the 2D fpRFDR spectrum of lyophilized SAF-p1/p2a nanofibers unambiguously confirm the formation of a majority α-helical structure population under the assembly conditions described by Woolfson and coworkers (*23*). Remarkably, solid state NMR experiments in the time elapsed following minimal rehydration of lyophilized SAF-p1/p2a nanofibers (Appendix A.2, Table 4) reveal a time-dependent structural conversion of the α-helical coiled-coil assembly to a β-sheet conformation. The clearest evidence supporting this conclusion comes from characteristic β-sheet ΔCS values (*98, 106*) calculated for every labeled backbone CO, C_α, and C_β from peak positions in the fpRFDR spectrum of the rehydrated sample (Figure 18). This result proves that SAF-p1/p2a exhibits polymorphism, and further suggests that this β-sheet structure may be the most thermodynamically-stable conformation for SAF-p1/p2a. Follow-up testing of the reversibility of the α-β structural transition (detailed in the next chapter) will conclusively determine whether the SAF-p1/p2a is a true molecular switch (*i.e.* capable of structural interconversion) or if the coiled-coil configuration is instead a metastable structure that irreversibly transitions to a β-sheet structure over time.

There is evidence in the 500 ms DARR spectrum of lyophilized SAF-p1/p2a that the Leu-Ile hydrophobic core interaction predicted by Woolfson's design hypothesis is qualitatively realized. However, the structural transition triggered by rehydration of the nanofibers presents an obstacle to examining this hydrophobic interaction in conditions relevant to co-assembly.

DARR crosspeaks between SAF-p1 K6 and SAF-p2a E15 in the dry nanofibers show unambiguous through-space contacts between the sidechain carbonyl carbon of SAF-p2a E15 and the C_β and C_γ of SAF-p1 K6, but not the C_ε of K6. This result indicates that these two residues are in close (<6 Å) proximity near the molecular fold of the coiled-coil, but do not pair to form a salt bridge as hypothesized by Woolfson and coworkers. A single C_γ-C_γ crosspeak between Lys and Glu is the only other unambiguous through-space contact present for this residue pair; all other couplings that may be present between the SAF-p1 K6 and SAF-p2a E15 spin systems are either lost in spectral overlap to intraresidue signals or possible minor signals from residues in a β-strand conformation. Hence, no further conclusions can be made with regards to the relative spatial configuration of SAF-p1 K6 and SAF-p2a E15.

Finally, TEM results show that MOPS plays a more important role than anticipated in guiding the assembly of SAF-p1/p2a into nanofibers matching the topology reported in literature (*30, 31*). Additionally, ^{13}C NMR signals were observed around ~48.5 and 65.1 ppm in all SAF-p1/p2a spectra. These peak positions do not correspond to any labeled ^{13}C sites for the sample, but they do match the ^{13}C chemical shifts for pure MOPS (*108*). The fact that these signals survive rehydration, which is expected to remove unbound MOPS from the sample by dissolution, indicates that MOPS serves as a structural component of the nanofiber assembly.

CHAPTER 5: RECOMMENDATIONS TOWARDS FUTURE WORK

The "big picture" question for this thesis concerns how my work contributes to the field of rationally-designed peptide systems. We have searched the literature exhaustively, and to our knowledge, my study of SAF-p1/p2a marks the first observation of an α-helical coiled-coil to β-sheet structural transition triggered by physiologically benign conditions in a multicomponent designer peptide system. Therefore, I have potentially opened up two new paths for future work in the field:

1. As previously discussed in Chapter 1, there are numerous applications in biotechnology (drug delivery, biosensor fabrication, and functionalized fusion peptides) for molecular switch biomaterials that adopt a β-sheet conformation in response to a trigger. The benefit of elucidating a process for engineering these technologies as molecular switches lies in the fact that, at present, the "rules" for designing amyloidogenic co-assembling peptides are more complex than those for their self-assembling counterparts (*63, 65*). With further characterization by solid-state NMR, the SAF-p1/p2a system could potentially provide an alternate route to the "bottom-up" approach commonly applied to designing β-sheet co-assemblies. The well-established design principles of coiled-coil assembly could be applied towards the design of an amyloidogenic binary peptide assembly starting from the desired amyloid structure, rather than from the peptide sequences themselves. By developing models for how the coiled-coil architecture rearranges into a β-sheet, a coiled-coil system could be rationally engineered, then triggered to undergo structural conversion, and finally tested against the model or desired

structure to set up the next step in development of a product. Elucidating how the α-helical coiled-coil accomplishes the structural transition to a β-sheet at atomic-length scale resolution would be a key step towards realizing this approach to design. As such, I expect that further solid state NMR study of the SAF system and novel systems inspired by SAF would benefit the field of rational biomaterial design. Enough iterations of this type of study could ultimately strengthen the *de novo* design principles of co-assembling β-sheet peptide systems to make the process more practical and straightforward.

2. The SAF-p1/p2a design can now be used as a starting point for rational design of novel co-assembling binary peptide systems as hydration-triggered α-to-β molecular switches, especially if a follow-up study is done test the ability of the other SAF variants to undergo the same structural transition. A preliminary study of rehydration effects with CPMAS alone could qualitatively identify other promising candidates from the SAF family that can affect a similar structural transition.

In closing, I have proposed some steps to replicate and clarify the results discussed in this thesis.

Analyzing the reversibility of the α-helical to β-sheet structural transition will provide some insight about the thermodynamics of the SAF-p1/p2a system. Re-suspension by vortex mixing of the rehydrated SAF-p1/p2a sample in 10 mM MOPS should be performed at a solution volume that approximately matches the 100 μM peptide concentration used during co-assembly. This re-suspended sample should be given at least 24 hours to incubate at

room temperature before lyophilization and analysis by fpRFDR. If the Δ CS values for the backbone and beta carbons are restored to those observed for the α-helical population, then SAF-p1/p2a will be the first co-assembled designer peptide system ever observed to be fully interconvertible between α-helical and β-sheet structure. Proof of concept would suggest exciting new possibilities for *de novo* co-assembling "molecular switch" systems that can be triggered by controlling water content. However, if the predominantly α-helical structure cannot be restored by re-suspension, then the β-sheet structure would be implicated as the most thermodynamically-stable conformation of the SAF-p1/p2a system; as such, the "knob-in-hole" coiled-coil structure proposed by Woolfson and coworkers would be determined to be metastable. To validate either conclusion, supporting data from circular dichroism and TEM analysis should be collected to monitor structural population distribution and topography of the SAF-p1/p2a sample as it undergoes structural transition.

The NMR data presented previously may be disambiguated through simple modifications to the experiments described. First, during the replication of our results, we propose including a 50 ms DARR experiment on the dry SAF-p1/p2a nanofibers in addition to the fpRFDR and 500 ms DARR. This additional step will separate through-space contacts from through-bond couplings within residues. If spectral overlap is still enough of a problem that we cannot identify an important through-space contact, then the experiments can be repeated with only one component of SAF-p1/p2a carrying labeled residues, *i.e.* one of the peptides used in co-assembly would be unlabeled. DARR spectra for a semi-labeled SAF-p1/p2a sample would then show only intramolecular crosspeaks. The data from the fully-labeled SAF-p1/p2a could then be reinterpreted with greater accuracy by overlaying DARR spectra for both samples.

To test the packing density of the hydrophobic core in its native state (*i.e.* nanofibers in aqueous media), a swinging-bucket ultracentrifuge attachment for a sedimentation NMR rotor (*111*) would be used to collect freshly assembled SAF-p1/p2a nanofibers that could be experimented upon immediately without lyophilization. If a 500 ms DARR contact is observed between the alpha carbons of SAF-p1 L12 and SAF-p2a I23 for this sample, then the Leu-Ile pairings may be considered to occur as described by Woolfson's design hypothesis (*31*). A quantitative measurement of intermolecular distance between the two residues using the ^{13}C-^{13}C PITHIRDS-CT (*112*) experiment could provide the final distance constraint for modeling the hydrophobic core interactions of SAF-p1/p2a.

Finally, the role of MOPS in the structural evolution of SAF-p1/p2a and the mechanistic interactions of SAF-p1 K6 and SAF-p2a E15 could be tested concurrently by analyzing a sample of SAF-p1/p2a assembled in pure water. The NMR experiment sequence performed for the 10 mM MOPS assembly would be repeated, and the secondary structure of the sample would again be evaluated from fpRFDR. If the epsilon carbon of SAF-p1 K6 shows a DARR contact with the sidechain carbonyl carbon of SAF-p2a E15, then it is likely that MOPS interferes with the salt-bridge pairing. However, if this contact remains unaccounted for, then we can conclude that SAF-p1 K6 and SAF-p2a E15 are more likely to be involved in lateral assembly interactions between coiled-coil protofibrils, rather than in stabilizing the coiled-coil interface within their own heterodimer.

APPENDIX A

PEPTIDE SAMPLE INFORMATION SUPPLEMENT

A.1 SAF-p1/p2a Certificates of Analysis

CPC scientific

Certificate of Analysis

Product Name:	SAF-p1, labeled K6 and L12:
Lot #:	CP-11-01618
Product #:	913258
Sequence:	Lys-Ile-Ala-Ala-Leu-Lys(U13C6,15N2)-Gln-Lys-Ile-Ala-Ser-Leu(U13C6,15N)-Lys-Gln-Glu-Ile-Asp-Ala-Leu-Glu-Tyr-Glu-Asn-Asp-Ala-Leu-Glu-Gln
Molecular Weight:	3188.6
Mass Spectral Analysis:	Electrospray "Exhibits correct MW" (see attached MS spectrogram)
HPLC Analysis:	Peptide purity: 93.0% (see attached RP-HPLC chromatogram)
Solubility:	1 mg/ml in water
Appearance:	White lyophilized powder
Counter Ion:	Trifluoroacetate
Cert. of Analysis Remarks:	

Remarks: Not for human use, research purpose only.

Quality Assurance By: Tina An Date: 12/26/16
Quality Control Department

CPC Scientific Inc.

Figure 25A: Certificate of Analysis cover sheet for SAF-p1, from CPC Scientific, Inc.

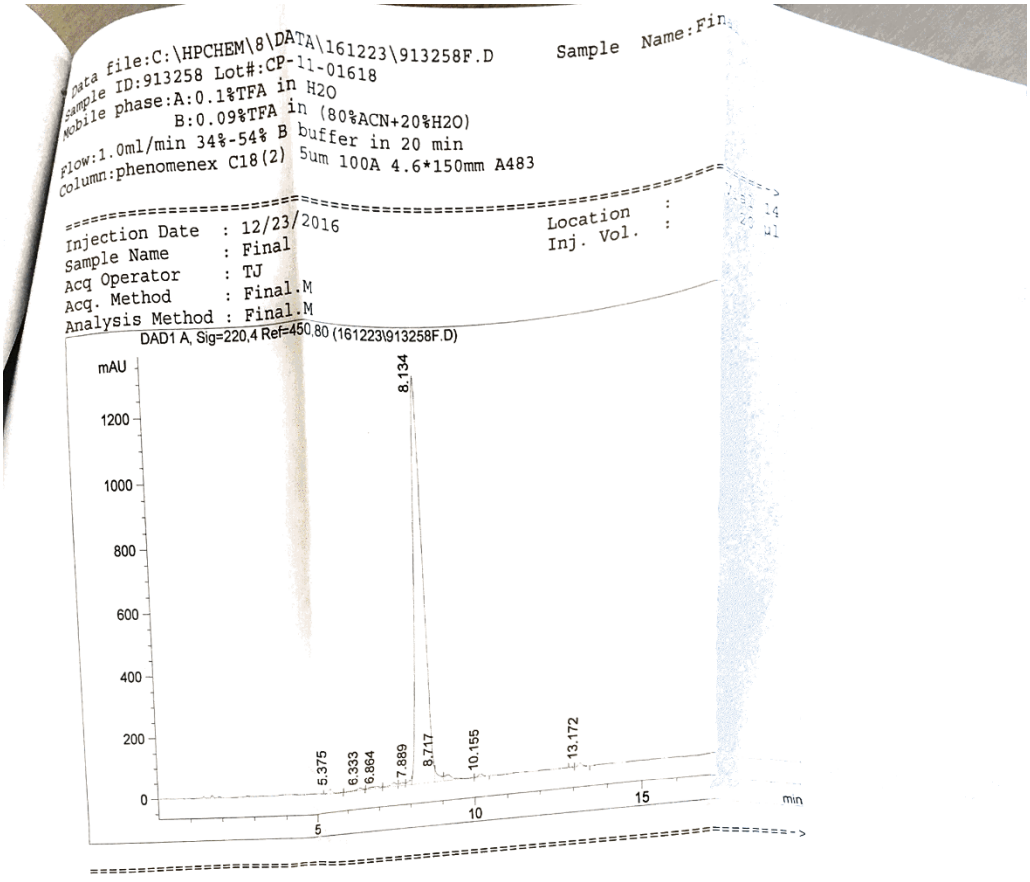

Signal 1:DAD1 A, Sig=220,4 Ref=450,80

Peak #	RT [min]	Type	Height	Width [min]	Area	Area %
1	5.375	PV	14.438	0.161	147.432	0.541
2	6.333	VV	8.826	0.194	120.147	0.441
3	6.864	VV	7.013	0.305	162.101	0.595
4	7.414	VV	13.870	0.200	200.149	0.734
5	7.680	VV	10.215	0.168	116.019	0.426
6	7.889	MF	17.020	0.142	145.515	0.534
7	8.134	FM	1315.866	0.321	25364.834	93.081
8	8.717	FM	43.804	0.146	382.922	1.405
9	9.125	VP	21.174	0.265	399.206	1.465
10	10.155	VP	9.837	0.151	95.274	0.350
11	12.899	BP	0.685	0.099	4.313	0.016
12	13.172	VP	12.937	0.133	112.425	0.413

*** End of Report ***

Page 1 of 1

Figure 25B: RP-HPLC chromatograph of SAF-p1, from CPC Scientific, Inc.

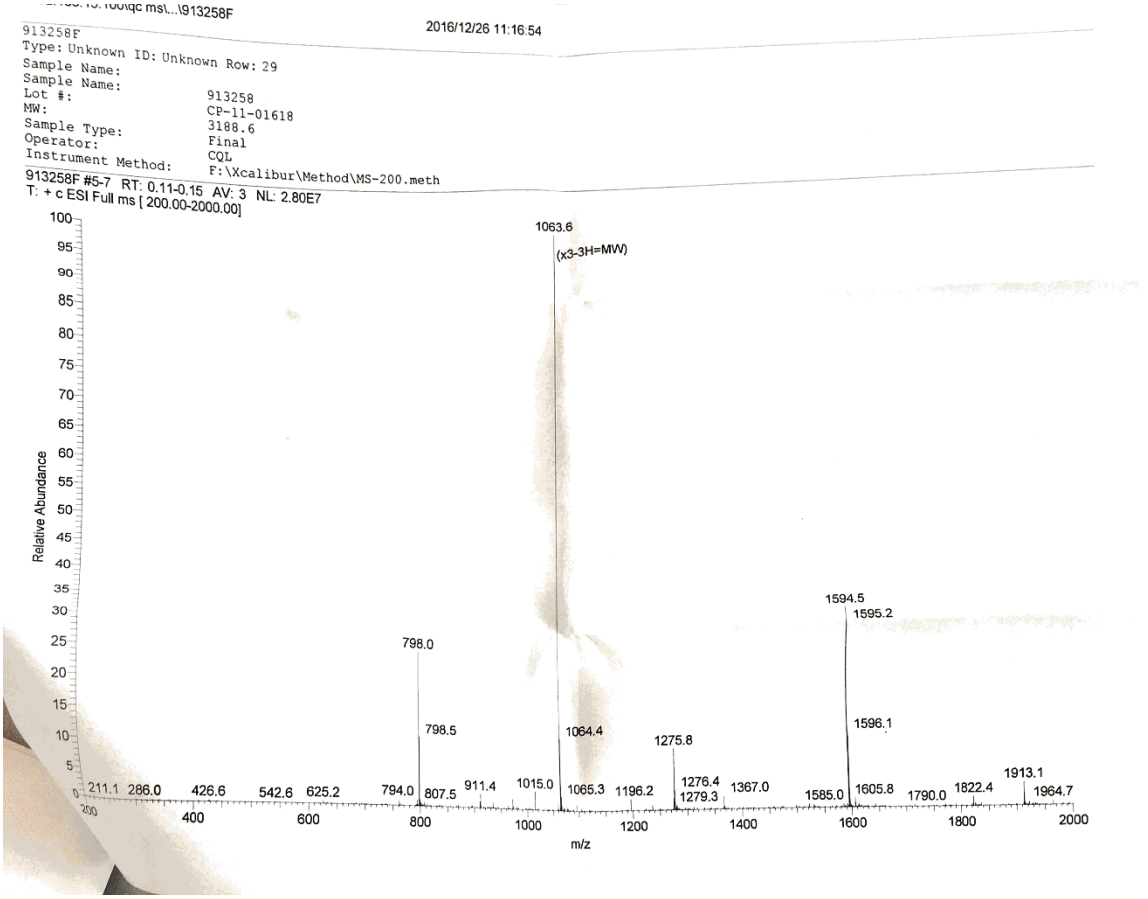

Figure 25C: ESI+ mass spectrometry readings for SAF-p2a, from CPC Scientific, Inc.

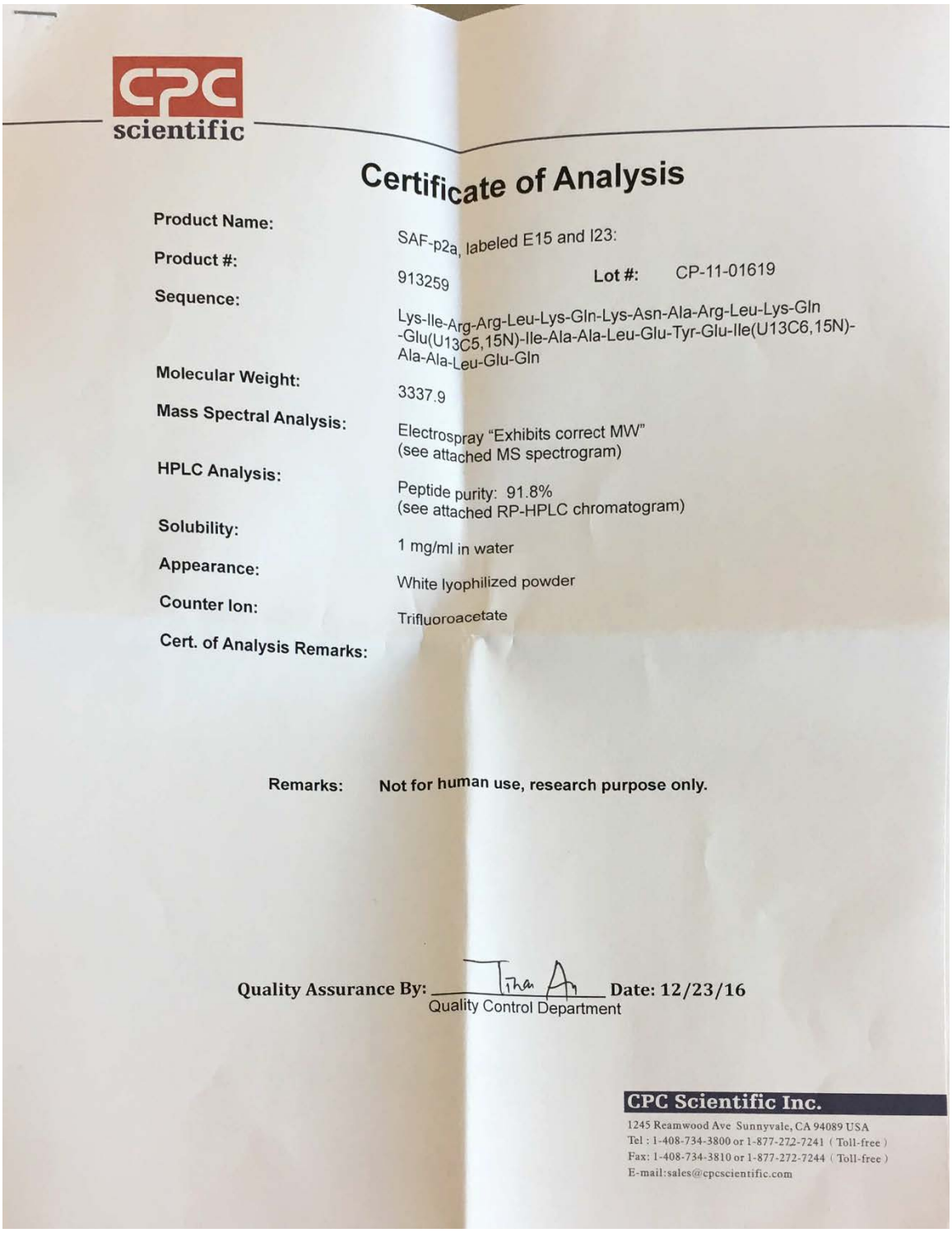

CPC scientific

Certificate of Analysis

Product Name:	SAF-p2a, labeled E15 and I23:
Product #:	913259 **Lot #:** CP-11-01619
Sequence:	Lys-Ile-Arg-Arg-Leu-Lys-Gln-Lys-Asn-Ala-Arg-Leu-Lys-Gln -Glu(U13C5,15N)-Ile-Ala-Ala-Leu-Glu-Tyr-Glu-Ile(U13C6,15N)- Ala-Ala-Leu-Glu-Gln
Molecular Weight:	3337.9
Mass Spectral Analysis:	Electrospray "Exhibits correct MW" (see attached MS spectrogram)
HPLC Analysis:	Peptide purity: 91.8% (see attached RP-HPLC chromatogram)
Solubility:	1 mg/ml in water
Appearance:	White lyophilized powder
Counter Ion:	Trifluoroacetate
Cert. of Analysis Remarks:	

Remarks: **Not for human use, research purpose only.**

Quality Assurance By: Tha An **Date: 12/23/16**
Quality Control Department

CPC Scientific Inc.
1245 Reamwood Ave Sunnyvale, CA 94089 USA
Tel : 1-408-734-3800 or 1-877-272-7241 (Toll-free)
Fax: 1-408-734-3810 or 1-877-272-7244 (Toll-free)
E-mail:sales@cpcscientific.com

Figure 25D: Certificate of Analysis cover sheet for SAF-p2a, from CPC Scientific, Inc.

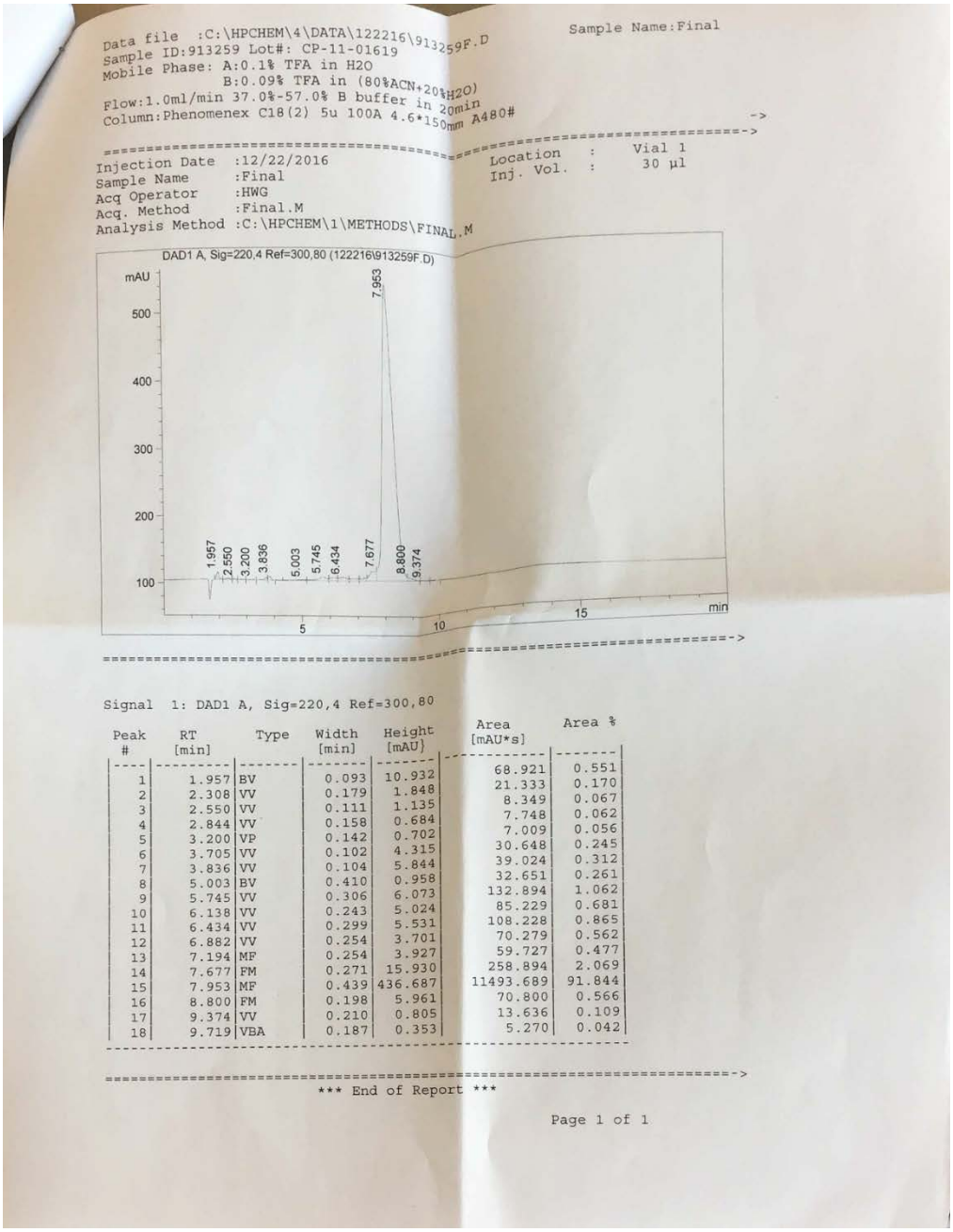

Data file :C:\HPCHEM\4\DATA\122216\913259F.D
Sample Name:Final
Sample ID:913259 Lot#: CP-11-01619
Mobile Phase: A:0.1% TFA in H2O
B:0.09% TFA in (80%ACN+20%H2O)
Flow:1.0ml/min 37.0%-57.0% B buffer in 20min
Column:Phenomenex C18(2) 5u 100A 4.6*150mm A480#

Injection Date :12/22/2016
Location : Vial 1
Sample Name :Final
Inj. Vol. : 30 µl
Acq Operator :HWG
Acq. Method :Final.M
Analysis Method :C:\HPCHEM\1\METHODS\FINAL.M

DAD1 A, Sig=220,4 Ref=300,80 (122216\913259F.D)

mAU
500
400
300
200
100
5
10
15
min
1.957
2.550
3.200
3.836
5.003
5.745
6.434
7.677
7.953
8.800
9.374

Signal 1: DAD1 A, Sig=220,4 Ref=300,80

Peak #	RT [min]	Type	Width [min]	Height [mAU]	Area [mAU*s]	Area %
1	1.957	BV	0.093	10.932	68.921	0.551
2	2.308	VV	0.179	1.848	21.333	0.170
3	2.550	VV	0.111	1.135	8.349	0.067
4	2.844	VV	0.158	0.684	7.748	0.062
5	3.200	VP	0.142	0.702	7.009	0.056
6	3.705	VV	0.102	4.315	30.648	0.245
7	3.836	VV	0.104	5.844	39.024	0.312
8	5.003	BV	0.410	0.958	32.651	0.261
9	5.745	VV	0.306	6.073	132.894	1.062
10	6.138	VV	0.243	5.024	85.229	0.681
11	6.434	VV	0.299	5.531	108.228	0.865
12	6.882	VV	0.254	3.701	70.279	0.562
13	7.194	MF	0.254	3.927	59.727	0.477
14	7.677	FM	0.271	15.930	258.894	2.069
15	7.953	MF	0.439	436.687	11493.689	91.844
16	8.800	FM	0.198	5.961	70.800	0.566
17	9.374	VV	0.210	0.805	13.636	0.109
18	9.719	VBA	0.187	0.353	5.270	0.042

*** End of Report ***

Page 1 of 1

Figure 25E: RP-HPLC chromatograph of SAF-p2a, from CPC Scientific, Inc.

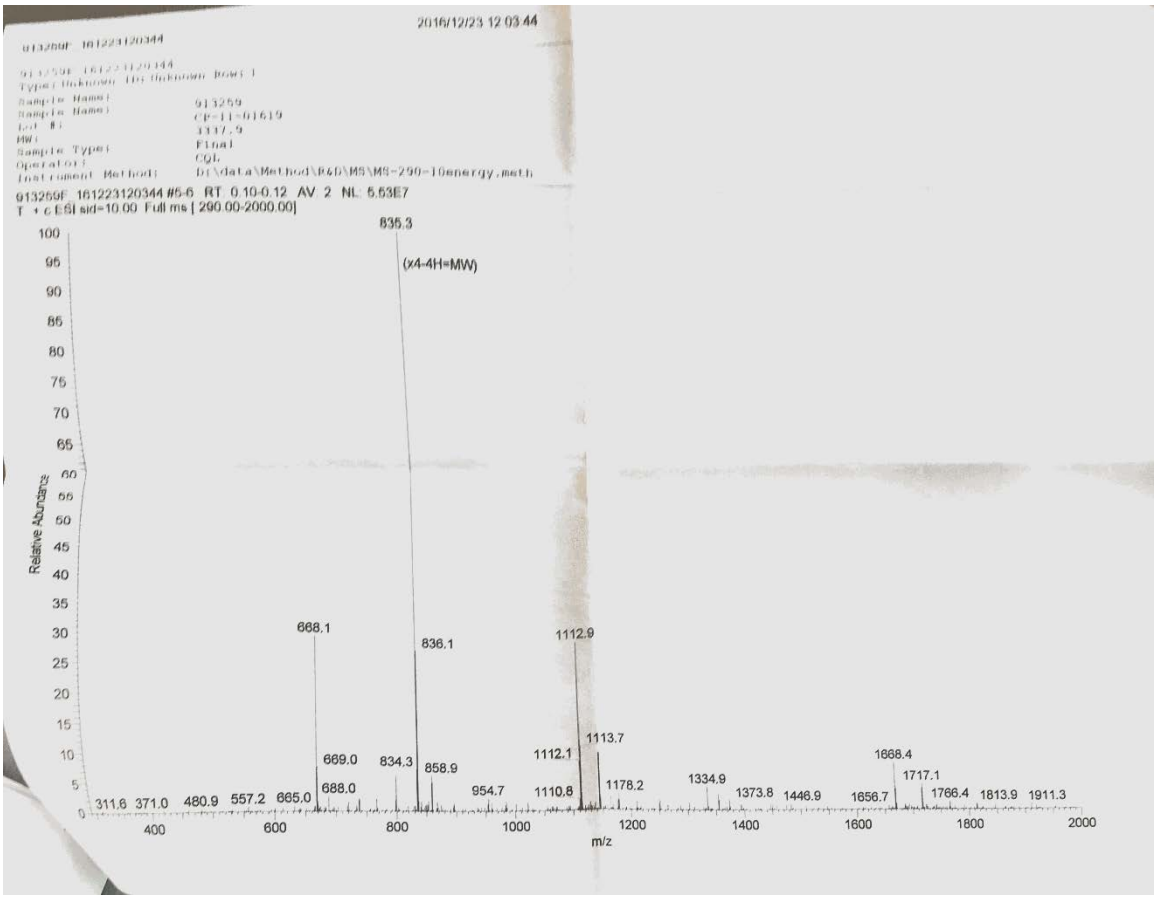

Figure 25F: ESI+ mass spectrometry readings for SAF-p2a, from CPC Scientific, Inc.

A.2 Sample Rehydration Log and Selected ^{1}H Spectra

Rehydration timeline for SAF-p1/p2a nanofibers

Table 4: Rehydration of SAF-p1/p2a nanofibers for solid state NMR experiments on β-sheet structure. For this sample, multiple rehydration aliquots were required to maintain the preferred level of hydration for our experiments.

Date	Sample Amount (mg)	Amount UPW Used (µL)	Notes
2/8/17	15.6	~16	1 drop UPW missed the sample, added ~6 µL UPW to correct for this.
2/10/17	10.4	4.3	Some sample lost while unpacking rotor. Rehydration here was to correct for dry sample added at 1 µL UPW per mg dry sample
2/16/17	10.4	10.0	Final rehydration performed under direction of Dr. Paravastu upon seeing diminished water peak in ^{1}H spectrum

Selected ^{1}H spectra following initial rehydration of SAF-p1/p2a sample

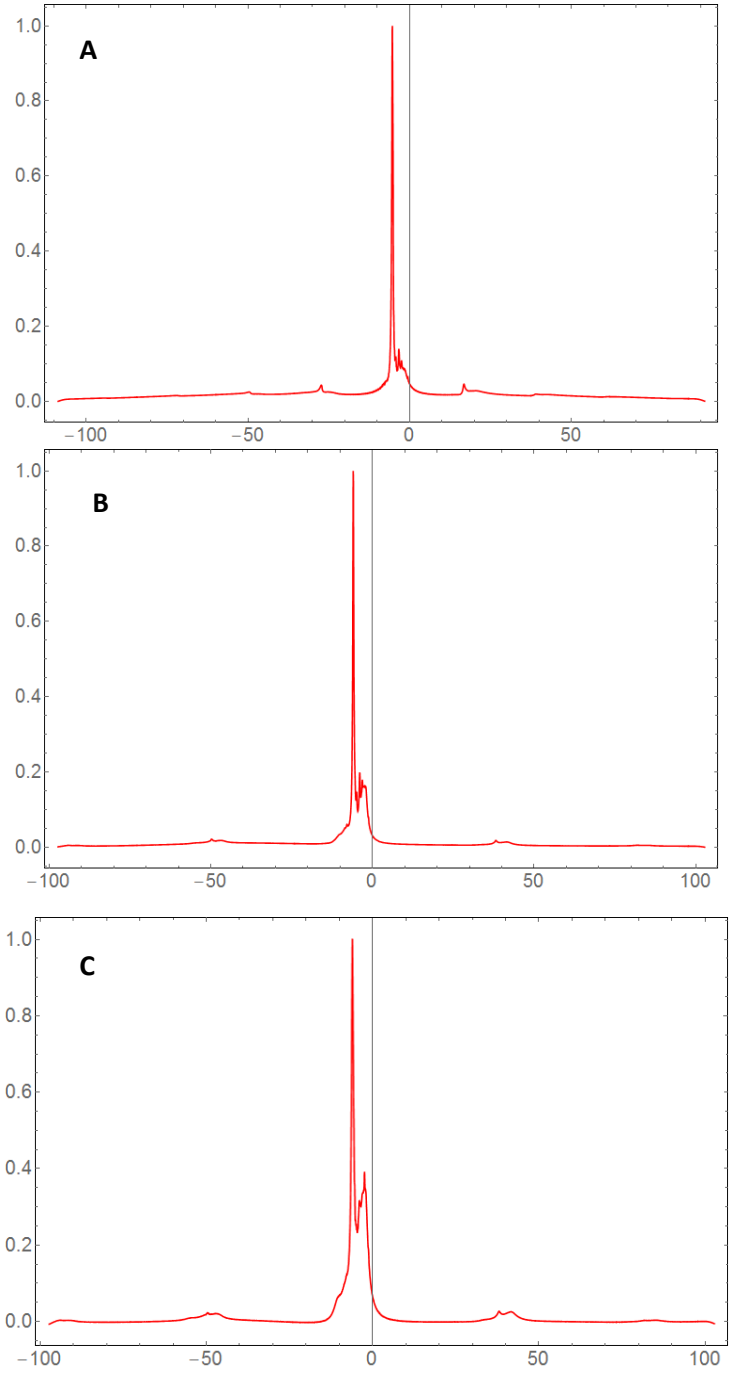

Figure 26A-C: ^{1}H spectra collected **(A)** 1 hr after initial hydration **(B)** 1 hr after second hydration **(C)** 1 day after second hydration

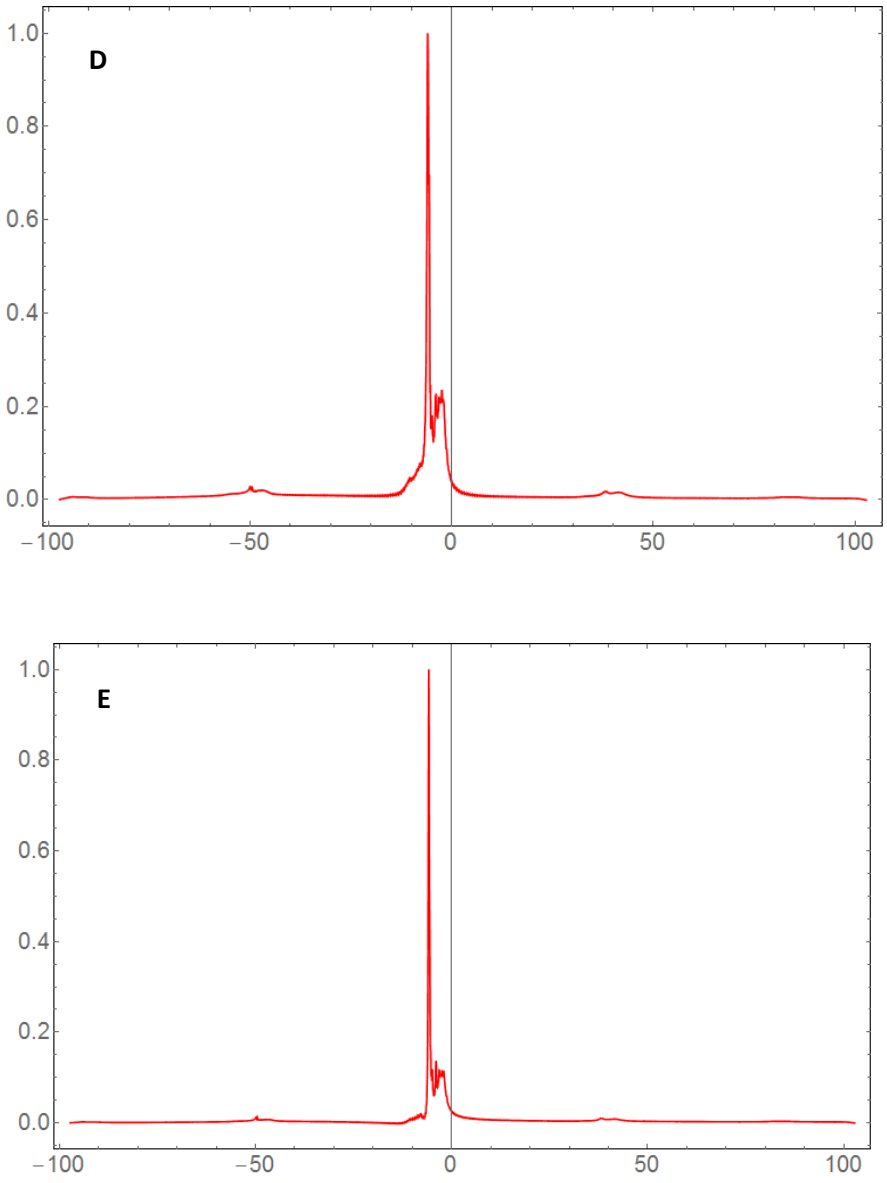

Figure 26D-E: ^{1}H spectra collected **(D)** 3 days after second hydration **(E)** 1 hr after final hydration

APPENDIX B

RAW SPECTRAL DATA

B.1 ^{13}C-^{13}C fpRFDR Spectra

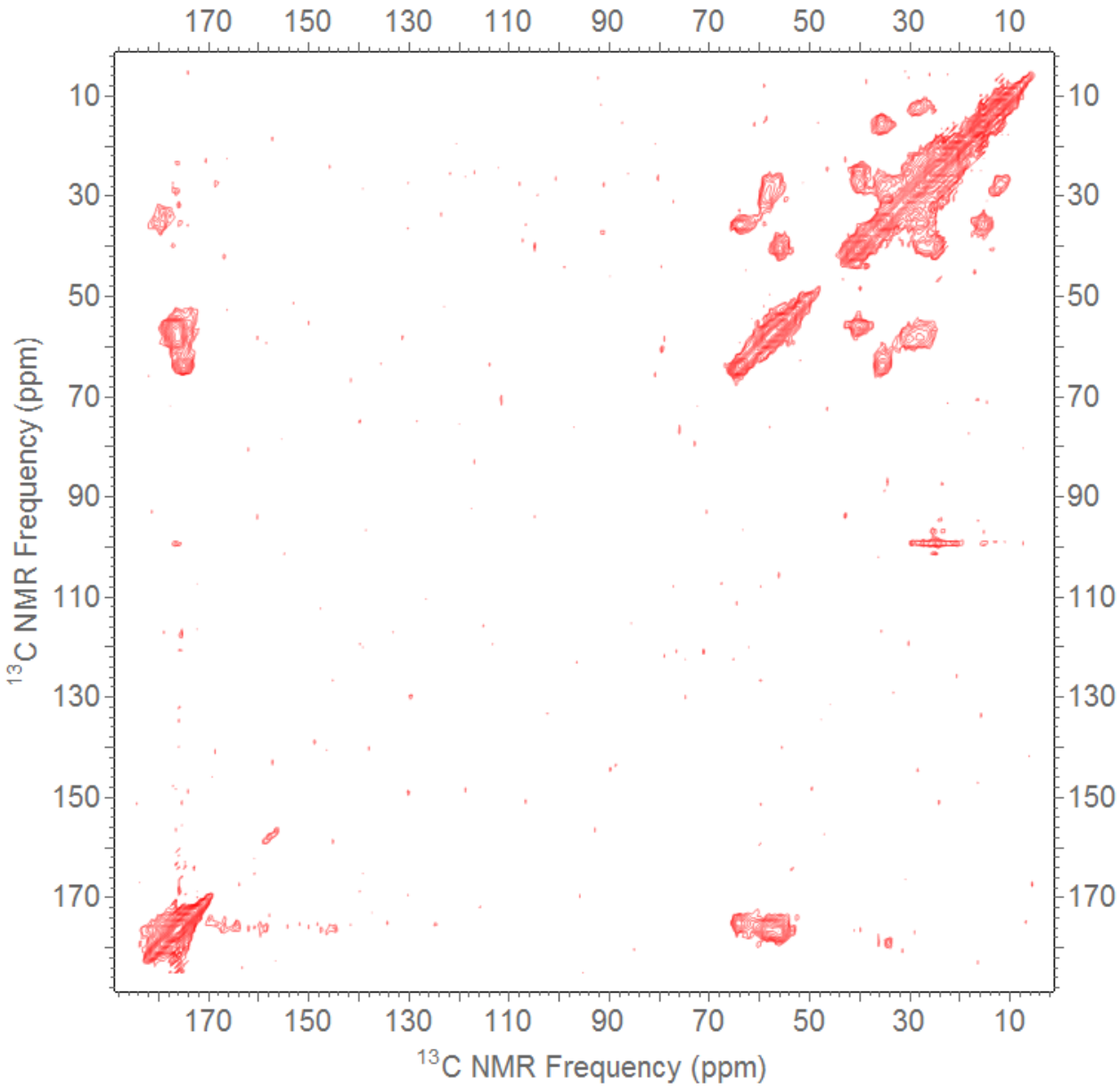

Figure 27A: 2D ^{13}C-^{13}C fpRFDR spectrum of dry SAF-p1/p2a nanofibers.

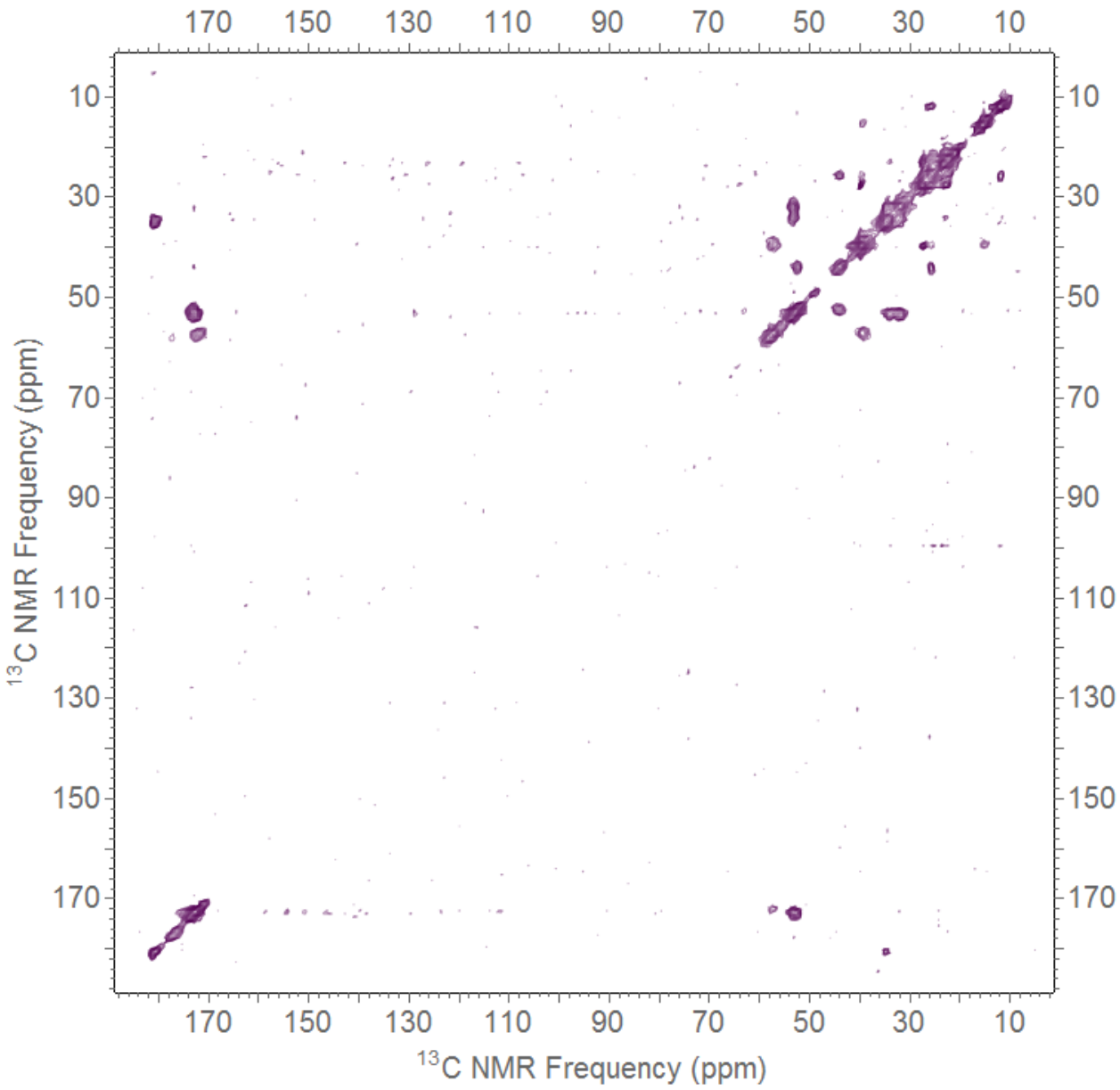

Figure 27B: 2D ^{13}C-^{13}C fpRFDR spectrum of rehydrated SAF-p1/p2a nanofibers.

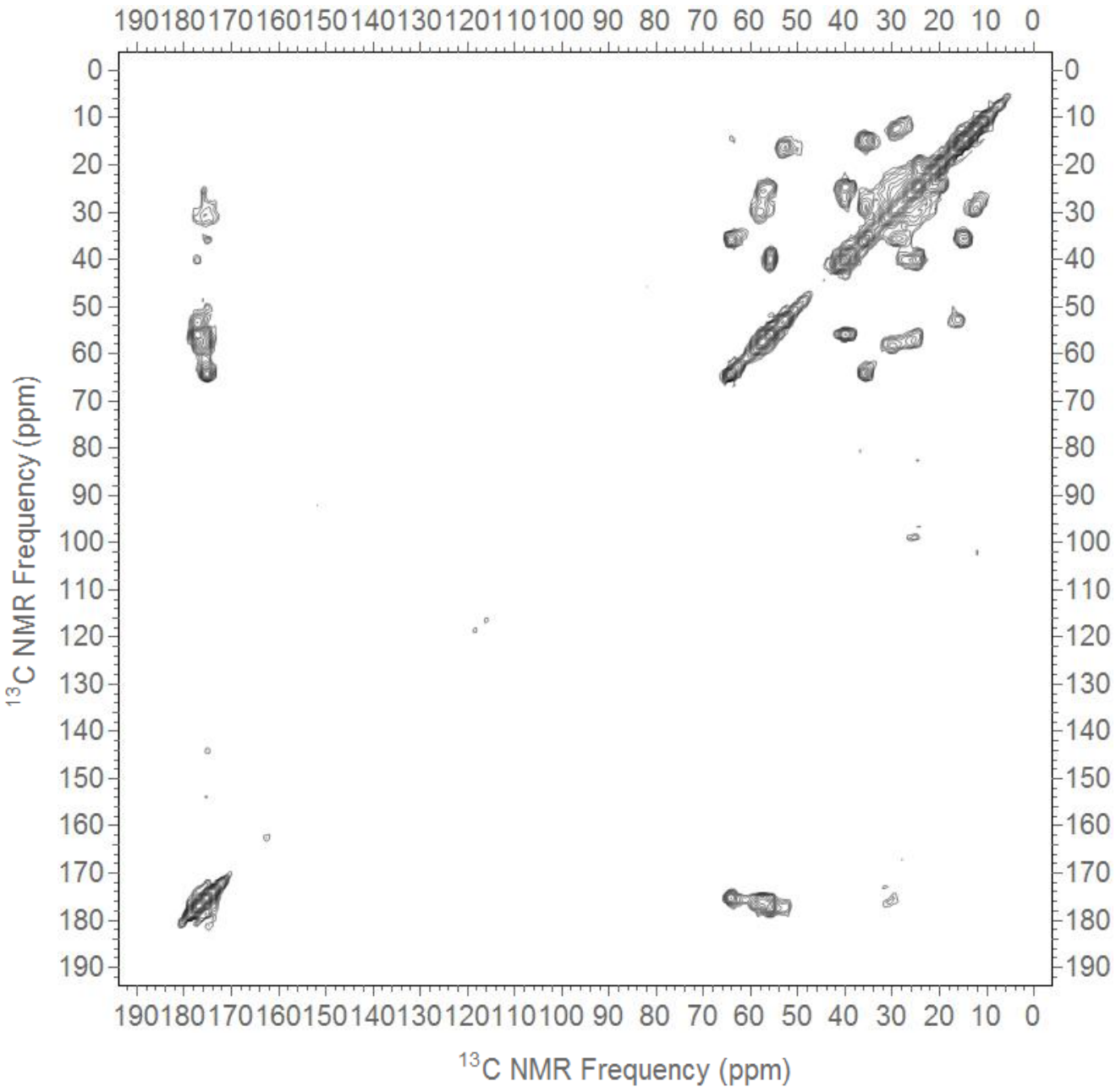

Figure 27C: 2D ^{13}C-^{13}C fpRFDR spectrum of dry hSAF$_{AAQ}$-p1/p2 nanofibers. Collected by Sarah R. Leonard.

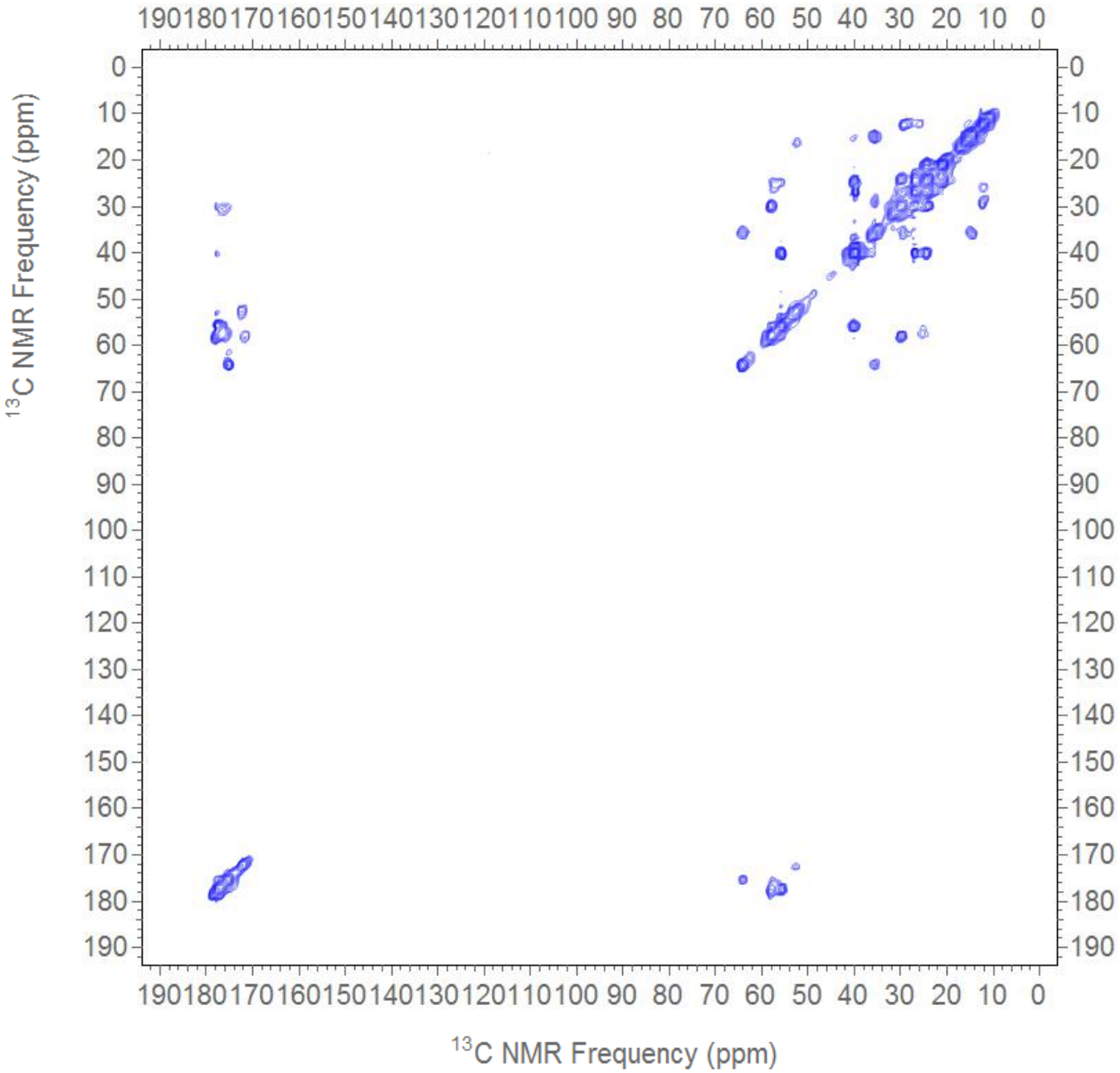

Figure 27D: 2D ^{13}C-^{13}C fpRFDR spectrum of rehydrated hSAF$_{AAQ}$-p1/p2 nanofibers. Collected by Sarah R. Leonard.

B.2 ^{13}C-^{13}C DARR Spectra

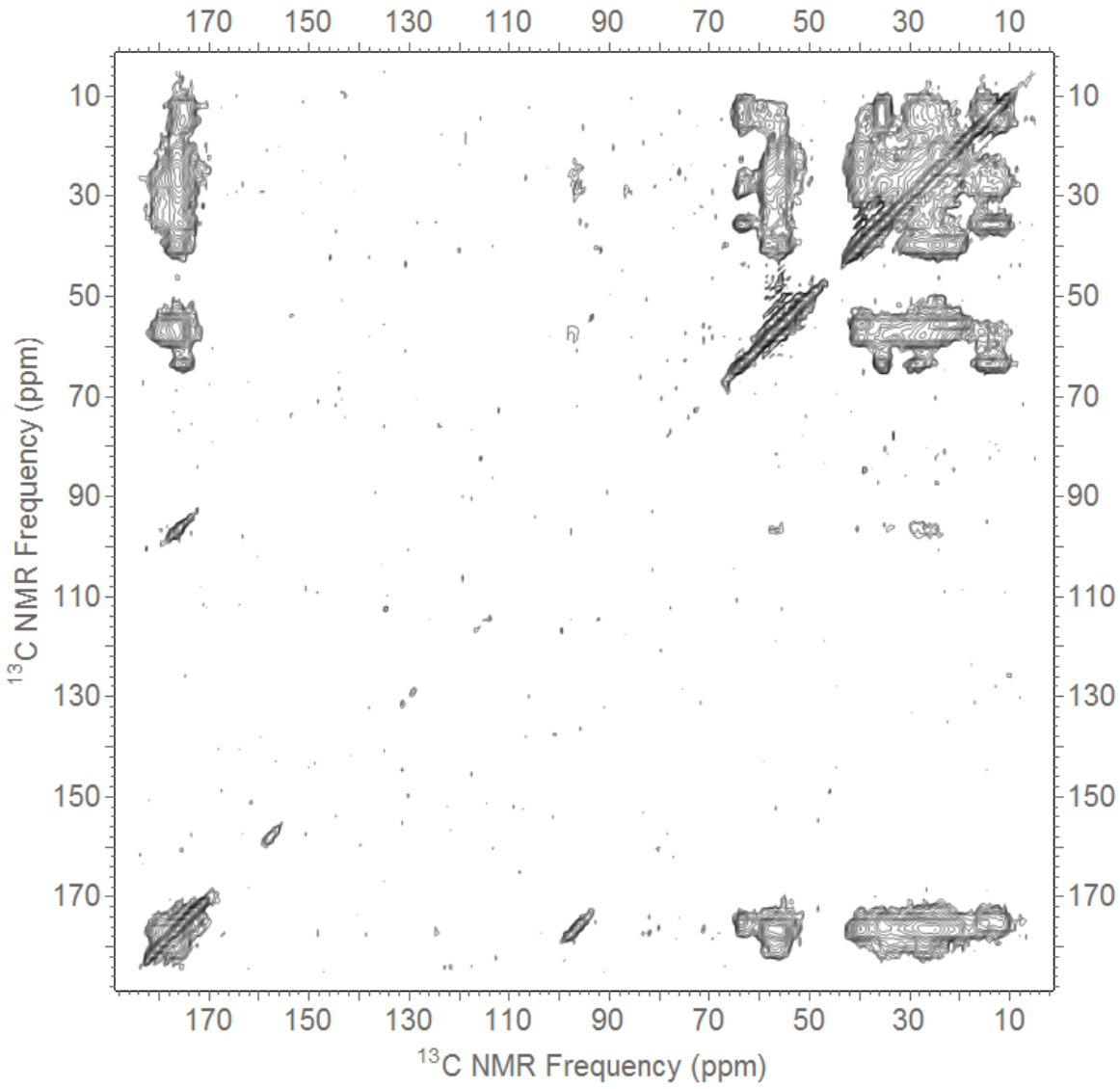

Figure 28A: 2D ^{13}C-^{13}C DARR spectrum of dry SAF-p1/p2a, collected at 500 ms mixing time.

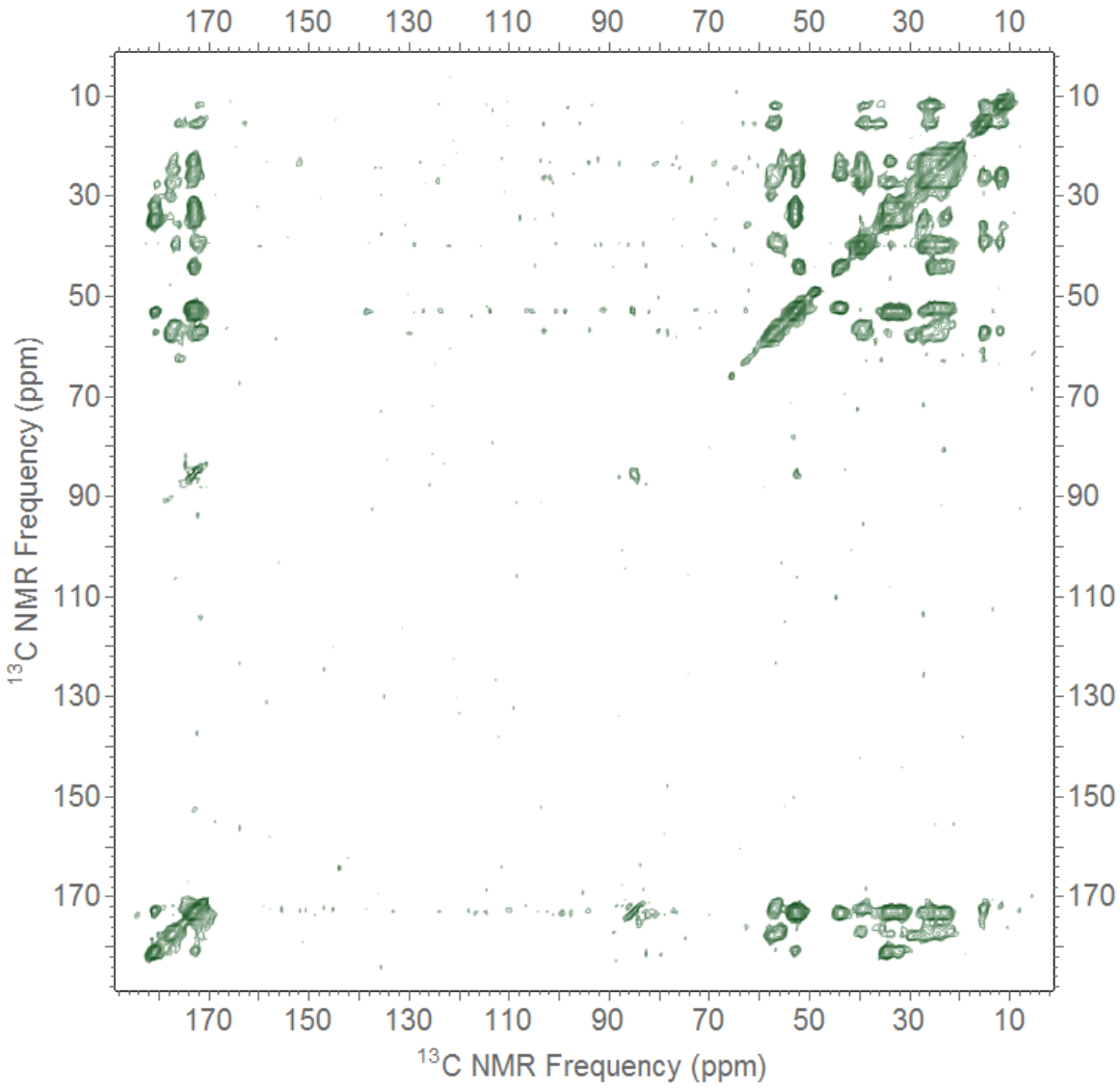

Figure 28B: 2D ^{13}C-^{13}C DARR spectrum of rehydrated SAF-p1/p2a, collected at 50 ms mixing time.

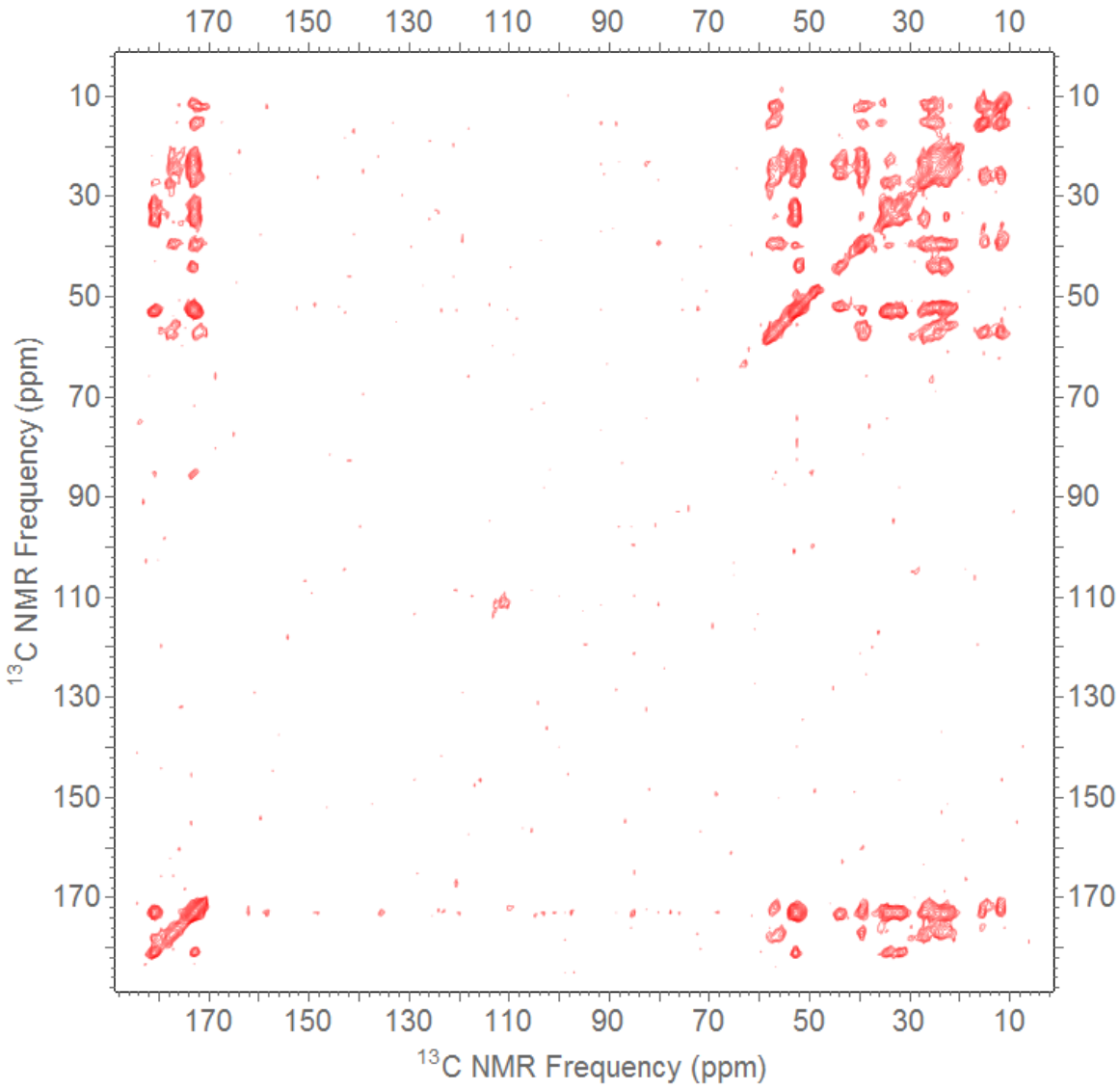

Figure 28C: 2D ^{13}C-^{13}C DARR spectrum of rehydrated SAF-p1/p2a, collected at 500 ms mixing time.

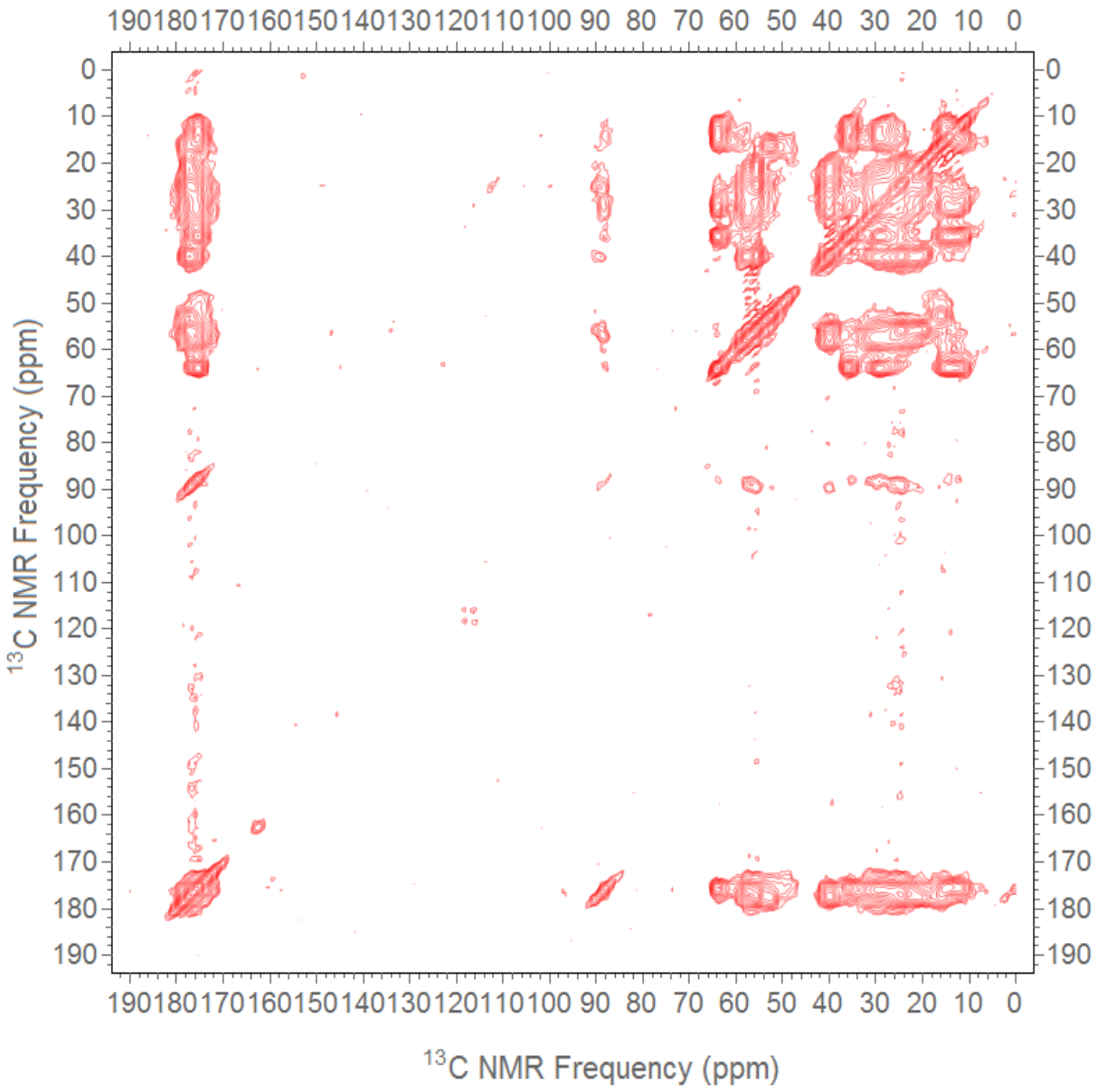

Figure 28D: 2D ^{13}C-^{13}C DARR spectrum of dry hSAF$_{AAQ}$-p1/p2, collected by Sarah R. Leonard at 500 ms mixing time.

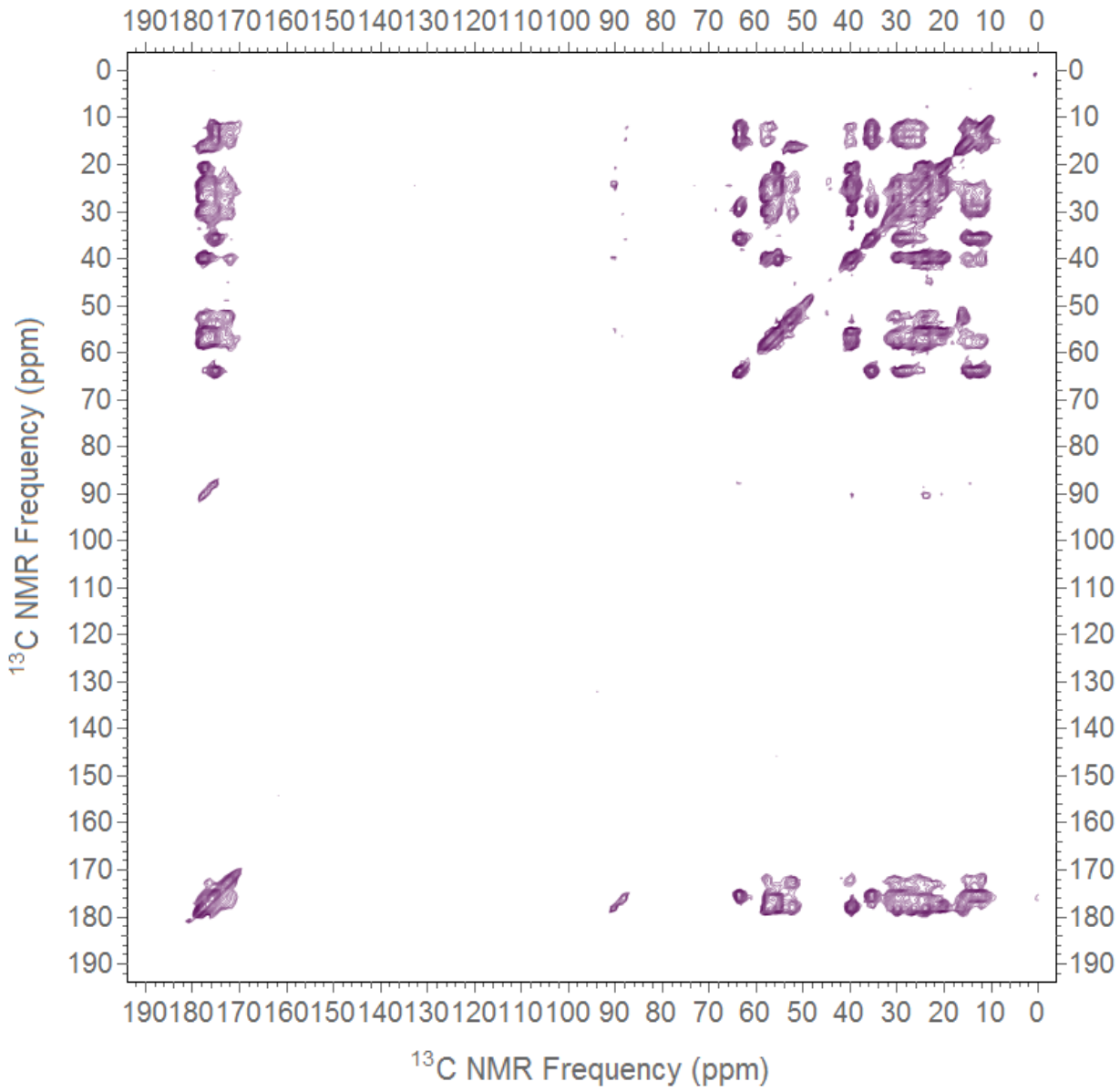

Figure 28E: 2D ^{13}C-^{13}C DARR spectrum of rehydrated hSAF$_{AAQ}$-p1/p2, collected by Sarah R. Leonard at 500 ms mixing time.

REFERENCES

1. C. Chothia, M. H. Levitt, D. Richardson, Helix-to-Helix Packing in Proteins. *J Mol Biol* **145**, 215-250 (1981).
2. C. Cohen, D. A. Parry, Alpha-helical Coiled Coils and Bundles – How to Design an Alpha-helical Protein. *Proteins* **7**, 1–15 (1990).
3. C. Cohen, D. A. Parry, Alpha-helical coiled coils: more facts and better predictions. *Science* **263**, 488-489 (1994).
4. J. F. Conway, D. A. D. Parry, Structural Features in the Heptad Substructures and Longer-Range Repeats of Two-stranded Alpha-fibrous Proteins. *Int. J. Biol. Macromol* **12**, 328–334 (1990).
5. P. Burkhard, J. Stetefeld, S. V. Strelkov, Coiled coils: a highly versatile protein folding motif. *Trends Cell Biol* **11**, 82-88 (2001).
6. W. Saenger, Principles of Nucleic Acid Structure. (1984).
7. J. R. Beasley, M. H. Hecht, Protein design: the choice of de novo sequences. *J Biol Chem* **272**, 2031-2034 (1997).
8. L. Pauling, R. B. Corey, Compound helical configurations of polypeptide chains: structure of proteins of the alpha-keratin type. *Nature* **171**, 59-61 (1953).
9. D. N. Woolfson, in *Fibrous Proteins: Coiled-Coils, Collagen and Elastomers*. (2005), vol. 70, pp. 79-+.
10. J. F. Conway, D. A. Parry, Three-stranded alpha-fibrous proteins: the heptad repeat and its implications for structure. *Int J Biol Macromol* **13**, 14-16 (1991).
11. M. A. Dwyer, L. L. Looger, H. W. Hellinga, Computational design of a biologically active enzyme. *Science* **304**, 1967-1971 (2004).
12. W. D. Kohn, R. S. Hodges, De novo design of Alpha-helical Coiled Coils and Bundles: Models for the Development of Protein-Design Principles. *Trends Biotechnol* **16**, 379–389 (1998).
13. L. L. Looger, M. A. Dwyer, J. J. Smith, H. W. Hellinga, Computational design of receptor and sensor proteins with novel functions. *Nature* **423**, 185-190 (2003).
14. C. E. MacPhee, D. N. Woolfson, Engineered and designed peptide-based fibrous biomaterials. *Current Opinion in Solid State & Materials Science* **8**, 141-149 (2004).
15. H. W. Hellinga, Rational protein design: combining theory and experiment. *Proc Natl Acad Sci U S A* **94**, 10015-10017 (1997).
16. R. B. Hill, D. P. Raleigh, A. Lombardi, N. F. Degrado, De novo Design of Helical Bundles as Models for Understanding Protein Folding and Function. *Acc. Chem. Res.* **33**, 745-754 (2000).
17. J. P. Schneider, A. Lombardi, W. F. DeGrado, Analysis and design of three-stranded coiled coils and three-helix bundles. *Folding & Design* **3**, R29-R40 (1998).
18. J. Ha, S. N. Loh, Protein Conformational Switches: From Nature to Design. *Chem. Eur. J.* **18**, 7984 – 7999 (2012).

19. M. M. Stratton, S. N. Loh, Converting a protein into a switch for biosensing and functional regulation. *Protein Sci* **20**, 19-29 (2011).
20. D. W. P. M. Lowik, E. H. P. Leunissen, M. van den Heuvel, M. B. Hansen, J. C. M. van Hest, Stimulus responsive peptide based materials. *Chemical Society Reviews* **39**, 3394-3412 (2010).
21. G. Grigoryan, A. E. Keating, Structural specificity in coiled-coil interactions. *Curr Opin Struct Biol* **18**, 477-483 (2008).
22. M. J. Pandya *et al.*, Sticky-end assembly of a designed peptide fiber provides insight into protein fibrillogenesis. *Biochemistry* **39**, 8728-8734 (2000).
23. D. N. Woolfson *et al.*, Assembly Pathway of a Designed alpha-Helical Protein Fiber. *Biophysical journal* **98**, 1668-1676 (2010).
24. M. G. Ryadnov, D. N. Woolfson, Engineering the morphology of a self-assembling protein fibre. *Nat Mater* **2**, 329-332 (2003).
25. M. F. Butler *et al.*, Rational design and application of responsive alpha-helical peptide hydrogels. *Nature Materials* **8**, 596-600 (2009).
26. N. Mehrban *et al.*, alpha-Helical peptide hydrogels as tissue engineering scaffolds. *International journal of experimental pathology* **92**, A9-A9 (2011).
27. E. K. O'Shea, J. D. Klemm, P. S. Kim, T. Alber, X-ray structure of the GCN4 leucine zipper, a two-stranded, parallel coiled coil. *Science* **254**, 539-544 (1991).
28. C. Aronsson, D. Woolfson, Self-sorting Heterodimeric Coiled Coil Peptides with Defined and Tuneable Self-assembly Properties. . *Sci. Rep* **5**, 14063 (2015).
29. D. N. Woolfson, D. Papapostolou, E. H. C. Bromley, C. Bano, Electrostatic control of thickness and stiffness in a designed protein fiber. *Journal of the American Chemical Society* **130**, 5124-5130 (2008).
30. A. M. Smith, E. F. Banwell, W. R. Edwards, M. J. Pandya, D. N. Woolfson, Engineering increased stability into self-assembled protein fibers. *Advanced Functional Materials* **16**, 1022-1030 (2006).
31. D. Papapostolou *et al.*, Engineering nanoscale order into a designed protein fiber. *Proc Natl Acad Sci U S A* **104**, 10853-10858 (2007).
32. M. G. Ryadnov, D. N. Woolfson, Self-assembled templates for polypeptide synthesis. *Journal of the American Chemical Society* **129**, 14074-14081 (2007).
33. D. N. Woolfson, Z. N. Mahmoud, D. J. Grundy, K. J. Channon, The non-covalent decoration of self-assembling protein fibers. *Biomaterials* **31**, 7468-7474 (2010).
34. J. Seo, C. Cohen, Pitch diversity in alpha-helical coiled coils. *Proteins* **15**, 223-234 (1993).
35. M. Altman, P. Lee, A. Rich, S. G. Zhang, Conformational behavior of ionic self-complementary peptides. *Protein Sci* **9**, 1095-1105 (2000).
36. Y. Zimenkov *et al.*, Rational design of a reversible pH-responsive switch for peptide self-assembly. *Journal of the American Chemical Society* **128**, 6770-6771 (2006).
37. K. Pagel *et al.*, Random coils, beta-sheet ribbons, and alpha-helical fibers: One peptide adopting three different secondary structures at will. *Journal of the American Chemical Society* **128**, 2196-2197 (2006).
38. S. G. Zhang, A. Rich, Direct conversion of an oligopeptide from a beta-sheet to an alpha-helix: A model for amyloid formation. *P Natl Acad Sci USA* **94**, 23-28 (1997).

39. H. Dong, J. D. Hartgerink, Role of hydrophobic clusters in the stability of alpha-helical coiled coils and their conversion to amyloid-like beta-sheets. *Biomacromolecules* **8**, 617-623 (2007).
40. R. E. Sallach *et al.*, Micelle density regulated by a reversible switch of protein secondary structure. *Journal of the American Chemical Society* **128**, 12014-12019 (2006).
41. A. Aggeli *et al.*, Responsive Gels Formed by the Spontaneous Self-assembly of Peptides into Polymeric β-sheet Tapes. *J. Am. Chem. Soc* **125**, 9619-9628 (2003).
42. S. T. Kumar *et al.*, Solvent Removal Induces a Reversible β-to-α Switch in Oligomeric Aβ Peptide. *J. Mol. Bio* **428**, 268-273 (2016).
43. Y. Takahashi, A. Ueno, H. Mihara, Optimization of Hydrophobic Domains in Peptides That Undergo Transformation from α-Helix to β-Fibril. *Bioorg. Med. Chem* **7**, 177-185 (1999).
44. D. H. T. Le, M. Kato, D. A. Tirrell, A. Sugawata-Narutaki, Self-assembly of Elastin-memetic Double Hydrophobic Polypeptides. *Biomacromolecules* **14**, 1028-1034 (2013).
45. G. Garcia-Iriepa, M. Marrazzi, A Biomimetic Molecular Switch at Work: Coupling Photoisomerization Dynamics to Peptide Structural Rearrangement. *Phys. Chem. Chem. Phys.* **18**, 6742 (2016).
46. E. Cerasoli, B. K. Sharpe, D. N. Woolfson, ZiCo: A peptide designed to switch folded state upon binding zinc. *Journal of the American Chemical Society* **127**, 15008-15009 (2005).
47. S. N. Dublin, V. P. Conticello, Design of a selective metal ion switch for self-assembly of peptide-based fibrils. *Journal of the American Chemical Society* **130**, 49-+ (2008).
48. G. Tuchscherer *et al.*, Switch-peptides as folding precursors in self-assembling peptides and amyloid fibrillogenesis. *Biopolymers* **88**, 239-252 (2007).
49. B. Apostolovic, M. Danial, H.-A. Klok, Coiled coils: attractive protein folding motifs for the fabrication of self-assembled, responsive and bioactive materials. *Chemical Society Reviews* **39**, 3541-3575 (2010).
50. K. Chockalingam, M. Blenner, S. Banta, Design and application of stimulus-responsive peptide systems. *Protein Eng Des Sel* **20**, 155-161 (2007).
51. B. Ciani, E. G. Hutchinson, R. B. Sessions, D. N. Woolfson, A designed system for assessing how sequence affects alpha to beta conformational transitions in proteins. *Journal of Biological Chemistry* **277**, 10150-10155 (2002).
52. M. J. Webber, E. A. Appel, E. W. Meijer, R. Langer, Supramolecular biomaterials. *Nature Mat* **15**, 13-26 (2015).
53. Z. Yu *et al.*, Engineering β-sheet peptide assemblies for biomedical applications. *Biomater. Sci.* **4**, 365-374 (2016).
54. S. Kalepu, K. T. Sunilkumar, S. Betha, M. Mohanvarma, Liposomal drug delivery system - A Comprehensive Review. *Int. J. Drug Dev. & Res.* **5**, 62-75 (2013).
55. B. S. Pattni, V. V. Chupin, V. P. Torchilin, New Developments in Liposomal Drug Delivery. *Chem. Rev.* **115**, 10938-10966 (2015).
56. V. P. Torchilin, Micellar Nanocarriers: Pharmaceutical Perspectives. *Pharm Res* **24**, 1-16 (2006).

57. Z. Ahmad, A. Shah, M. Siddiq, H. Kraatz, Polymeric micelles as drug delivery vehicles. *RSC Adv.* **4**, 17028–17038 (2014).
58. W. Gu, C. Wu, J. Chen, Y. Xiao, Nanotechnology in the targeted drug delivery for bone diseases and bone regeneration. *Int J Nanomedicine* **8**, 2305-2317 (2013).
59. E. V. Giger *et al.*, Gene delivery with bisphosphonate-stabilized calcium phosphate nanoparticles. *Journal of Controlled Release* **150**, 87-93 (2011).
60. M. R. Newman, D. S. W. Benoit, Local and targeted drug delivery for bone regeneration. *Curr Opin Biotechnol* **40**, 125-132 (2016).
61. T. Ponnapakkam, R. Katikaneni, J. Sakon, R. Stratford, R. C. Gensure, Treating osteoporosis by targeting parathyroid hormone to bone. *Drug Discovery Today* **19**, 204-208 (2014).
62. T. Vo-Dinh, in *BioMEMS and Biomedical Nanotechnology*, M. Ferrari, R. Bashir, S. Wereley, Eds. (Springer, 2007), vol. 4, chap. Biosensors and Biochips, pp. 20.
63. P. J. S. King *et al.*, A modular self-assembly approach to functionalised beta sheet peptide hydrogel biomaterials. *Soft Matter* **12**, 9 (2016).
64. J. Boekhoven, S. I. Stupp, Supramolecular Materials for Regenerative Medicine. *Adv Mat* **26**, 1642-1659 (2014).
65. D. T. Seroski *et al.*, Co-Assembly Tags Based on Charge Complementarity (CATCH) for Installing Functional Protein Ligands into Supramolecular Biomaterials. *Cellular and Molecular Bioengineering* **9**, 16 (2016).
66. Z. Qin, M. J. Buehler, Molecular Dynamics Simulation of the alpha-Helix to beta-Sheet Transition in Coiled Protein Filaments: Evidence for a Critical Filament Length Scale. *Physical Review Letters* **104**, 4 (2010).
67. S. Kim, J. H. Kim, J. S. Lee, C. B. Park, Beta-Sheet-Forming, Self-Assembled Peptide Nanomaterials towards Optical, Energy, and Healthcare Applications. *Small* **11**, 3623-3640 (2015).
68. J. Ryu, S. Y. Lim, C. B. Park, Photoluminescent Peptide Nanotubes. *Adv Mat* **21**, 1577-1581 (2009).
69. A. S. Bommarius, B. R. Riebel, *Biocatalysis: Fundamentals and Applications*. (John Wiley & Sons, 2007).
70. J. Kopecek, J. Yang, Smart Self-Assembled Hybrid Hydrogel Biomaterials. *Angew Chem Int Ed Engl* **51**, 7396 – 7417 (2012).
71. L. Taboada, E. Nicolás, E. Giralt, One-pot full peptide deprotection in Fmoc-based solid-phase peptide synthesis: methionine sulfoxide reduction with Bu4NBr. *Tetrahedron letters* **42**, 1891-1893 (2001).
72. E. R. Andrew, A. Bradbury, R. G. Eades, Removal of Dipolar Broadening of Nuclear Magnetic Resonance Spectra of Solids by Specimen Rotation. *Nature* **183**, 1802-1803 (1959).
73. J. Schaefer, E. O. Stejskal, C-13 Nuclear Magnetic-Resonance of Polymers Spinning at Magic Angle. *Journal of the American Chemical Society* **98**, 1031-1032 (1976).
74. A. Pines, M. G. Gibby, J. S. Waugh, Proton-Enhanced NMR of Dilute Spins in Solids. *Journal of Chemical Physics* **59**, 569-590 (1973).
75. X. L. Wu, K. W. Zilm, Cross Polarization with High-Speed Magic-Angle Spinning. *Journal of Magnetic Resonance, Series A* **104**, 154-165 (1993).

76. A. E. Bennett, C. M. Rienstra, M. Auger, K. V. Lakshmi, R. G. Griffin, Heteronuclear Decoupling in Rotating Solids. *J Chem Phys* **103**, 6951-6958 (1995).
77. D. L. Vanderhart, W. L. Earl, A. N. Garroway, Resolution in C-13 NMR of Organic-Solids Using High-Power Proton Decoupling and Magic-Angle Sample Spinning. *Journal of Magnetic Resonance* **44**, 361-401 (1981).
78. C. P. Grey, R. Tycko, Solid-state NMR in biological and materials physics. *Physics Today* **62**, 44-49 (2009).
79. M. T. Nelson *et al.*, NAMD: A parallel, object oriented molecular dynamics program. *Int J Supercomput Ap* **10**, 251-268 (1996).
80. D. A. Case *et al.*, The Amber biomolecular simulation programs. *J Comput Chem* **26**, 1668-1688 (2005).
81. C. D. Schwieters, J. J. Kuszewski, N. Tjandra, G. M. Clore, The Xplor-NIH NMR molecular structure determination package. *J Magn Reson* **160**, 65-73 (2003).
82. A. K. Paravastu, R. D. Leapman, W. M. Yau, R. Tycko, Molecular structural basis for polymorphism in Alzheimer's β-amyloid fibrils. *Proc Natl Acad Sci U S A* **105**, 18349-18354 (2008).
83. A. R. Cormier, X. Pang, M. I. Zimmerman, H. X. Zhou, A. K. Paravastu, Molecular structure of RADA16-I designer self-assembling peptide nanofibers. *ACS Nano* **7**, 7562-7572 (2013).
84. D. Huang *et al.*, Antiparallel beta-Sheet Structure within the C-Terminal Region of 42-Residue Alzheimer's Amyloid-beta Peptides When They Form 150-kDa Oligomers. *J Mol Biol* **427**, 2319-2328 (2015).
85. K. Nagy-Smith, E. Moore, J. Schneider, R. Tycko, Molecular structure of monomorphic peptide fibrils within a kinetically trapped hydrogel network. *Proc Natl Acad Sci U S A* **112**, 9816-9821 (2015).
86. J.-X. Lu *et al.*, Molecular structure of β-amyloid fibrils in Alzheimer's disease brain tissue. *Cell* **154**, 1257-1268 (2013).
87. A. T. Petkova *et al.*, Self-propagating, molecular-level polymorphism in Alzheimer's β-amyloid fibrils. *Science* **307**, 262-265 (2005).
88. R. Tycko, Physical and structural basis for polymorphism in amyloid fibrils. *Protein Sci* **23**, 1528-1539 (2014).
89. V. Rangachari *et al.*, Amyloid-beta(1-42) rapidly forms protofibrils and oligomers by distinct pathways in low concentrations of sodium dodecylsulfate. *Biochemistry* **46**, 12451-12462 (2007).
90. M. R. Nichols *et al.*, Growth of β-amyloid(1-40) protofibrils by monomer elongation and lateral association. Characterization of distinct products by light scattering and atomic force microscopy. *Biochemistry* **41**, 6115-6127 (2002).
91. D. M. Walsh *et al.*, Amyloid b-protein fibrillogenesis: Structure and biological activity of protofibrillar intermediates. *J. Biol. Chem.* **274**, 25945-25952 (1999).
92. L. Gonzalez, R. A. Brown, D. Richardson, T. Alber, Crystal structures of a single coiled-coil peptide in two oligomeric states reveal the basis for structural polymorphism. *Nature Structural Biology* **3**, 1002-1010 (1996).
93. A. E. Bennett, J. H. Ok, R. G. Griffin, S. Vega, Chemical-Shift Correlation Spectroscopy in Rotating Solids - Radio Frequency-Driven Dipolar Recoupling and Longitudinal Exchange. *Journal of Chemical Physics* **96**, 8624-8627 (1992).

94. A. E. Bennett *et al.*, Homonuclear radio frequency-driven recoupling in rotating solids. *Journal of Chemical Physics* **108**, 9463-9479 (1998).
95. W. M. Tay, D. Huang, T. L. Rosenberry, A. K. Paravastu, The Alzheimer's Amyloid-β(1-42) Peptide Forms Off-Pathway Oligomers and Fibrils that are Distinguished Structurally by Intermolecular Organization. *J. Mol. Biol.* **425**, 2494-2508 (2013).
96. D. Wishart, B. Sykes, The 13C Chemical-Shift Index: A simple method for the identification of protein secondary structure using 13C chemical-shift data. *Journal of Biomolecular NMR* **4**, 171-180 (1994).
97. D. S. Wishart, C. G. Bigam, A. Holm, R. S. Hodges, B. D. Sykes, 1H, 13C and 15N random coil NMR chemical shifts of the common amino acids. I. Investigations of nearest-neighbor effects. *J Biomol NMR* **5**, 67-81 (1995).
98. D. S. Wishart, Interpreting protein chemical shift data. *Prog Nucl Mag Res Sp* **58**, 62-87 (2011).
99. Y. Shen, F. Delaglio, G. Cornilescu, A. Bax, TALOS plus : a hybrid method for predicting protein backbone torsion angles from NMR chemical shifts. *Journal of Biomolecular NMR* **44**, 213-223 (2009).
100. A. T. Petkova *et al.*, Solid state NMR reveals a pH-dependent antiparallel beta-sheet registry in fibrils formed by a beta-amyloid peptide. *Journal of Molecular Biology* **335**, 247-260 (2004).
101. A. T. Petkova, Y. Ishii, R. Tycko, Probing the structure of Alzheimer's beta amyloid fibrils by two-dimensional C-13-C-13 and C-13-N-15 solid state NMR methods. *Biophysical Journal* **82**, 320A-320A (2002).
102. A. T. Petkova, W. M. Yau, R. Tycko, Experimental constraints on quaternary structure in Alzheimer's β-amyloid fibrils. *Biochemistry* **45**, 498-512 (2006).
103. K. Takegoshi, S. Nakamura, T. Terao, 13C-1H dipolar-assisted rotational resonance in magic-angle spinning NMR. *Chemical Physics Letters* **344**, 631-637 (2001).
104. E. Crocker *et al.*, Dipolar assisted rotational resonance NMR of tryptophan and tyrosine in rhodopsin. *Journal of Biomolecular Nmr* **29**, 11-20 (2004).
105. W. Humphrey, A. Dalke, K. Schulten, VMD: Visual molecular dynamics. *Journal of Molecular Graphics & Modelling* **14**, 33-38 (1996).
106. D. S. Wishart, B. D. Sykes, F. M. Richards, Relationship between Nuclear-Magnetic-Resonance Chemical-Shift and Protein Secondary Structure. *Journal of Molecular Biology* **222**, 311-333 (1991).
107. A. C. Zane, C. Michelet, A. Roehrich, P. S. Emani, G. P. Drobny, Silica morphogenesis by lysine-leucine peptides with hydrophobic periodicity. *Langmuir* **30**, 7152-7161 (2014).
108. G. Zhao, N. D. Chasteen, Oxidation of Good's Buffers by Hydrogen Peroxide. 262-267 (2006).
109. S. B. Lim, I. Rubinstein, H. Onyuksel, Freeze Drying of Peptide Drugs Self-Associated with Long-Circulating, Biocompatible and Biodegradable Sterically Stabilized Phospholipid Nanomicelles. *Int. J. Pharm* **355**, 345-350 (2008).
110. T. O. Omosun *et al.*, Catalytic Diversity in Self-Propagating Peptide Assemblies. *Nat. Chem*, (2017).

111. I. Bertini, C. Luchinat, G. Parigi, E. Ravera, SedNMR: On the Edge between Solution and Solid-State NMR. *Acc. Chem. Res*, (2013).
112. R. Tycko, Symmetry-based constant-time homonuclear dipolar recoupling in solid state NMR. *J. Chem. Phys.* **126**, 064506-064506 (2007).